A Critical Review of Multi-Phase Materials and Optimization Strategies for Additive Printing Technologies

W. Elliot McAllister

Thesis submitted to the faculty of the Virginia Polytechnic Institute and State University in partial fulfillment of the requirements for the degree of

Master of Science

In

Materials Science and Engineering

ShashankPriya, Chair

Carlos T. Suchicital.

Alex O. Aning,

May 2, 2013

Blacksburg, VA

Keywords: 3D Additive Printing, Selective Laser Sintering, Boron, NBT-BT, PVDF, Al-Si

A Critical Review of Multi-Phase Materials and Optimization Strategies for Additive Printing Technologies

W. Elliot McAllister

Abstract

The focus of this thesis is the critical review of Additive Printing (AP) or 3D-printing, and optimization strategies for the introduction of new materials. During the course of tenure, four classes of solids were investigated to determine the hurdles presented from each system. Specifically, the investigation developed techniques for optimization of ink production, green-film deposition, and laser sintering parameters surrounding the Optomec AJP system (AJP). In the assessment, statistical experimental design, analysis and material characterization techniques have been utilized. Final recommendations disseminate current best practices for new ink and material development, along with factor analysis of input variables for phase and material properties, along with insights for future research of these systems.

The first chapter provides a general introduction to the field of AP. The second chapter focuses specifically on Optomec aerosol-jet process (AJP) techniques, and expands the discussion to process parameters, information concerning the fabrication/characterization procedure followed for each system, and includes: a detailed description of the materials investigated. This is important because printing parameters, optimization, and approach may be divergent for optimization within each strain; and is meant as an aid to resolve some technical issues for future investigators. The third chapter is fully dedicated to the results concerning the fabrication and the characterization of amorphous boron powder to film. Chapter four discusses future research options, ideas and directions. Appendices are provided for any which wish to investigate the orthogonal arrays used, or the combinatory effects resulting in the attributes of the material system final products.

Contents

Figures:

Tables:

Chapter 1 Overview of Technology

1.1 Additive Printing: Overview of Technology

This first chapter provides a general introduction to the field of additive printing. This initial section focuses on the description and hierarchy of different printing systems and compatible material classes, traits, abilities, compliments and detractors. Although it is introduced in this chapter, those interested in aerosol jet process (AJP) should direct their inquiry to the chapter following as it is dedicated to printed electronics applications with specific orientation to and opportunities presented for the AJP system and applications.

Over the past 30 years, the home based printer has vaulted from sole use desktop publishing to desktop prototyping. In essence, allowing an at-home innovator to produce circuit-boards, models, devices or prototypes of varying complexity utilizing a variety of materials. News reports from financial companies like Forbes have portrayed 2013 as the year of the 3D printer; recently some companies have even argued that 3d printing can fill Americas manufacturing void- allowing innovation to reign again in the capitalist market [2] The appeal of this kind of technology can be linked directly to; introduction of new materials, low entry cost ($650 for DIY), flexible platforms, rapid prototype iteration periods, and the rapid learning curves of these machines [3]

Additive fabrication or additive manufacturing (AM) and 3D Printing (3D) technology have been available since the late 1980s with the advent of stereolithography (SL) [4, 5] Several processes have since been introduced, helping to expand the number of applications and the industries that employ this technology. Most readers are familiar with computer numerically controlled machining (CNC or numerically controlled-NC); its attributes and acceptance within the manufacturing world. The distinction between each is the process direction: In a CNC processes, the material is introduced to the machine as a solid billet or brick; the CNC machine removes material (as much as 95%) to reveal the final part, the reverse is true in AM as the part is built layer by layer from the raw material with minimal waste [5]

Within the manufacturing realm, many are relying on the future this technology promises; creation parts of the same strength as current items with lower weight, to overcome the hurdle of

intricate hollows within solid shapes, and reduction of time to market. Some examples in the recent press have been advances to Unmanned Aerial Vehicles (UAVs) through both printed energy scavenging components or antenna on wings[6], lighter more integrated parts, the company Aerobus which hopes to print an aircraft at 60% of current weight[7, 8] Ford, GM and other automakers have also made investments in 3D printing with aims to reduce the weight of their vehicles without sacrificing safety, significantly increasing gas mileage to meet new federal requirements[3, 9]. The shifting market and expectations for shorter design cycles is exemplified by Shapeways of the Netherlands which in 2007 developed the concept, design and manufactured a protective cover for the Apple iPad within four days of market introduction[10]. The realization of these long term goals requires direct efforts in further development of suitable materials for use in these applications. Over the past 10 years significant growth has been acquired in the reduction of post-processing for completed parts, increased ultimate yield strength of materials processed by AM, and the availability of newer materials from industry favored alloys[4, 5]. The scenarios for new materials and phase selection through laser sintering have required new ideologies regarding these materials[11].

One of the most difficult hurdles to clear for 3D printing remains still one of the largest detractors- the introduction of new materials. In its nebulous, 3D printing employed a limited materials list. Additionally, the characteristics of those available materials after processing were not comparable to those of a machined part; powders were brittle, plastics were weak and emerged from the process malformed[12, 13]. However, with a more thorough understanding of the thermodynamics and science behind the new processes like powder lasing; materials are beginning to achieve new plateaus and allow tunable characteristics-- meeting the end user needs. The new understandings of driving forces within these transformations are beginning to allow new characteristics to be optimized and realized as well as transference of the process concept to other materials [14-16].

In many cases, CNC machining still holds residual advantages over 3D printing. For example, to use some industry favored alloys, AM must employ non-ambient environments equipped with vacuum chambers, environmental controls, necessitating restrictive platform sizes for production and part geometries along with others [8,11,15]. However, AM also exists because of restrictions to the CNC process. CNC is purely subtractive process in nature, up to 95% of the

material from the original blank is removed, and it is a 2.5D process, as one side of the object must always be linked to the platform, isolated from the concerns of the designer[13].

1.2 Machine Language

These two processes (CNC and AP) are practically identical in operation; this begets the nature of machine communication language is nearly the same as well. Before continuing on, it is important for the reader to realize how AM understands a 3D image and converts it to sequential 2D layers; stacking each such that the end result is a model indicative of the original computer generated image. An excellent visualization of the tessellation process can be seen in the movie TRON™ when the protagonist, Flynn, is pulled into the computer, one byte at a time.

In the real world, systems rely on a form of Standard Tessellation Language (STL) file or object file (.obj), parametric slicing software[17] developed by 3D Systems in 1987 in coordination with the development of steriolithography (Fig 1.2). The language was uploaded to the public domain, allowing vendors easy integration to their own systems and made STL the standard for AM[18, 19]. Currently several other programs are attempting to gain traction as a replacement to this language and are slated for public domain use.

In STL, the object is converted into a series of layers, and each layer then to a series of small triangles, to describe the surfaces for construction in the vertical direction. Each triangle is defined by three points for the area, and a normal vector originating at the surface, the magnitude and direction of this triangle lie to the outside of the object and orient it to the surrounding volume. Each small volume is termed a voxel. Most defect issues for high-resolution printing arise from inconsistencies between the algorithms and machine processor abilities. Some increased flexibility and attributes are offered through paring of auxiliary programs such as Mathematica which can be paired with STL files as well as other variants of the STL file: obj EOS (CLI), HP (HPGL), steriolithography-contour from Stratasys, and Fockle and Schwarze (IGES) [17, 18, 20, 21].

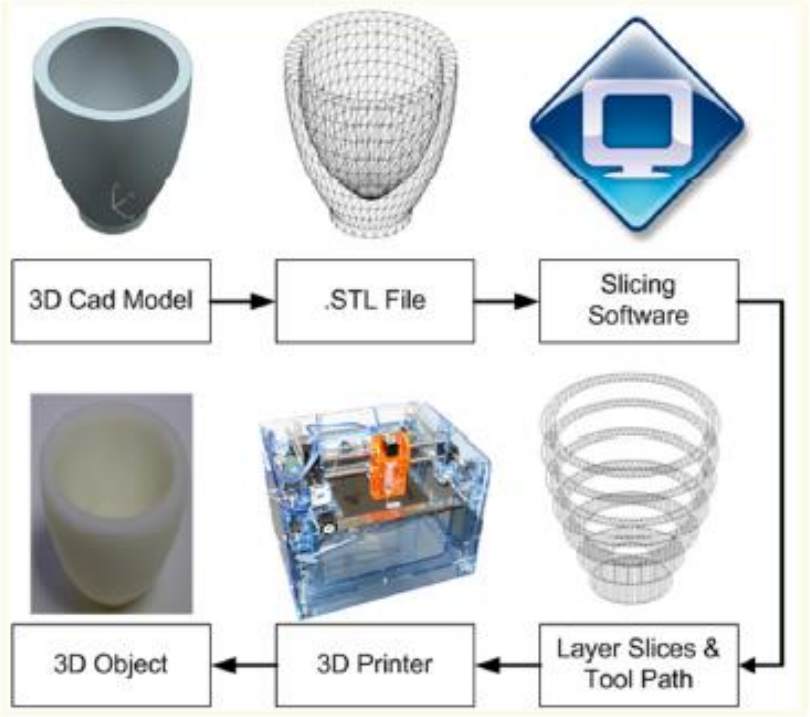

Figure 1.1: Translation Process

Originally, it was the demand for CNC and NC machining that pushed the rapid development of CAD and now Computer Aided Manufacturing (CAM) to the point it is now. As both the machine and computer progressed in processor speed, complex geometric capabilities, and ability to coordinate the data, the applicability for use in industry increased exponentially.

Still for NC machining three main limitations are present: Like Michelangelo's David, all processes rely on the removal of material and the removal of extraneous parts to reveal the final product. All machining is done from the approach vector- the stock material must be held in a precise location and orientation and acts as the attachment point, eliminating at least one surface from attention. Second, each removal section is done piece-wise in many cases requiring multiple steps in the removal process. Third, the original part must enclose the final volume; any parts that are removed can be considered waste; in these ways CNC machining is more 2.5 D than true 3D [13].

AM was the first truly CAM that utilized and required the program to have a completely enclosed 3D surface for rendering. Though the part drawing may be perceived as a complete 3D solid by the observer, the computer and subsequent processes realize most solids are incomplete

and not entirely enclosed solids. As such, CAD/CAM programs evolved using interesting solutions such a tolerance variations and splines for proper communication to the printer and NC machine. Between each of these programs for CAD and Computer Aided Milling (CAM), the integration of a variety of programs can become complex[19].

1.3 3D Printing Hierarchy

3D Printing (3DP) was originally developed by MIT and is utilized improperly in most cases, becoming a misleading term. The original system ,3DP, relates to a discrete particle system with binder additives. Within literature 3D Printing is an umbrella term and often referred to as 3DP, though it covers several distinct methods of fabrication, all of which are additive in nature and have individual challenges.

Several classification methods have been developed in the past but confusion often exists in some of the cross-over technologies [22-24]. In this document the chosen method of identification is a reconsideration of Pharm's Method wherein each separate technology is separated via machine design and differentiated through cross-overs through a second dimension describing how each layer is constructed[25]. The base groupings are: Liquid Systems (LS), and Solid Systems (SS). Further delineation allows each to be further subdivided into contact (CLS) where there exists no separation between liquid, deposition tip, and substrate; and non-contact liquid systems (NCLS), where particles or liquid droplets are not in-contact with both deposition head and substrate at the same time. Finally Hybrid Systems which can be further quantized through a description of final product finishing methods that may be either a combination of the above, thermal, light, oxidation and employ both additive and subtractive processes. As with many categorization methods, some have aspects of more than one group, or lie outside the boundaries of the general class. In this thesis, there are no additional differentiations for multi-channel (1D vs. 2D) methods of deposition or binding.

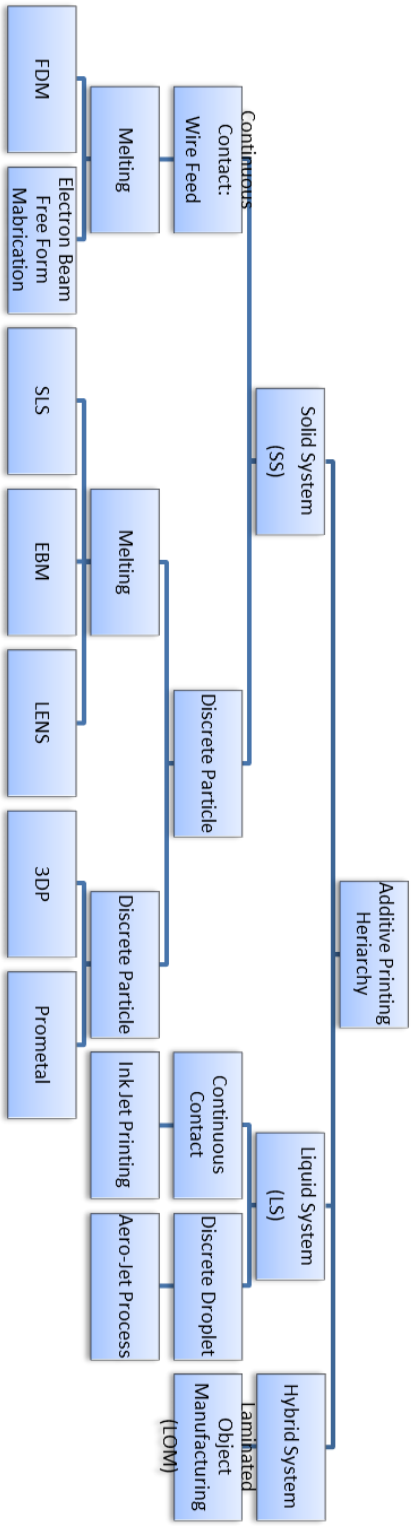

Figure 1.2: Additive Process Hierarchy

To be sure, some Rapid Prototyping (RP) schemes are outliers to this system and this list cannot be considered complete. Interested parties are referred to the bibliography at the end of this section for further reading. Initial separation for hierarchy begins with initial state of material, solid and liquid. Beyond this initial separation, groups are further delineated by continuous contact or discrete deposition groupings and through phase transformation mechanism or energy source, (thermal heat ramp via heating platen or laser raster, UV polymerization, or cooling). Through this classification six distinct categories are seen to exist, (Fig1.3). The liquid-and powder-based processes appear more promising than solid-based processes of which LOM is the predominant one today. Prior Pharm's 2004 work many of these systems including EBM, Lens, Polyjet and Prometal were underdevelopment [26]. Additional lists for those processes beyond the scope of this introduction and arising new technologies are listed after these descriptions. Considered in this chapter's discussion are stereolithography (SLA), fused deposition modeling (FDM), laminated object manufacturing (LOM), 3D printing (3DP), selective laser sintering (SLS), laminated engineered net shaping (LENS), and electron beam melting (EBM), Ink Jet Printing (IJP), Aerosol Jet Printing (AJP).

1.3.1 Solid Systems

Laminated Object Manufacturing (LOM)

Perhaps the earliest illustration of AM technologies, LOM combines both additive and subtractive techniques to realize the final object from thousands of thin material sheets as seen in Figure 1.3 LOM utilizes a laser, blade or other cutting instruments to create a 2D layer from the STL file. Helisys USA, Kira Japan, and Solid-dimension from Israel offer some examples that can use metal foils, wood or paper that are systematically cut into shape and laminated on top of one another building the model from the ground up. These systems use material from a continuous roll or individual sheets of the same size as the working area. One detriment to the early systems of was the stereotypical steps on the profile of new object construction. In newer systems, these steps can be somewhat mitigated via an angled cut made to the edges of the layer such that the bottom edge of the upper part mates with the upper edge of the lower layer. Bonding one layer to the next can be achieved from ultrasonic welding, heat reactive binder or glues [48, 49]. Adhesives can be drawn with a separate plotter head or sprayed on.

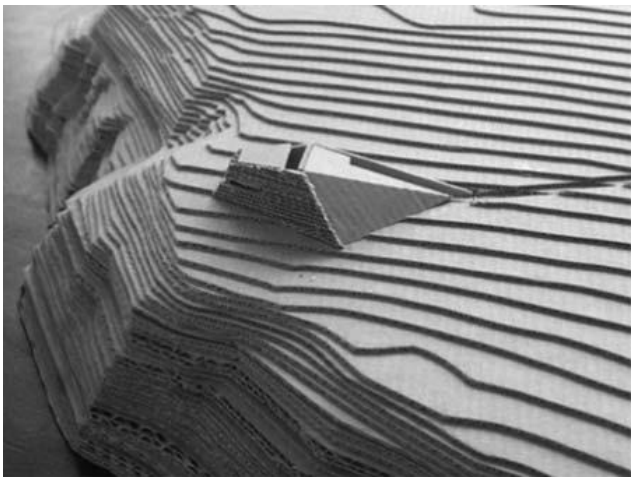

Figure 1.3: Laminated Object Manufacturing

Advantages include low cost, relatively little post processing, no deformation, shrinkage or phase changes, no support structures need to be employed for overhangs. [14, 16, 50] Disadvantages include waste material, low surface definition with characteristic steps visible on the part profile (each layer only has the z-resolution of the sheet 50-100 μm) and material properties that are dependent on direction/orientation can be difficult to work with. Internal cavities or complex voids can be hard to form.

3DP

These are similar to the SLA, however instead of an unpolymerized liquid; this process uses particles on a bed, which are then bound via a liquid binder or direct energy source, see Figure 1.4. Originally this technology was developed at MIT and licensed as 3DP, currently owned by Z-Corp. The process can use a wide variety of ceramics, metals, and polymers can be annealed to create a solid in a layered process [14, 15, 20]. As each layer is finished, a new layer of the raw material is leveled over the previous surface. This technique of backfilling the previous surface allows excellent support of overhangs and voids that other techniques have difficulty with. 1D or multiple channel approaches are the similar in function and process to the above. Limitations on the systems exist through difficulties maintaining material characteristics from the raw input through phase transitions to final state. Specifically, polymers must exhibit enough thermoplasticity to allow melt-remelt bonding between each layer, and in the case of pizeoelectrics the crystal formation which enables the reaction to stress must not be disrupted.

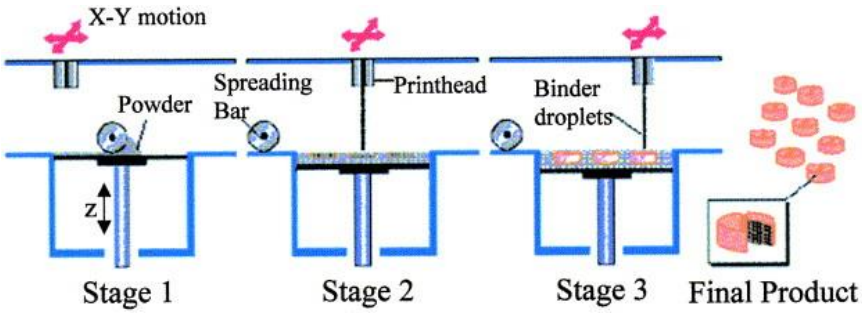

Figure 1.4: 3DP Process

Two main types of polymer systems are available from 3D systems, and EOS[27-30]. Binders and glues can be tailored to the base materials allowing very rapid construction at excellent resolution. Post construction some materials are sintered in an oven to reach final state, others are used as molds for castings in foundries, etc. The most successful approaches are using low-cost starch, sand and plaster based powders with companies like ZCorp which is able to produce blanks of $1m^3$ volume for metal pouring within eight hours, Soligen with its Direct Shell Production casting (DSCP)[30, 31], EOS in from Germany uses a very similar system with Selective Laser Sintering (SLS) discussed below. One additional use of 3DP can be to create complex parts for drug delivery rates as from Therics[32, 33].

Prometal

A separate 3D powder based process; Prometal is a method of producing injections tools and dies from stainless steel. It works very similarly to the 3DP process described above, except liquid binders are used on steel powder with final part finishing taking place through sintering at 350^oC for 24 hours[14, 15]. If the final requirements are for a less porous specimen, an infiltration process with bronze may be employed and the part heated to more than 2000 ^oC [30]. This interesting case has found use with Zr-Cu alloys for use in rocket nozzles and exhibits material properties surpassing the previous standards [34].

Selective Laser Sintering (SLS)

Selective Laser Sintering uses a CO_2 laser to target and heat with extreme precision a small area of the powder bed and fuse particles together. Initially the chamber is heated to nearly that of the melting point of the base material. An inordinate amount of knowledge is necessary for this process; including heating only the required area, thermal heat transfer between the particles and rates of densification. SLS offers flexibility in the vast variety of materials including plastics,

metals, and ceramics [20, 35, 36]. Some examples of the polymers utilized are acrylic styrene, and polyamide (Nylon). Already many processes for materials commonly used in industry have been optimized, allowing the same mechanical properties to that of injection molded parts [35, 37]. Polyamide fiberglass and reinforced composites have found favor with this process. The current limitations stem from use and removal of binders, and in the case of metals oxidation rates due to high heat. In general if a pure alloy is necessary, the binder can be treated for removal by heat. [35, 36, 38] An example is that of alumina particles fuse with a PVA organic binder [14, 39]. Additional advantages include the ability to reuse materials that were not sintered, and near 100% use of expended materials [37].

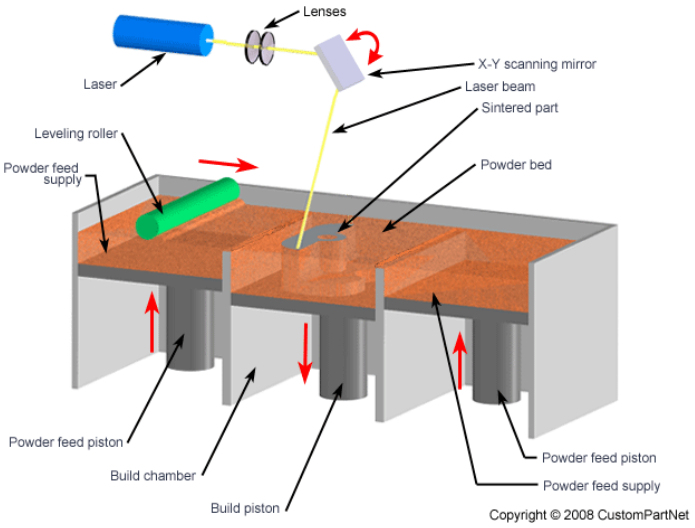

Figure 1.5: Selective Laser Sintering

Disadvantages are restrictions on part size due to the necessity of inert environments (heavy oxidations take place with sintering metals at high heats in oxygen rich environments), subsequent steps for heat treatments in the case of furnaces being used, and geometrical restraints of the[40] system for inert atmosphere. In the case of accuracy, the limitations are placed by the particles sizes and for many nano-particle systems they can range from 4nm to a few μm [41].

Electron Mean Melting (EBM)

Another variant of the SLS system above uses Electron Beam Melting, the Swedish company Arcam is an excellent example of this technology. This process uses a high powered electron laser powered by high voltage (30-60kV) to melt powder as it is selectively focused and deposited in the target area. The main difference between SLS and EBM are exhibited by the fact that EBM necessitates a high vacuum chamber to avoid oxidation issues and to increase the Mean-Free Path (MFP) of electron travel. The additional requirement of a vacuum makes the process identifiable as one process that can produce products in space [42, 43]. EBM lends itself to producing parts of exacting tolerances capable of use for implants and final products of net shape that are exact replicas of the CAD models. The main negatives affecting the system are the same as those for selective laser sintering.

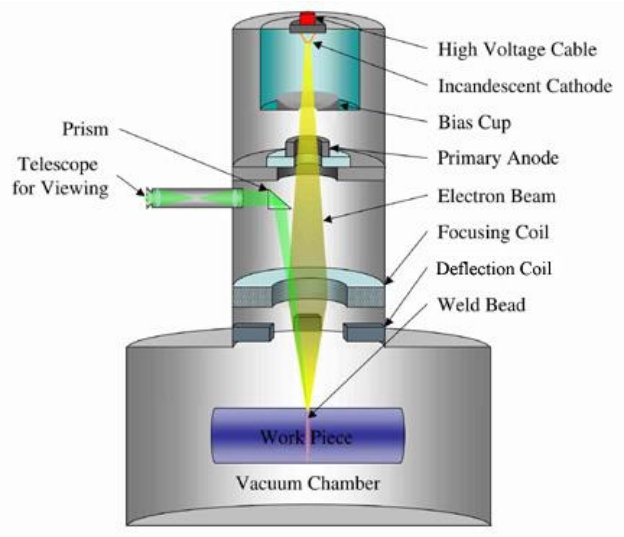

Figure 1.6: Electron Beam Melting

1.3.2 Non-Contact Solid Systems

LENS or Laser Engineered Net Shaping is another very similar process to EBM with the exception that the process takes place in a sealed argon environment container. Particles are directed to the target area and liquefied by a laser as they impinge on the surface of the part. In this way the process can be used with nickel based alloys, Ti (6/4), tooling steels, copper alloys and aluminum alloys. One drawback to the process is some yet unresolved thermal stress problems caused by uneven heating and cooling processes. These residual material stresses can

cause significant issues with high strength parts, yet it has shown promise in the applications where other methods have failed to achieve success [14, 20, 43-45]. Systems like the Optomec LENS and Germanys EOSint systems have been available for a number of years and utilize the point wise building process [46, 47]. These systems use discrete powder particles in their systems

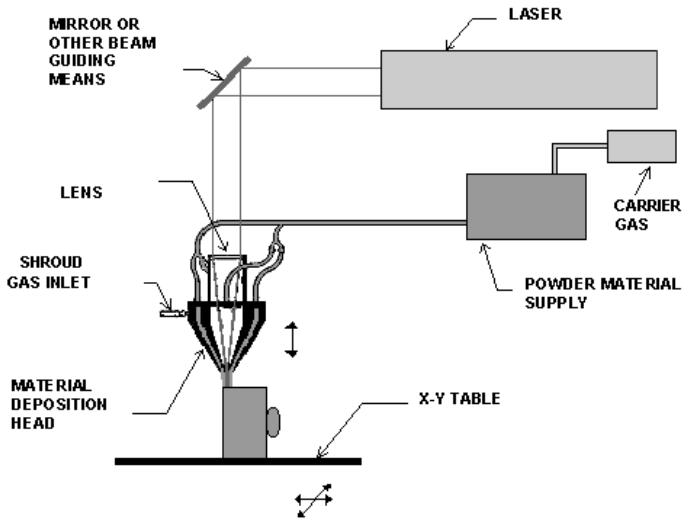

Figure 1.7: LENS

1.3.3 Liquid Systems

Steriolithography (SLA)

The first system to enter the commercial market for RP was the 3D systems Steriolithography. The process is based on a photo-reactive polymers which when exposed to a focused UV light reacts and polymerizes. This system, originally restricted to polymers, has found some renaissance with alternative direct energy sources, experimental hydrogels currently in development as well as suspended ceramics within the liquid phase polymer. [25] Fab@home developed at Cornell and Reprap from the Bath in the UK use polymer systems of similar machine architecture and cure the object via focused beams other than UV wavelengths [51, 52].

In this process a platform lays just below the surface of a polymer within a container. Initially, the polymerizing source rasters across the surface hardening the base of the structure as 2D slice of the part. Multiple channels can be employed to speed up the process. Once the layer is complete, the piston lowers the stage below the liquid surface and the next layer is constructed.

The completed part has one of the most dramatic reveals, rising out of the liquid like the Lady of Lake Avalon revealing King Arthur's Sword. Remaining unreacted liquid can be reused, or evacuated an a separate polymer with different material properties can be flooded into the tank for other part features [14-16]

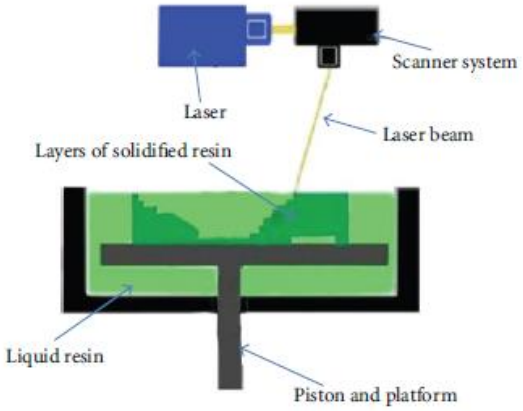

Figure 1.8: Steriolithography

Significant improvements to the above have been shown with introduction of digital micro-mirror devices (DMMD), eliminating the need of a raster scans with resolutions to 10um thicknesses. [20, 53] The Viper line of stereolithography apparatuses (SLA's) manufactured by 3D Systems is an excellent example of this technology. The material properties from systems like Objet can be altered by limiting the processing time or creating fractal areas of solid/void sections, or adding separate polymers in subsequent processes. Parts can vary between hard and rubber like feel from this process. [54]

Errors to final parts can be introduced from over-curing in the case of cantilevered sections, and line shaped scans where unwanted polymerization takes place. In addition most polymers employed are of high viscosity and can cause layer thickness variability. [55] In the case of multi materials mentioned above, all original material must be drained from the container to introduce the second, slowing the process [56]. Additionally, suspended ceramics within the liquid polymer causes difficulties in curing from changes to the liquid refraction angle and viscosity because of solids loading. The general tolerances for commercially available SL are 100um in x-y and approximately 30 μm in the vertical direction

1.3.4 Contact Liquid Systems

Fused Deposition Modeling (FDM)

Fused Deposition Modeling (FDM) creates models by heating and extruding a filament of material usually glass, wax or plastic, the thickness of the material can be selected via alteration of the main parameters of heat, federate, speed, and tip aperture. It is generally a 1D channel system with a piezoelectric valve used to control deposition within close proximity to the substrate. It is considered a contact based deposition method. Filament thicknesses on the order of 0.25mm are the standard. Plastics which lend themselves to this process are: polycarbonate (PC), acrylonitrile butadiene styrene (ABS), polyphenylsulfone (PPSF), PC-ABS blends, and PC-ISO, which is a medical grade PC, PLA and PCL have both been used to reform calcaneus bone within the body as they have similar compression rates.

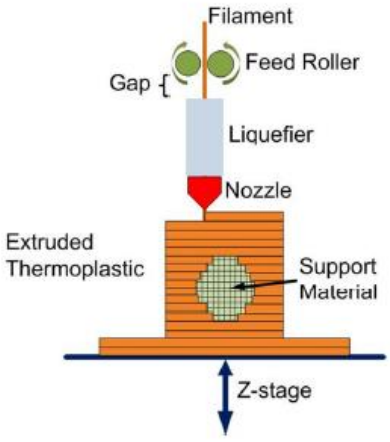

Figure 1.9: Fused Deposition Modeling

Systems like the Solidscape employ two print heads or more. This application leads to increased rates of product rendering when the same material is used in both heads. In the case of dissimilar materials; strength in one area while allowing flexibility in another, or as a sacrificial support of the main structure to be removed later by either heat or chemical etching. Cube from Stratysys uses this type of technology to construct 3D parts. Part precision can be further enhanced by using a planar leveling blade to keep tolerances between each layer. The precision offered by some of the wax based systems have allowed them employment for precision castings in jewelry, medical, dental industries.

The main advantages of this process are exhibited through: no chemical post-processing requirements, no resins to cure, lower initial investments in the machine, and materials resulting in a more cost effective process [14, 57]. The main disadvantage beyond available materials is lower resolution, especially the z axis, as compared to other AM processes (0.1mm (100 micron) in z-axis and an x-y resolution of 0.0025 (2.5 microns)). Further, to produce a smooth surface, FDM can be a slow process sometimes taking days to build large complex parts. To save time some models permit two modes; a fully dense mode and a sparse mode that save time but obviously reducing the mechanical properties [14, 16, 30]. It should be noted that because of the relative ease and well understood mechanical properties for the base materials, they have found a huge following in the Do-It-Yourself (DIY) computer crowd. In 2011 many have reported construction of High-Resolution machines capable of 20 μm z-resolution and 0.4 μm x-y resolution, though these can require special resins [58] as seen in figure 1.10.

Figure 1.10: High Resolution FDM

1.3.5 Non-Contact Liquid Systems

Ink Jet Printing Technologies

Ink-jet and droplet based technologies have the ability to deploy discrete areas of material for sintering via curing, UV sintering, or laser based heating. The high resolution, color flexibility and speed of these machines make them very attractive for use in 3D systems. In contact based systems standoff heights vary between 1-3 mm, production is achieved either through thermal volume increases or a piezoelectric impulse to expel a droplet of 10-30 μl to the target below. It is possible to control sizes of the droplets of a variety of materials of varying viscosities 0.1-20

cP and temperatures. It is even possible to work with molten or UV curable materials to some degree. These systems use the technology of current printing systems produced on the market.

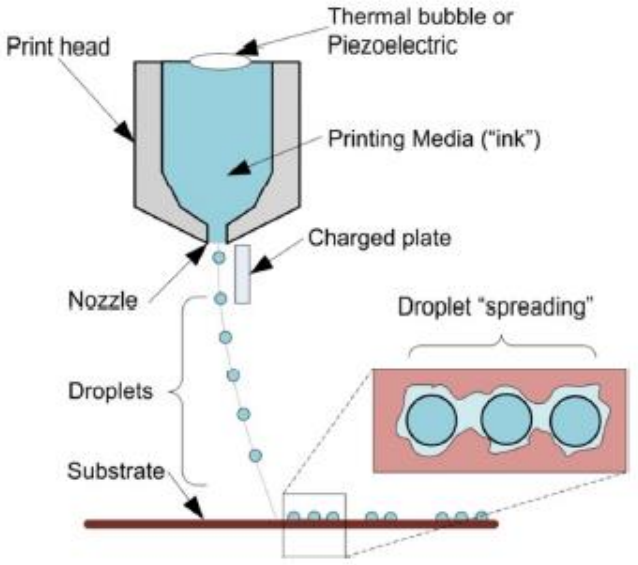

Figure 1.11: Ink Jet Printing

In the selected example from Polyjet, inkjet technology is used much like a plotter for architectural designs. The print head is moved in the x-y position depositing a photopolymer that is cured with a UV light. Additional charged plates may be employed for directional, diffuse or focused patterns to be realized on the substrate. Thickness to 16 μm can be achieved for exacting resolutions. In general parts produced from this process are lower in Ultimate Yield Strength UTS than the standard steriolithography and SLS. To support overhanging features, a gel polymer is employed and water jetted to remove after the part is complete. [57, 59, 60]

Expectations for resolutions are in the 10 μm for x-y and several hundred nm range for feature heights.

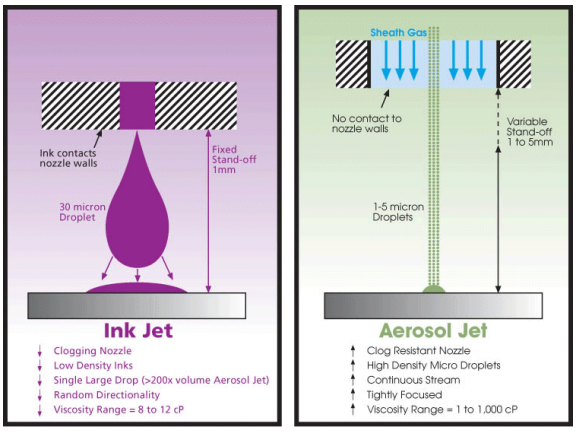

Figure 1.12: Ink Jet v.s. Aerosol Jet Process

Aerosol Jet

One of the most promising newer technologies for microscale printing is the Optomec Aerojet System. It has the ability to produce droplets from 1-5 µl, at distances of up to 10 mm above the substrate and is capable of developing patterns on curved and 3D structures with z-height angles approaching 30 degrees. The AJP utilizes aerosol deposition for laying down lines and features as small as 10 µm and thicknesses as low as 100 nm. To produce these delicate elements, nanoparticles of up to 1 µm can be suspended in a colloidal mix or polymers are dissolved in a solvent mixture. The mixtures viscosity can vary in a huge range from 1 to 1000 cP. Utilizing one of two methods of agitation, ultrasonic or pneumatic, the mixtures are initially aerosolized in small containers and further refined for proper size in a "virtual impactor" then transmitted to the print head through a thin tube. In this way the AJP can deposit any type of solid provided the nano-particle size does not exceed 1-2 µm. The ultrasonic attachment works in the optimum range of 1-10 cP depending on the surface tension and material density. This technique utilizes mainly aqueous, alcohol and acetone base solvents. The Pneumatic disperser can handle much higher viscosity solvents, and uses inks with base solvents of Xylene, Turpineol, and Ethylene Glycol.

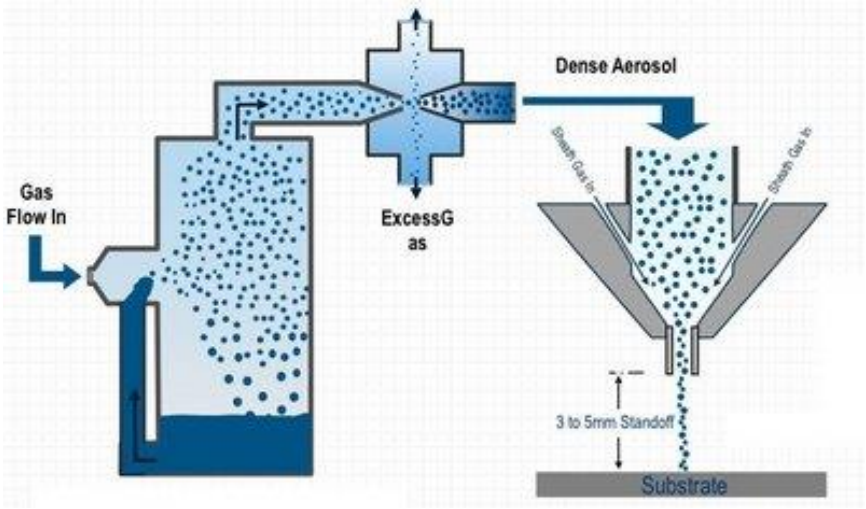

Figure 1.13: General Aerosol Jet Process

The material stream is then aerodynamically focused using a flow guidance deposition head, which creates an annular flow of sheath gas to collimate the aerosol, (figure above). The co-axial flow exits the flow guidance head through a nozzle directed at the substrate, which serves to focus the material stream to as small as a tenth of the size of the nozzle orifice (typically 100μm). Patterning is accomplished by attaching the substrate to a computer-controlled platen with motion in the x-y plane. The relatively large standoff distance from the deposition head to the substrate allows accurate deposition on even non-planar substrates, over existing structures and into channels.

Once deposited, the materials may undergo a thermal or chemical post-treatment to attain final electrical and mechanical properties and adhesion to the substrate. As part of this portion, the system uses a 2 Watt- 830 nm CW diode laser that can be focused to approximately 20 μm. This allows a low temperature, small Heat Affected Zone (HAZ) surrounding the target area. The end result is a high-quality thin film (as fine as 10nm) with excellent edge definition and near-bulk properties.

The AJP system works with a variety of inks and has partnered with many companies to further develop additional materials for their system. A wide range of materials has been successfully deposited, including diluted thick film pastes, thermosetting polymers, UV-curable epoxies, and solvent-based polymers like polyurethane and polyimide. A combination of chemistry and post-

treatment allows functional electronic structures to be fabricated directly on low temperature substrates. Conductor inks including Ag, Pt, Pd, and Cu have been developed with cure temperatures down to 150 C°, and higher temperature ceramics, ruthenates, and ferrites can be cured using the laser energy source. Semiconductor, resistor, dielectric adhesives, and etch resist formulations also have been deposited for Aerosol Jet on a wide variety of substrates including polyester, polyimide, glass, C-Si, ceramic, FR4 and metal materials. Even biomaterials such as proteins and DNA have been deposited with Aerosol Jet without denaturing or loss of bio-activity.

The main drawbacks to the AJP system are that it is generally a 2D system that requires programming by the operator to perform calculations for the layering techniques described in the tessellation section above. While it is easy to enable it to produce simple 3D shapes like cylinders, cubes and pyramids, hollows and complex geometries that are non-planar present significant issues. More specifically any overhang or internal roof to a void is difficult to control with current inks available.

Complications can arise in the production of inks for particle size distributions outside of the range listed above. Fundamentally, there exists a lack of base knowledge associated to working at this size regime and with these systems and the development of inks. This thesis hopes to elaborate on the pitfalls and discuss best current practices and elucidate both engineering and science principles related to operations at this level in the following chapter and closing appendices.

1.3.6 Hybrid Systems

The educated reader can easily see the hybridization to processes that are additive and subtractive. Some of the above examples can be characterized in this manner and while they are still rapid prototyping technologies, the added steps required machining and/or removing materials increase process time and waste of material. This theme can be found in SL, LOM and IJ processes. Similarly many additive processes that employ support materials that are then removed post construction as in FDM and SLA can be thought of in this regard. One final note on a process that was developed specifically with this in mind is Stratoconception. In this system, the original CAD file is converted into small machinable parts of the construct and then assembled with adhesives. It can work quite well with complex or large parts that may exceed

the working space of the machine, or when a 2.5D CNC machine would have difficulty with the entire part. It has been applied to wood, metal, polymer and foam shapes. Intricate bonding surfaces can be created to increase surface area and bonding strength for structural components. [58] In addition, these structural parts can be bonded from dissimilar materials making use of high-strength and low density materials in the same part, other key examples are companies like SRP from Poland, Shaped Deposition Modeling from Stanford-Carnegie-Mellon [61].

1.3.7 Techniques Not Discussed

Soft Contact Printing: These techniques are very similar to the original printing presses where an ink is spread over the lettered block or relief and a sheet of paper or other substrate is pressed creating the originals mirror image. These techniques were a stepping stone to new technologies and have some very large limitations in the materials that are applicable, substrates, inks, solvents etc. Broad examples include roll to roll (R2R) printing, flexography, Soft lithography and gravure printing [13, 62, 63].

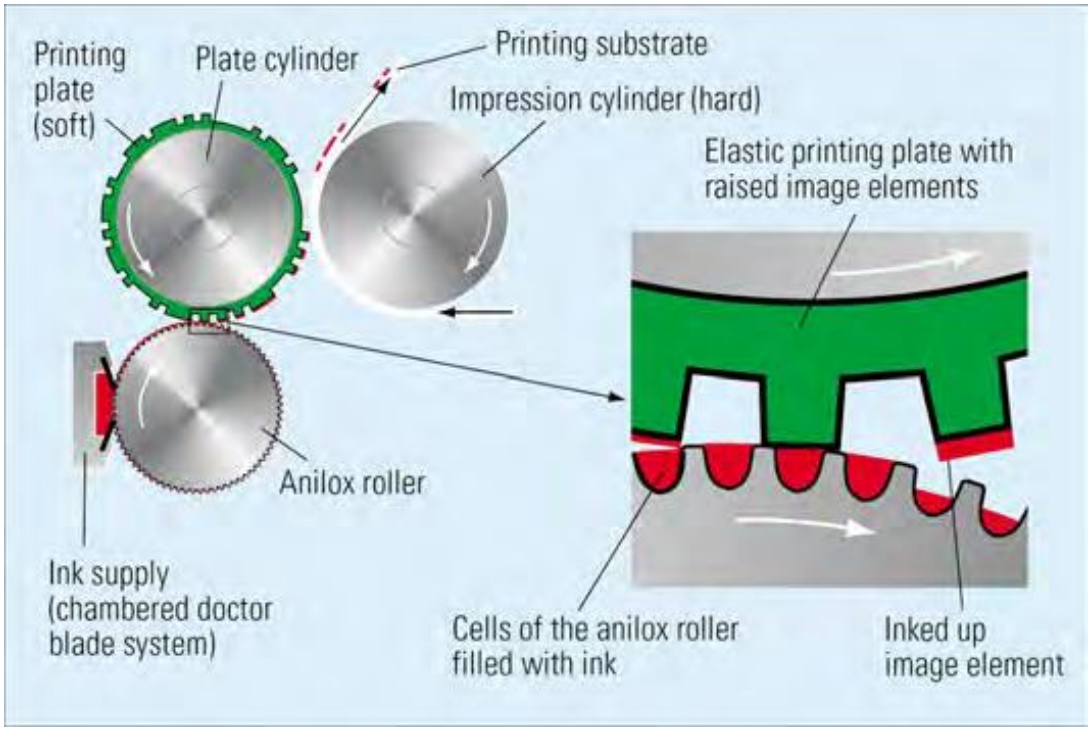

Figure 1.14: Soft Lithography

Up and Coming Technologies

This section is dedicated to technologies that have yet to materialize and develop into the 3D realm but show significant progress. The reason for non-inclusion is really the lack of controllable deposition either in direction or sustainable process. Selected examples of this technology are Pressure Assisted Micro-Syringes or PAM and Electrospinning. In PAM, a liquid, usually a polymer is transferred to a syringe which is held in a translation stage. This stage can be rastered across the x-y plane to direct the liquid from the syringe needle. Compressed air aids the evacuation of the syringe. Some highlights from the PAM system are shown below as utilized for intricate scaffolds for tissues. While this system is not a 3D printing system, it can be used to place 2D layers directly on top of the preceding layer and build a framework or woven texture for help in tissue regeneration.

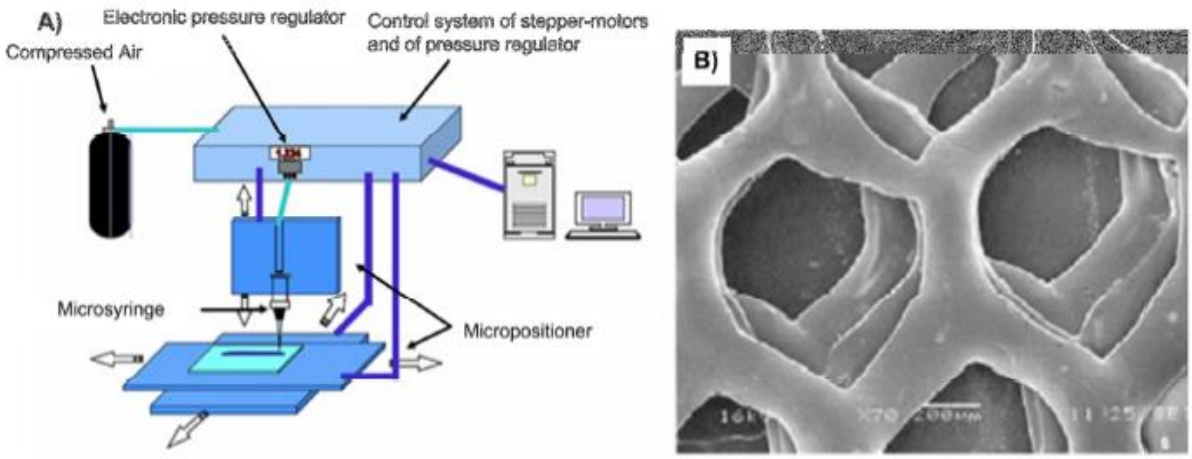

Figure 1.15: MicroSyringe process and example of work

Electrospinning uses a high potential electrical field to extend the liquid into a Taylor Cone, eventually fibers can be created and are ejected from the cone due to driving force changes. The fiber that is ejected from the cone continues to move towards the substrate and any solvent that may initially be brought from the cone is evaporated prior to deposition. Although the exact placement of the deposition cannot be confined for exact placements, it is not a far jump to recognize the same charged plates from IJP may be someday employed here for focusing technology. Currently this technique can be used for fabricating polymers and it is hoped with further research that it will be able to make complete fabrics. One significant advantage it offers over the above techniques can be seen in an example of the polymer PVDF.

Currently, PVDF is the only piezoelectric polymer that can be used within the body. However in order to generate the piezoelectric affect the polymer must be processed in a very specific way of stretching and poling it. Electrospinning offers the only known method of completing both these steps in one process. Other methods employ not only poling and stretching but also intermediate electroding and cleaning steps to accomplish this.

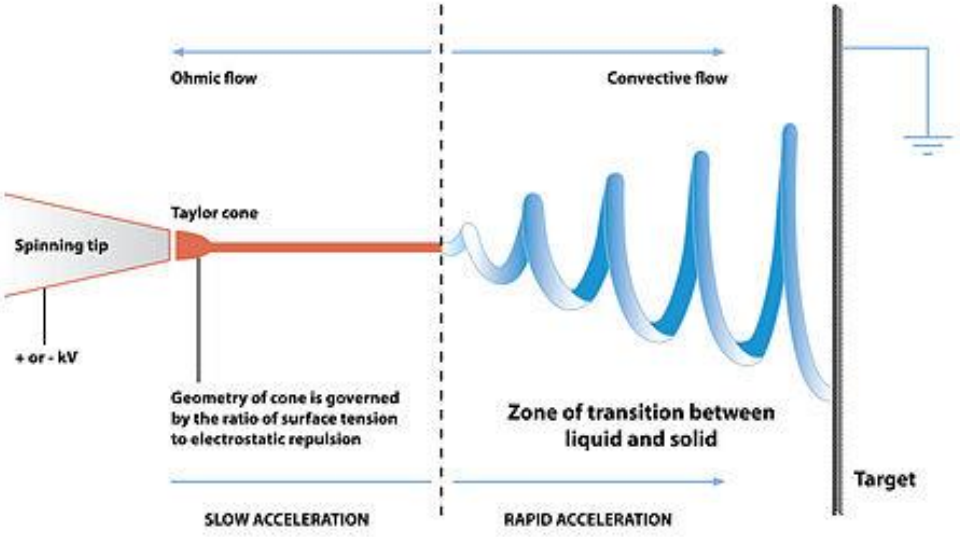

Figure 1.16: Electrospining

1.4 Conclusions:

3D Printing refers to a set of technologies used to fabricate a wide range of physical and electronic devices employing many materials and methods. In the previous decades, printing technologies, e.g. flexography, soft lithography, screen, gravure and inkjet printing, gained the attention of electronic and manufacturing industries thanks to their low-cost, scale up to high volume and high-throughput production of electronic components or devices. The methods listed above show the ubiquity of 3D printing, from polymers and ceramics to metallic based inks and ceramic inclusions direct prints.

Organic materials are easily processed in the liquid phase and their inclusion to printing processes illustrates the potential realization of batteries, shielding, capacitors and inductors. Other abilities have shown capabilities in Organic Diodes, LEDs, Photovoltaic cells and displays.

As the resolution, speed and materials that can be employed by 3D systems continues to encroach on CNC system, so too will the applicability of 3D systems rival and replace these processes. Many of the necessary electronic components and processes are already in use within industry and while not at the current level of electronic lithography, (high density and switching capabilities) and able to be used as a replacement, they will continue to make strides in this direction. It should be noted that not all processes for electronics have the need for the level of intricacy and concentration of features. And the elimination of traditional high-costs associated with Printed Circuit Boards (PCBs) can be realized through this technology especially those for rapid prototyping.

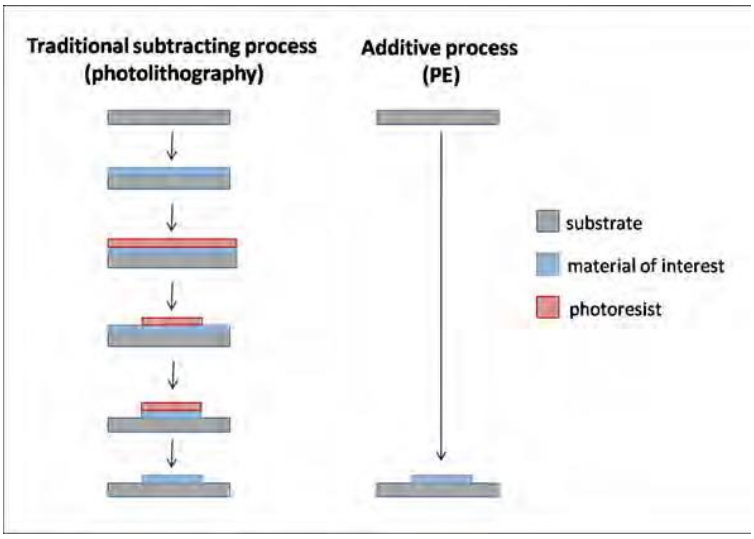

Figure 1.17: Standard vs Additive Lithography Steps

Compared to traditional lithography techniques, 3D manufacturing allows the elimination of several wastes from the traditional processes and is illustrated in the figure above.

Realizations from the real world have begun to creep in, solar voltaic cells have been reduced from $80/W to $3/W or even less with the newer Optomec technologies [64]. High throughput technologies for OLED on transparent and flexible substrates is some of the most attractive technology to arise from contact printing technologies [65] "Negative" printing for dielectrophoresis, bio-sensors or detectors and microfluidics, wherein the inverse pattern is printed for small wells, vias and channels is starting to be explored. 3D technology has been exploited for innerconnects and additive maskless printing at resolutions down to 10 μm currently the limit for the technology. So while the technology cannot replace current PCB

technology, it has allowed the realization of a “lab on a chip” and paper-chip healthcare diagnosis (G.M. Whitesides et al.). [62, 63, 66-68]

Recently other companies outside of the academic setting have also shown interest in adhesive/non-adhesive backgrounds and it is not secret that inkjet technology has been used for encapsulation and delivery of drugs, and implants (stents). [33, 69-71]3D printing and RP is yet to be at the level necessary for common use in manufacturing and daily lives, it is readily apparent the time is coming. New materials and inks are under development and the relentless progress of technologies continues to accelerate.

References Chapter 1

1. Eric Savitz, *Manufacturing The Future: 10 Trends To Come In 3D Printing.* Forbes, 2012(http://www.forbes.com/sites/ciocentral/2012/12/07/manufacturing-the-future-10-trends-to-come-in-3d-printing/).
2. Wadhwa, V., *The End of Chinese Manufacturing and Rebirth of U.S. Industry.* Forbes, 2012(http://www.forbes.com/sites/singularity/2012/07/23/the-end-of-chinese-manufacturing-and-rebirth-of-u-s-industry/).
3. Hopkinson, N., *Additive Manufacturing: What's happening and where are we going with printing in the third dimension?* Word Document available at http://www. Becta. org. uk, 2010.
4. Campbell, I., D. Bourell, and I. Gibson, *Additive manufacturing: rapid prototyping comes of age.* Rapid Prototyping Journal, 2012. **18**(4): p. 255-258.
5. Olson, P. *Airbus Explores Building Planes With Giant 3D Printers - Updated With Video*. Forbes 2012 [cited 2012 7-11-2012].; TECH:[
6. Levy, G.N., R. Schindel, and J.-P. Kruth, *Rapid manufacturing and rapid tooling with layer manufacturing (LM) technologies, state of the art and future perspectives.* CIRP Annals-Manufacturing Technology, 2003. **52**(2): p. 589-609.
7. Cable, J., *GM, Ford and Chrysler Get Big Chunk of Advanced-Vehicle Funding.* http://www.industryweek.com/global-economy/gm-ford-and-chrysler-get-big-chunk-advanced-vehicle-funding, 2011.
8. Anonymous, *All together now; Collaborative manufacturing*, in *The Economist*2012, The Economist Intelligence Unit: London. p. 18-19.
9. Maxey, K., *IBM Sees 3D Printing Changing Manufacturing.* http://www.engineering.com/3DPrinting/3DPrintingArticles/ArticleID/5478/IBM-Sees-3D-Printing-Changing-Manufacturing.aspx, 2013.
10. Wohlers, T., *Additive Printing Technology.* MoldMaking Technology, 2012.
11. Gibson, I., D.W. Rosen, and B. Stucker, *Additive manufacturing technologies: rapid prototyping to direct digital manufacturing*. 2010: Springerverlag Us.

12. Cooper, K.G., *Rapid prototyping technology: selection and application*. 2001: Marcel Dekker, Inc.

13. Kruth, J.-P., *Material incress manufacturing by rapid prototyping techniques.* CIRP Annals-Manufacturing Technology, 1991. **40**(2): p. 603-614.

14. Noorani, R., *Rapid prototyping*. 2006: Wiley.

15. Jamieson, R. and H. Hacker, *Direct slicing of CAD models for rapid prototyping.* Rapid Prototyping Journal, 1995. **1**(2): p. 4-12.

16. Roscoe, L., *Stereolithography interface specification.* America-3 D Systems Inc, 1988.

17. Specification, S.I., *The STl Format.* Valencia, CA: 3Dsystems Inc, 2000.

18. Halloran, J.W., et al., *Photopolymerization of powder suspensions for shaping ceramics.* Journal of the European Ceramic Society, 2011. **31**(14): p. 2613-2619.

19. Sachs, E., M. Cima, and J. Cornie, *Three-dimensional printing: rapid tooling and prototypes directly from a CAD model.* CIRP Annals-Manufacturing Technology, 1990. **39**(1): p. 201-204.

20. Kruth, J.-P., M. Leu, and T. Nakagawa, *Progress in additive manufacturing and rapid prototyping.* CIRP Annals-Manufacturing Technology, 1998. **47**(2): p. 525-540.

21. Chua, C.K., K.F. Leong, and C.C.S. Lim, *Rapid prototyping: principles and applications*. 2010: World Scientific Publishing Company.

22. Burns, M., *Automated fabrication: improving productivity in manufacturing*. 1993: Prentice-Hall, Inc.

23. Pham, D. and R. Gault, *A comparison of rapid prototyping technologies.* International Journal of Machine Tools and Manufacture, 1998. **38**(10-11): p. 1257-1287.

24. Wong, K.V. and A. Hernandez, *A Review of Additive Manufacturing.* ISRN Mechanical Engineering, 2012. **2012**.

25. Shivpuri, R., et al., *Evaluation of 3D printing for dies in low volume forging of 7075 aluminum helicopter parts.* Rapid Prototyping Journal, 2005. **11**(5): p. 272-277.

26. Systems, E.d.p. *e-Manufacturing Systems*. Available from: www.EOS.com.

27. Systems, d. *Stereolithography and selective laser sintering machines*. Available from: http://www.3dsystems.com.

28. Systems, d. *ZCorp Systems*. Available from: http://www.zcorp.com/en/home.aspx.

29. *Soligen*. Available from: http://www.soligen.com.

30. Sachs, E., *Three dimensional printing*, 2001, DTIC Document.

31. Pfister, A., et al., *Biofunctional rapid prototyping for tissue-engineering applications: 3D bioplotting versus 3D printing.* Journal of Polymer Science Part A: Polymer Chemistry, 2004. **42**(3): p. 624-638.

32. Lipke, D.W., et al., *Near net-shape/net-dimension ZrC/W-based composites with complex geometries via rapid prototyping and Displacive Compensation of Porosity.* Journal of the European Ceramic Society, 2010. **30**(11): p. 2265-2277.

33. Tang, H.-H., M.-L. Chiu, and H.-C. Yen, *Slurry-based selective laser sintering of polymer-coated ceramic powders to fabricate high strength alumina parts.* Journal of the European Ceramic Society, 2011. **31**(8): p. 1383-1388.

34. Salmoria, G.V., et al., *Microstructural and mechanical characterization of PA12/MWCNTs nanocomposite manufactured by selective laser sintering.* Polymer Testing, 2011. **30**(6): p. 611-615.

35. Kruth, J.-P., et al., *Binding mechanisms in selective laser sintering and selective laser melting.* Rapid Prototyping Journal, 2005. **11**(1): p. 26-36.

36. Taminger, K.M. and R.A. Hafley. *Electron beam freeform fabrication: a rapid metal deposition process*. in *Proceedings of the 3rd Annual Automotive Composites Conference*. 2003.

37. Liu, Z., et al. *Selective laser sintering of high-density alumina ceramic parts*. in *Proceedings of the 35th International MATADOR conference*. 2007. Springer.

38. arcam. *Electron beam welding*. 2012; Available from: www.arcam.com.

39. Exner, H., et al., *Laser micro sintering: A new method to generate metal and ceramic parts of high resolution with sub-micrometer powder.* Virtual and physical prototyping, 2008. **3**(1): p. 3-11.

40. Murr, L.E., et al., *Metal fabrication by additive manufacturing using laser and electron beam melting technologies.* Journal of Materials Science & Technology, 2012. **28**(1): p. 1-14.

41. Kummailil, J., *Process Models for Laser Engineered Net Shaping*, 2004, WORCESTER POLYTECHNIC INSTITUTE.

42. Balla, V.K., S. Bose, and A. Bandyopadhyay, *Processing of bulk alumina ceramics using laser engineered net shaping.* International Journal of Applied Ceramic Technology, 2008. **5**(3): p. 234-242.

43. Liao, Y., H. Li, and Y. Chiu, *Study of laminated object manufacturing with separately applied heating and pressing.* The International Journal of Advanced Manufacturing Technology, 2006. **27**(7-8): p. 703-707.

44. *LENS System*. 2012; Available from: www.optomec.com.

45. Atwood, C., et al., *Laser engineered net shaping (LENS (TM)): A tool for direct fabrication of metal parts*, 1998, Sandia National Laboratories, Albuquerque, NM, and Livermore, CA.

46. Corp, K.; Available from: www.kiracorp.co.jp/EG/pro/rp/top.html

47. dimensions, S. *Solido Machine*. Available from: www.solidimension.com

48. Vaupotič, B., M. Brezočnik, and J. Balič, *Use of PolyJet technology in manufacture of new product.* Journal of Achievements in Materials and Manufacturing Engineering, 2006. **18**(1-2).

49. *Fab@home*. Available from: www.fabathome.org.

50. Reprap.

51. Facchini, L., et al., *Microstructure and mechanical properties of Ti-6Al-4V produced by electron beam melting of pre-alloyed powders.* Rapid Prototyping Journal, 2009. **15**(3): p. 171-178.

52. Grimm, T., *User's guide to rapid prototyping*. 2004: Sme.

53. Kim, H., J.-W. Choi, and R. Wicker, *Scheduling and process planning for multiple material stereolithography.* Rapid Prototyping Journal, 2010. **16**(4): p. 232-240.

54. Szilvśi-Nagy, M. and G. Matyasi, *Analysis of STL files.* Mathematical and Computer Modelling, 2003. **38**(7): p. 945-960.

55. Wohlers, T., *Wohlers Report*, 2009, Fort Collins, Colorado, USA: Self. www. wohlersassociates. com.

56. *<Capillary-Assembled Microchip for Universal.pdf>*.

57. Singh, R., *Process capability study of polyjet printing for plastic components.* Journal of mechanical science and technology, 2011. **25**(4): p. 1011-1015.

58. Petrovic, V., et al., *Additive layered manufacturing: sectors of industrial application shown through case studies.* International Journal of Production Research, 2011. **49**(4): p. 1061-1079.

59. Prinz, F.B. and L.E. Weiss, *Novel applications and implementations of shape deposition manufacturing.* Naval research reviews, 1998. **50**: p. 19-26.

60. Martinez, A.W., et al., *Programmable diagnostic devices made from paper and tape.* Lab Chip, 2010. **10**(19): p. 2499-504.

61. Whitesides, G.M., *The origins and the future of microfluidics.* Nature, 2006. **442**(7101): p. 368-73.

62. Glunz, S., *High-efficiency crystalline silicon solar cells.* Advances in OptoElectronics, 2007. **2007**.

63. Jain, K., et al., *Flexible electronics and displays: High-resolution, roll-to-roll, projection lithography and photoablation processing technologies for high-throughput production.* Proceedings of the IEEE, 2005. **93**(8): p. 1500-1510.

64. Lankelma, J., et al., *Paper-based analytical device for electrochemical flow-injection analysis of glucose in urine.* Anal Chem, 2012. **84**(9): p. 4147-52.

65. Martinez, A.W., et al., *Patterned paper as a platform for inexpensive, low-volume, portable bioassays.* Angew Chem Int Ed Engl, 2007. **46**(8): p. 1318-20.

66. Martinez, A.W., S.T. Phillips, and G.M. Whitesides, *Three-dimensional microfluidic devices fabricated in layered paper and tape.* Proc Natl Acad Sci U S A, 2008. **105**(50): p. 19606-11.

67. Sachs, E., M. Cima, and J. Cornie, *Three-Dimensional Printing: Rapid Tooling and Prototypes Directly from a CAD Model.* CIRP Annals - Manufacturing Technology, 1990. **39**(1): p. 201-204.

68. Xiong, Z., et al., *Fabrication of porous scaffolds for bone tissue engineering via low-temperature deposition.* Scripta Materialia, 2002. **46**(11): p. 771-776.

69. Mironov, V., G. Prestwich, and G. Forgacs, *Bioprinting living structures.* J. Mater. Chem., 2007. **17**(20): p. 2054-2060.

Chapter 2 Optomec AJP System and Process Variables

As briefly introduced in Chapter 1, the Aerosol Jet Processor (AJP) from Optomec presents capabilities which hope to overcome some issues with current methods for production. This chapter further addresses the operation controls, processing, and fabrication of thin films on multiple substrates via the Optomec Aerosol Jet Printing system (AJP or AJP). In addition, it discusses various processing parameters related to ink development, as well as green film development and selective laser sintering (SLS).

2.1 Introduction to Aerosol Deposition Machine Controls

The AJP deposition system from Aerosol Jet Optomec is equipped with an ultrasonic atomizer, a print-head, a 1000 mW-830 nm CW diode laser sintering tool, and a Process Control Module (PCM). Optimization of the AJP system requires adjustment for several processing variables related to the deposition and laser sintering.

2.1.1 Process Description

The AJP can be used to fabricate intricate structures with feature sizes down to 10 μm and particles as large as 1 μm by depositing inks, pastes etc. on multiple substrates. It is a non-contact process which uses a nozzle orifice at a general height of 1-6 mm above the substrate. To enable the deposition of ink, the liquid is atomized into droplets of 1-5 μm in diameter in either the Ultrasonic Atomizer (UA) or Pneumatic Atomizer (PA). Once a significantly dense mist has been formed, the droplets are entrained within a gas stream and directed to the print head through a transfer tube where an annular flow of gas (N_2) collects, condenses and directs the droplets to the substrate at a high velocity.

The ink must be a combination of liquid precursors, and may contain other additions such as solvents and solid particulates. Once deposited, the material may be post-processed if necessary via Selective Laser Sintering (SLS) and/or the heated platen for evaporation of solvents, crystallization, and adherence to the substrate. The AJP system has been successfully utilized for deposition of metals, ceramics and polymers [72-75]. In addition the AJP system has been used for Direct Write Biologics (DWB) for cells, enzymes, proteins, nucleic acids and others [74].

2.2 General Description of the Aerosol Jet Process

2.2.1 Ultrasonic Atomization

The ultrasonic atomizer (UA) (Figure 2.1) uses an ultrasonic transducer to develop high-frequency pressure waves, which are transmitted to the ink through coupling fluid and the containing vial, atomizing the ink into 1-5 μm diameter droplets. Once a significantly dense mist is produced, it can be siphoned off and directed to the print-head for subsequent deposition using a dry N_2 gas.

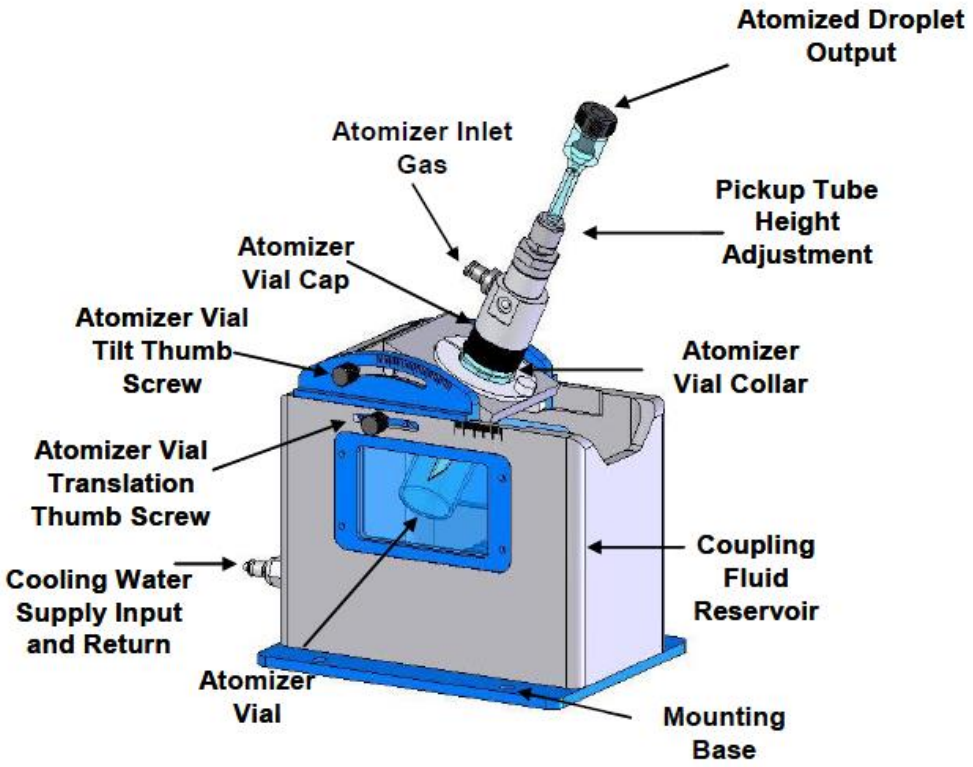

Figure 2.1: The schematic of the ultrasonic atomizer

The UA was found to work optimally for solutions having viscosity ≤7 cP [74, 75]. However, for inks having high viscosity (e.g. pastes, colloidal suspensions, particulates and long chain solvents), the Pneumatic Atomizer (PA) atomizer provided better results. This difference may be due to a limiting factor of solid to liquid within droplet formation that may be ejected from the ink and energy generated within the UA vial. This process comprises of complex interaction among the vapor pressure, surface tension and viscosity [74] as discussed below. For higher density solids, the particulate size should be kept below 50 nm. However, the experimental

results, presented in chapter 3, suggested that the cut-off limit for low-density is approximately 200 nm.

2.2.2 Pneumatic Atomization/Virtual Impactor

The pneumatic atomizer (Figure 2.2) employs a high-velocity gas stream, which shears the liquid stream into droplets. In this process, the compressed gas is expanded through the atomizer nozzle producing a high-velocity jet and drawing the ink from the reservoir to the atomizer nozzle. Here, the liquid stream is expanded into droplets and suspended within the flow. The high-velocity gas stream, including suspended droplets, exits the nozzle and impinges on the sidewalls of the atomizer reservoir. The larger droplets drain back after impact; smaller particles remain suspended in the gas and travel downstream to the virtual impactor where excess gas is removed from the process stream, allowing viable material to continue downstream. [74, 75]

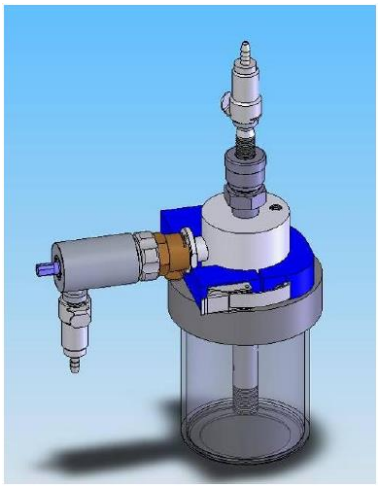

Figure 2.2: Schematic of the pneumatic atomizer

As discussed in previous paragraph, the pneumatic atomizer may be used for inks, pastes, or other materials having higher viscosity (up to 1000 cP), higher vapor pressures (>0.1mm Hg), higher density materials, or particulates in the range of 200+ nm [74]. Particulate suspensions are atomized more readily because of higher power and the shear forces exerted on the ink [76-80]. Generally, suspended particles should be on the order of ≤ 0.5 μm for high quality product [74, 75]. During the investigation with Sodium Bismuth Titananate (NBT-BT) it was found that particles up to 1 μm in size were deposited, however significant fouling of the deposition jet

occurred and was a common occurrence. Use of solvents with a low to medium vapor pressure is desirable as the solvents with high vapor pressure (e.g. alcohols) may exhibit excessive drying leading to a powdery or porous deposition.

2.2.3 Print Head

The print head (Figure 2.3) is capable of printing lines with low standard deviation and good resolution to 10 μm onto nearly any substrate with varying topography. The aerosol stream is directed down the transfer tube and focused within the head via a gas stream, which confines, focuses, and accelerates the droplets to the substrate directly below the ceramic nozzle. The nozzle aperture is pre-set by the user before processing (100 to 300 μm in 50 μm increments). The size of the tip is selected based on the type of the ink being used. The height of the tip is kept between 1-6 mm from the substrate. During the printing process, depending upon the programming, the print head is raster scanned over the surface (x-y). A shutter is used to deflect the stream of droplets and eliminate overspray or unwanted material. The height of the nozzle is generally left at a preset height, but it can be programmed (by modifying code of the STL file) to adjust at varying points along the trajectory and may be included as a factor for tuning especially in the case of overspray.

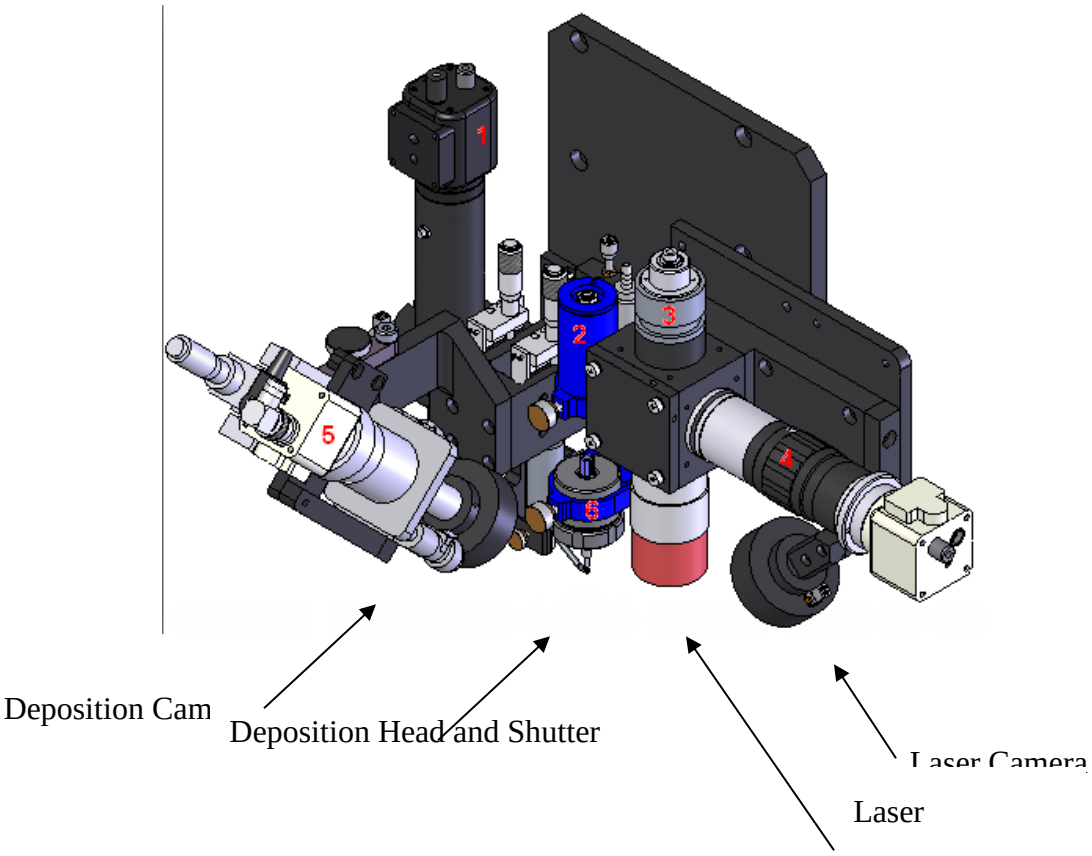

Figure 2.3: Schematic of the print head

2.2.4 Monitoring System

The user may monitor the printing process via either of the two cameras (Figure 2.3): deposition camera and sintering camera. These cameras can also be used for:

- Manual alignment of the tool-path to specific features on a substrate
- Imaging for semi-automated alignment of the tool-path to the substrate
- Setting offset values for system calibration

2.2.5 Constant Wavelength (CW) 830 nm Laser

The AJP is also equipped with an 830 nm laser (labeled as 3 in Figure 2.3), which is used to post-process (annealing and sintering) of printed material. Prior to sintering step, in order to burn organics, the substrate temperature can be raised to illuminate deleterious effects of evaporated

organics like porosity. The laser sintering enables us to obtain rapid heating and cooling of the material. This method can be used to select required phase of the material and to eliminate possible damage to the low temperature substrates.

2.2.6 Process Control Module

The process control module (PCM) houses controls and support electronics for the AJP system. The PCM contains a programmable logic controller (PLC), electronic connection points, mass flow controllers (MFC), pressure transducers, connecting gas lines, process-shutter control board, and an optional ultrasonic atomizer power supply.

2.3 New Material Development Process

Along with the use of a commercial ink with a known deposition recipe, development of a new ink or alteration of a current one for use with the AJP machine requires three separate Design of Experiment (DOE) blocks completed in order for optimization (see appendix for experiment design and chapter 3 for discussion).

1. Optimization of solution and dispersant and component parameters
2. Optimization of deposition parameters
3. Optimization of laser sintering parameters

2.3.1 Introduction to Process Variables

Consideration and investigation of the following parameters are paramount as they are related to the quality of the final product. Suggested characterization methods for investigating specific variable are listed in table 2.1.

Table 2.1: Response Variables for Decision Matrix

Response Variables:	
I. Presence and purity of material phase (i.e. amorphous, crystalline orientation) [XRD, XPS].	V. Thickness of film, growth rate calculation [SEM].
II. Remainder of binders/plasticizers [XRD, EDS].	VI. Delineation of lines, (Standard Deviation from mean edge) [SEM].
III. Apparent porosity or density of film [SEM, AFM].	VII. Continuous Film, [SEM]. (Laser blow-outs / vaporization of material)
IV. Location, diameter and percent-fill by voids [SEM].	VIII. Adherence to substrate [AFM, tape test].
	IX. Additional material properties

To get a high quality uniform and dense film, a high quality green film (without post processing) is required. Table 2.2 below describes 12 important factors for the development of aerosol mist and its transmission to the substrate during aerosol deposition process. All factors listed can be controlled by the user via the user interface (GUI) or are set during the translation (STL file creation) between Auto CAD drawing and the process motion file. Alternatively, these can be set via programming logic at the line level after the translation file has been commuted.

Table 2.2: Deposition Parameters

Deposition Parameters with ranges:			
Factor	**Range**	**Factor**	**Range**
1. Atomizer power	1-50 V	7. Number of passes	5 to 15
2. Sheath	1-100 cfm	8. Overlap percentage	10-30%
3. Atomizer	1-100 cfm	9. Fill Method (serpentine or raster)*	
4. Platen Temperature	1-200 ^{o}C	10. Trace width	0.02-0.1
5. In-Line Temperature	1-100 ^{o}C	11. Z-axis height	1-6 mm
6. Deck Speed	0.01-5 mm/s	12. Nozzle size	100-300 μm

*Serpentine method traces the outline of the part from the outside towards the center. The raster method begins on a selected side of the part, placing the next layer directly parallel to the first. In this manner the raster method usually progresses in an x or y direction although it can be rotated to follow an angled part.

Atomizer Power:

Inside the ultrasonic atomizer system, the vial is placed in contact with the liquid container. The tilt (angle) and the offset (translation) are manually set by the user to achieve higher mist rate. This rate is a direct result of proper ultrasonic energy transmission and fluid coupling. In practice, watching the 1-2 cm liquid spurt within the vial and maximizing this efficiency prior to final atomizer power selection, is the most rapid method of adjustment. The highest efficiency is reached when the terminal end of the liquid stream produces as small as possible droplets. The atomizer power affects the vaporization and misting concentration in the ambient gas of the vial. Generally this power is set between 35 to 50 Volts for solutions in the 1-5 cP range.

Sheath and Atomizer: These flow parameters work in tandem to build the green film and have a high level of interaction. The atomizer selects the amount of reagent from the vial, the sheath gas acts to coalesce and confine the stream of reagents, and propel them to the substrate. The difference between the two is known as the “misting rate”, which controls the deposition rate or mass transfer rate to the substrate.

In general the optimum range was found to be 10-30 cfm difference. Smaller (200-500 nm) and lighter particulates with spherical shape will tend toward the upper end of the range, however, heavier particulates or higher solid loadings find optimization in the lower end of the spectrum. The material having mixture of substances of varying densities or volumetrically dissimilar distributions (e.g. mixed multi-materials) perform better at the lower end of the range. During the aerosol deposition process, the clogging of tip could be alleviated by lowering the difference.

Platen Temperature: The process of developing a particulate solution and depositing it on a substrate can be thought of as a small solid sphere encapsulated by a surrounding liquid traveling through the transfer tube with accompanying gas and interacting with the atmosphere after exiting the nozzle. The interaction time with the dry N_2 gas within the transfer tube is the longer of the two, and is the responsible factor for removal/evaporation of the solvent. The issue of rapid evaporation could be solved by adding a co-solvent to the dry N_2 using a bubbler (discussed in the appendix). The trajectory of the droplets terminates at impact with the substrate. Depending on the liquid-gas, liquid-solid surface tensions, system exhibits a hydrophobic or hydrophilic nature. In either case, it is preferred to have the liquid: solid ratio as small as possible allowing the solvent to flash-off prior to the next droplet impact for dense green film. The temperature of the substrate in AJP system can be raised to 200 ^{o}C, and can be used for organic solvent removal, low temperature material sintering, and relief of thermal shock during laser sintering.

In Line Temperature Control: As in the above case, this system can be helpful in removing excess liquid from the aerosol mist and can aid with higher viscosity liquids. In present work, this parameter was not used as the inks were synthesized using solvents of lower vapor pressure and viscosity.

Number of Depositions: Once the processing conditions and parameters are optimized, proper control exists over the green film formation and density. Now, the AJP can be programmed for additional depositions/coatings over selected areas, developing a thicker film. Initial green films with optimized depositions and low variations in high stacking densities can be attained at approximately 3x the initial particulate diameter [81]. This initial thickness is optimum for SLS, see discussion below.

Overlap Percentage: As the nozzle in AJP system rasters over the substrate, the overlap percentage controls how much of the first deposition is covered in the subsequent depositions/coatings. Optimization for this parameter is also a direct result of interaction between ink-substrate (hydrophobic/hydrophilic interaction), control over the Marangoni effect and low variations in process [76, 82]. Most disparities between seemingly incompatible substrate-ink may be overcome with the addition of Ethylene Glycol or alcohols for altering the interaction of the two components and the wetting ability of the ink.

Fill Method: The AJ system can fill an angular object by two methods, a standard raster pattern from top to bottom or left to right, or a serpentine method that traces the outline of the object from the perimeter to the center. Both of these methods were tested. In addition, the raster pattern may be rotated from the initial deposition. This angle adjustment is in 1 degree offsets. In the case of circular objects, capability of depositing a spiral pattern could be utilized.

Trace Width: The attempted width of a line of green material deposited on the substrate is generally set in the range of 10-100um. In order to have a proper setting for trace width, it is important to understand the interaction between the ink and substrate to obtain the proper profile of the green film. A "line" or "dot" in the case of a high-resolution, generally requires low trace width, and high solids content as well as lower wetting factor. A "film" generally consists of lower solids contained within the ink and has a high-wetting factor. The wetting parameter is generally a function of the major solvent-substrate interaction. If the trace width is set too far apart, the resolution will not be attainable, allowing skips or spaces between rasters to be visible.

Nozzle Height: The height of the nozzle above the substrate (z) is adjustable. For most of the experiments, the height was set in the range of 1.0-6.0 mm. During printing of lines with high precision, the height of the nozzle is set in the range of 2-3 mm. The rule of thumb generally seems to be, the smaller the tip aperture, the lower the stand-off. This height can be optimized initially by moving the z-height to 1 mm increments and manually fluttering the shutter open/closed for a given time. Inspection of the green-film pattern under a low powered microscope allows visual confirmation of low overspray and proper focus.

Deck Speed: The platen motion velocity can be programed between 0.01 mm/s to more than 15 mm/s. This allows optimization of the deposition thickness and laser sintering parameters. Most

of the processes used a single optimized speed for deposition; however access through the STL file allows further control over sections of the program for varied treatments.

Jet Aperture: The size of aperture ranges from 100-300 μm with the increments of 50 μm with different two lengths. The selection of the proper jet has a great effect on the back-pressure, clogging, development of moisture in application lines, and can eliminate any chance of deposition. It is important to maintain proper profile (data logging) jets to have control over processes, and select jet to match each ink because rheology can greatly affect the droplet size and interaction with the trajectory of the droplets as they exit the system.

2.4 Ink Development

The transition of the liquid ink contained in a vial to that of an atomized mist is a complex phenomenon that is not well understood [76-78, 80, 83, 84]. The classic description of fluid breakup is through flow instabilities; the assumption that wave formations occur slowly, and droplet sizes are highly influenced by the viscosity [76-78]. The complexity in the case of this discussion is further confounded by the existence of particulates in inks (solid loading percentage) which can change during the deposition, thereby affecting local density and frequency affects in the ultrasonic realm. In addition the reader should realize, the term "solid inclusions" suggests that this system cannot be treated as a Newtonian fluid. Discussions on this subject are beyond the scope of the paper, however additional information are included in the section below, more in depth information is can be found through the bibliography. A more complete review of non-Newtonian fluids, readers can be located in: Bubbles, Drops, and Particles in Non-Newtonian Fluids, Second Edition by Chhabra [77] or Liquid Atomization by Bayvel and Orzechowski[78].

In the 2008, Aliseda et al. investigated several fluids for mean droplet size and utilized many of the same solvents used in the research presented herein[76, 80]. In general, inks constructed for the Optomec machine include components in the chart listed below. This table has been further divided to delineate proper use of either the pneumatic or ultrasonic atomizer.

A recent paper on Solid Oxide Fuel Cells (SOFC's) inks shows that they were constructed with an excess of five constituents [85, 86]. This fact is surprising given that the most critical factor in atomization for the AJP system is the viscosity [74-76]. Additionally, the major solvent and solids loading profile most heavily influence both the ability and longevity of solvency for a

particular mixture and selection of UA or PA for aerosol generation. A more complete understanding of an ink with a low number of ingredients was of great interest. Experiments revealed better results for simple base-inks developed on atomizer style, solid class and initial loading profile. These base inks can be easily altered for use with a variety of substrates and solid classes.

2.4.1 Ink Categories

Inks used with the AJ fall into one of three categories

1. Those inks specifically designed for use with the AJP
2. Inks not specifically designed for use, but general parameters are acceptable for re-engineering the solution. Here the major factors involved are: initial viscosity, proper solvent or co-solvent selection, stability, solids loading, particle size (or filtering), vapor pressure.
3. Custom designed ink from the basic precursors. Additional factors include: shelf life, type of ink (colloid, polymer etc.). This category will be the focus of discussion.

Custom Designed Inks:

The first step in the process is selecting the atomizer. In the case of most ceramics and metals, or multi-materials the pneumatic atomizer is the optimum choice. In the case of aqueous, low boiling point alcohols, polymers, smaller (<200nm) or lower density particles the ultrasonic is the more appropriate choice. Inks are comprised of three main constituents: Major and Minor Solvents, Solids or Deposition Material, and Surfactants or viscosity adjusters. The table below shows selection criteria for atomizer type based on liquid properties, solids loading etc.

Table 2.3: Selection of Atomizer based on Ink Constituents

Atomizer Selection:					
Pneumatic				**Ultrasonic**	
Major Solvent Properties:				Major Solvent Properties:	
Low Vapor Pressure	0.1 mmHg			High Vapor Pressure	
High Boiling Point	>180			Low Boiling Point	
High Viscosity	>10 cP			Low Viscosity	<5-7 cP
Higher Particle Density				Lower particle density	
Larger size particulates	>500 nm			Lower particle size	< 200 nm
Solids Loading	Percentage (wt.)			Solids Loading	Percentage (wt.)
High Resolution	50-70%	cP 1-50		Coatings	3-5%
Coatings	20-50%	cP		high resolution	20-40%
Stability	can use stirring rod			Stability	2-4 hours
Examples:				Examples:	
High Solids Loading	>40%			Efficient Usage of materials for high cost inks	
Ceramics from ball milling				Alcohols (IPA) Organics (Acetone)	
Metals				Metal Nanoparticles	
Continuous stirring option				Lower viscosity than H2O	
Viscous Alcohols				Use Chiller to reduce solvent evaporation	

Major Solvents:

These are pure liquids and the main body of liquid used within the ink. Examples are H_2O, alcohols, organics such as Acetone, Xylene, and Turpineol etc. In some cases, such as the organics with higher evaporation rates, it is wise to use a different transfer tube. The typical polyethylene tube which is standard should be replaced with a PFTE tube to reduce condensation. PFTE is more hydrophobic and aids in reduction of premature failure via nozzle clogging due to condensation. Condensation will present as droplets, which get collected in the tube traveling into the jet nozzle and disrupts gas flow. Many issues with overspray can be resolved with proper solvent selection and nozzle height adjustments. Higher boiling point solvents greatly reduce extraneous solvent evaporation prior to substrate impingement.

Co-Solvents:

These include some from the above range, though typically below 15% of the total solvent content and are used to modify the surface tension for better atomization, or evaporation rate. Most often, the solvents used were an alcohol to reduce the surface tension enabling easier atomization. Conversely Ethylene Glycol was used to reduce the evaporation rate, while its use is described further in the green-film section below.

Polymers:

PAA was employed to enhance attachment to substrate and surrounding particles after flash off of the organic compounds. Other researchers have used PVA, PVB and other cross-linking carbomers in addition to these as well. [76, 86]

Known compatible solvents are listed below:

Table 2.4: Optomec Solvent Compatibility

Current Known Solvents and Additions:		
Pneumatic	Ultrasonic	Co-Solvents
Butyl Carbitol	Acetic Acid	Acetone/Cyclohexane
Butyl Ether	Acetonitride	Chloroform/Terpineol
Carbitol Acetate	Ammonium Hydroxide	Mixed Alcohols
Dimethyl Acenimide	Butyl Acetate	Water/Ethylene Glycol
NMP*	Dichlorobenzene	Xylenes/Terpineol*
Terpineol*	DMF*	Chlorobenzene/ Dichlorobenzene
Ethlyene Glycol*	Dodecane	
	Ethyl Acetate	
	Formic Acid	
	IPA*	
	Perfluro FC43	
	Teralin	
	Toluene*	
	Water*	
	Methanol*	

*Used in current study. Ethylene Glycol can be used in Ultrasonic as well, primarily as an evaporation modifier. IPA is not listed as a solvent, but is compatible and is used in these experiments as a viscosity and evaporative modifier.

In either choice of atomizer, the AJ system will only develop droplets within 1-5 μm, and as such generally limits particulate size to less than 2um. There is a high correlation between the solvent density and particles which are transmitted via that solvent, higher density solvent weight transmits higher particulate size and weights. Table 2.5 summarizes the results listed here. During the experiments listed in Chapter 3, only particulates up to 1 μm were observed in NBT-BT. However, in case of boron, particulates having sizes in the range of 200-500 nm, were observed. PVDF was solvent when ejected, however, Al-Si was not attempted due to time constraints. It was reported that this solution would have been within the limits already shown from the data above as the Al nanoparticles were 200nm and Si nanoparticles were between 4-9 nm [87].

Table 2.5: Ink and Atomizer Pairing

		Ultrasonic	Size Nm		Pneumatic	Size nm	Notes:
Material	Boron	Yes	200-500		N/A	N/A	PA was not attempted as UA provided adequate dispensation
	NBT-BT	Yes	NR		Yes	500+	UA was easily clogged, moved to PA.
	PVDF	in solution			in solution		Solution enabled both to be used
	Al-Si	N/A			N/A		Time constraints prevented attempts

It is important to keep in mind some recommendations for handling:

- All solvents are used with gas flow and can leak out of the chamber; as such they should be of low inhalation hazard.
- Shear thinning is preferential, Newtonian required for all generators
- Surfactants volumes of 3-5% are typical from manufacturers and in custom inks if necessary but should be kept as low as possible [75]
- Particle size cut off: 2 μm, droplet size is 1-5 μm. No particles found larger than 1μm were observed to be printed in the study conducted for this thesis.
- Sheath Gas is N_2 for both and is usually dry without a bubbler system which may aid the overlap in higher VP solvents used in the pneumatic generator.

(See Chapter 4 for more information.)

2.5 Green Film Deposition

Commonly used methods for manufacturing wet ceramics include tape casting, screen printing, spray and dip coating as well as spin techniques. These methods while simple are incompatible for some scale-up for production lines and can be limited by geometries they can create [80, 88]. Issues such as highly complex geometries, serial depositions for co-firing or layered techniques can be overcome by incorporation of the AJP system. Other positives already mentioned in this Chapter 1 are use of materials, elimination of wastes, and elimination of many of the masking layer techniques of standard lithography. Tables 2.6 and 2.7 list some of the differences in conventional sintering and laser sintering.

Table 2.6: Sintering Comparison between Furnace and Laser Sintering Process [89]

Factor	Standard Furnace Treatment	Laser Sintering
Size	mm^2	μm^2
Volume interaction	Piecewise	Selected area - μm^3
Process	Complete part	Serial, possible repeats
Compaction prior to Furnace Ramp	pellet press or Hydraulic	None suitable
Pre Heat Time	Hours	µ seconds
Sintering time	Hours (several ramps)	µ seconds
Cool Time	Hours	µ seconds
Environment	Gas feed	environment*
Consolidation Time	Hours	µ seconds
Inclusions	controlled burn off time	evaporation at rapid rate

In general the sintering driving forces are controlled by liquid-sintering mechanisms:

Table 2.7: Consolidation and Driving forces for Compaction [89]

Consolidation Driving Forces		
Surface diffusion	Non-densifying	Diffusion of atoms along the surface of a particle
Vapor transport	No-densifying	Evaporation of atoms which condense on a different surface
Lattice-Surface diffusion	Non-densifying	atoms from surface diffuse through lattice
Lattice-Grain Bound. Diff.		atom from grain boundary diffuses through lattice
Grain Boundary diffusion		atoms diffuse along grain boundary
Plastic deformation		dislocation motion causes flow of matter

Before continuing the discussion on green film deposition, it is important to include a small discussion about sintering for full comprehension. In pressureless sintering, the main driving force is the reduction in surface area per unit volume [90, 91]. During densification, the reduction in size or elimination of pores, requires constant capillary force and can be described by the Young-Laplace equation:[77]

$$p_c = \frac{2\gamma cos\theta}{r}$$

Where γ is the surface tension of the liquid and θ the wetting angle formed between the liquid and solid portions of the particles, and r the pore diameter size. Generally in SLS the work function of surface tension is severely limited in function due to the minuscule time available for action (on the order of 10^{-5}sec). This force can be increased by programming longer duration laser treatments. However, this force is limited by material properties and possible need of phase selection [92].

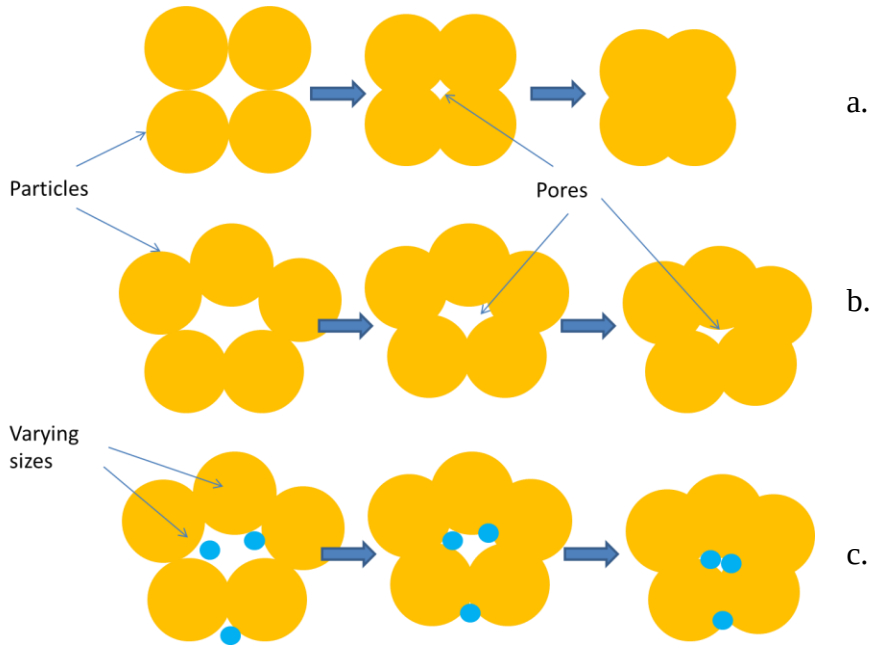

Figure 2.4: Compaction and Void Elimination during Sintering.

Illustrating (a) proper density of green film, (b) low initial density and incomplete porosity elimination, (c) variation of particle size and possible elimination of larger size pores.

Therefore, in sintering via SLS, the density of the thin film is highly dependent on the achievable and consistency of the packing density of the particles being consolidated. The theoretical densities for spheres of equal sizes would in close packed cubic or hexagonal range between 0.61 and 0.52 [93-95]. At a density of 1, the particles would exhibit the same density to those of bulk material. The missing portion accounts for the volume (air or other material) between solid particles. In dry powders, this is driven by interparticle friction. In the case of aerosol jet printing, the packing density is not controlled by the interparticle friction, but the competition of several forces:

1. **Varying size distributions:** As smaller particles may preferentially fill in voids or become lodged between larger particles, keeping them separate and reducing flow and pore sealing during sintering. Alternatively this may be a wanted affect as in the case of two dissimilar materials one that has a lower T_m than the counterpart that is used to fuse the alloy together.
2. **Binder Volume:** Excess non-evaporated solvent or polymers intended to adhere the substrate may act to keep particles apart from each. When the green film is heated and

the binder volume is too great or restricted by above layers, pock-marking or miniature eruptions may cause surface irregularities and poor sinterability. a

3. **Surface tension**: Remaining liquid carriers which have not evaporated previous to impact can act to combine and compact the slurry on the surface of the substrate. The time window created by this excess liquid allows sections numbered 4 and 5 to occur. To drive down the time available for surface rearrangement and variability introduced by this factor, elevated temperatures of the platen are commonly used for organics, high vapor pressure solvent elimination, as well as binder drying to promote adhesion.
4. **Surface Energies from Particulate Geometries:** Severe deviations from the assumed particle shape (sphere) will show via increasing irregularity with pore sizes, locations and other characteristics. The AFM images from the boron study clearly show peaks from the sintering process. These peaks were also observed in the pre-sinter state as evidenced by the long focal distance while being observed under the confocal microscope. These peaks have been attributed to preferential alignment while the solids are suspended in the liquid carrier. [84]

   In some cases with MEMS this effect may be desirable. The G.Whitesides et. al has excellent article regarding how surface energies may be harnessed for particle orientation [96]. While particles in this manuscript were all observed to be spherical in nature, this point is mentioned for illustrative purposes, should the particles have large heterogeneities in geometry.
5. **Marangoni Effect:** As excess liquid dries, the evaporation continues to exert a driving force on the placement of particles. As evaporation continues, an inter-droplet flow develops. This can give rise to "coffee-ring" profile as seen in the figure below. This is called the Marangoni Effect, which was experimentally alleviated with the addition of 10-15% vol/vol Ethylene Glycol to the ink and reduced the rate of evaporation.

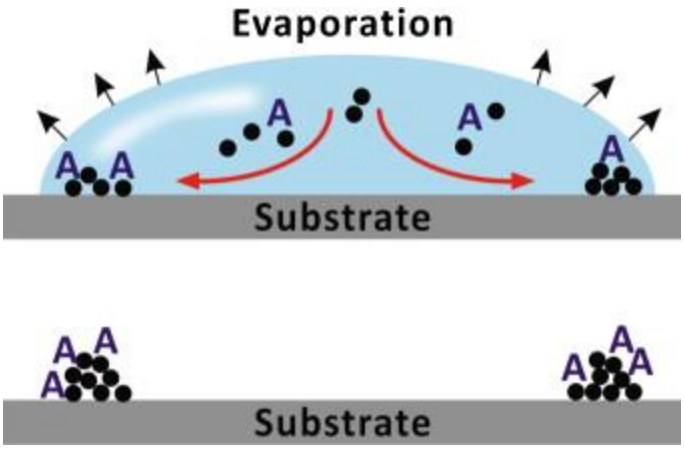

Figure 2.5: Marangoni Effect

6. **Multi-Material melt temperatures:** As in the case of NBT-BT, the lower melt temperature of bismuth causes unpredictable overheating areas. In this case, the material simply evaporates surrounding the grains and eliminates possibility of a successful sinter operation. Interestingly this phenomenon is more likely to occur in ceramics over metals and other compounds [81]. Additionally this applies to melt temperature between substrate and powder films as well as between initial sintered layer and subsequent layer sintering. If the interstitial layers are not properly heated, or are dimensionally dissimilar either in height or coefficient of thermal expansion (CTE), non-adherence or peeling can result.

2.6 Sintering

The past several decades have allowed the realization of optimized processes for thin-film and bulk sintering of materials. These processes generally share several commonalities, namely: pre-processing compaction, temperature ramping in ovens, gas flows or atmospheric controls, and selection of final composition oxidation layers, crystallographic orientations and superior control of grain sizes of final material characteristics. Other methods for thin film generation include: sputtering, CVD or PVD. These methods apply inert or reduced atmospheric pressures in specially designed chambers to produce printed electronics. Extensive studies in the effects of all factor has enabled comprehensive knowledge and enabled extremely precise control over oxide thicknesses, growth rates and multi-layer components, generally these processes produce an initially amorphous orientation which can be post process treated. These processes have become well understood through the last several decades of experimentation and in some cases

these are only available methods of specific material production [95]. As such, volumes of knowledge and vast arrays of experimentation become available on these systems. Currently, laser sintering does not afford this specialization or comprehensive knowledge base [81, 91].

Lasers have been around since the 1950's, serious efforts to use lasers for sintering have only been within the last 20 years, as such this portion of the science is still in its fledgling stages [37]. Thermodynamically, the influences of millisecond processing times, 10^5 or 10^{12} ^oC/sec heating rates create an inability to observe the process during reaction, limiting the understanding and data collection. The standard tube or electric furnace ramp and hold rate temperature curves exist on a time scale of minutes to hours, possess sample sizes on the order of millimeters as listed in Table 2.6. Conversely, a laser sintering process employs a sintering time on the order of nano-seconds for heating and cooling to ambient condition and interaction volumes are on the order of nm to μm. Additionally, direct energy systems are heavily influenced by porosity, plume effects and microstructure or crystal sizes. In many cases, the reason for non-industrial adoption is because of this knowledge gap. Simply put all factors affecting these systems are not understood or cataloged *[81]*.

2.6.1 Laser Sintering

The introduction of laser was heralded as, "a solution in pursuit of a problem", not initially the welcome befitting of one of Nature's top 25 inventions of 1900's [97]. Most of the original research dealing with lasers was directed towards standard practices of the time. Additive processes revolved around piece-wise additive manufacturing, surface treatments, welding parts. Subtractive ones involved: drilling, scribing, and machining. Concentrated efforts for lasers seemed to be focused in these areas until the late 70's [98]. Recently, it has been investigated for additive processes such as powder sintering [99-101]. Cannon et al. used the laser as a chemical vapor deposition heat source to prepare SiC or Si_3N_4 powders [102]. Realistically this function is more befitting of its stature. As a direct heating source, the laser has several advantages: it can (1) serve as a pure heat source, (2) generate high temperatures in extremely short periods of time, (3) provide local heating with controllable interaction areas, and (4) allow easy control of the sintering atmosphere (5) due to frequency interactions, it can selectively heat individual constituents of the matrix. [103]

2.6.2 AJP 830 nm Laser Factors

The following section is dedicated to the discussion of the 830 nm CW laser used in present AJP system. It will specifically deal with theory behind direct processing of powder materials though SLS, key process variables and considerations for material has selections, as well as introduce the controls background in developing a process with the AJP. Shown in Table 2.8 below are the key factors and for SLS through the AJP system. A brief discussion about various factors related to laser sintering is provided as follows:

Table 2.8: Laser Process Variables

Laser Factors:			
Laser Wattage	0.1-2.0 Watts	Raster Method (s/p)	Method
Deck speed	0.01-15 mm/s	Trace width	10-30 μm
Rotation of next pass	Degrees	Presence of Environmental Gas	Cu-ft/min
Percentage Overlap	0-100%	Number of passes	Number
Response Variables:			
Complete Sinter		Adherence	
Uniformity/Void Content		Proper Phase	

The Optomec AJP system allows a multitude of controls on the sintering process. Altering the factors of laser power (P), deck speed (v), number of depositions/passes (P), and raster spacing (RS) allow control over beam diameter (~20 μm), layer thickness (LT). The dwell time can be calculated by beam area/deck speed. For all experiments conducted for this thesis investigation, the laser programming was turned on at the beginning of the trace, and off at the completion of the process. The time to full power for the CW laser installed on the AJP is not a factor as programing allowed for the laser to come to full wattage before initiating movement. The overlap percentage (function of RS) or number of passes is set to allow multiple exposures of the laser. In order to get better material characteristics, equal care needs to be taken for increasing density and phase selection. From the materials point of view, laser sintering follows the below figure: [91]

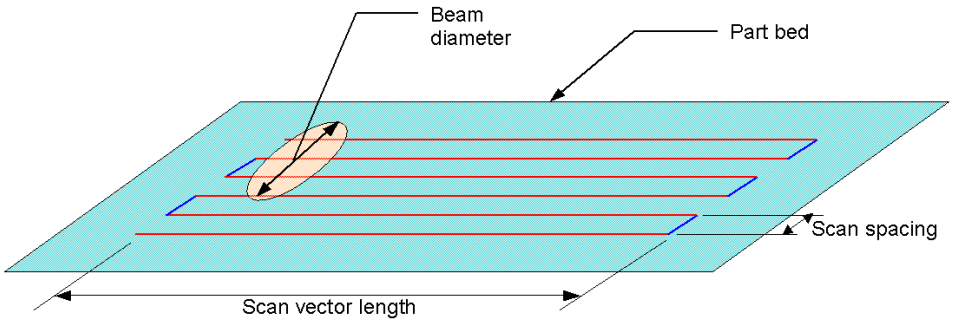

Figure 2.6: Laser Scanning Pattern [104]

In the same way the deposition head from the AJP traces the pattern created by the user, the laser traces the STL file generated from the same AutoCAD screen. During rendering, prior to commutation of the machine, the Graphical User Interface (GUI) allows the designer to visually inspect the trace pattern, direction and decide if alterations in segment order are needed. Once transplanted and uploaded to the computer, the manual settings are input and the sample is placed under the laser section of the deck. The process is self-sufficient once initiated and at completion turns off major sources of power or sub-systems which can damage operators. The laser heats up the area immediately surrounding the particle, this interaction between the beam and powder begins to consolidate the matrix. This consolidation is typically attributed to the liquid sintering (2). The density, achieved during the sintering process, depends on the initial density of the powder and the actual temperature reached. The temperature achieved during this processing is a function of the above parameters and the length of time the system remains under given conditions. This temperature model is discussed below. Multiple passes can be used for increased densification as well as phase selection and surface finish.

Laser sintering of Powder Beds

This section provides a brief description about the factors related to laser sintering. Plasma generation at point of laser impact is not considered, and is considered beyond scope for this work.

While laser usage in manufacturing has become widely accepted for a number of materials, a full understanding of various phenomena involved in this process are not understood. Overall, it is a complex process which involves physical characteristics: variability in shape, density and consistency of the green film, multi-material combinations, solid classes, binder additives and minute ratio changes of binder: solid in localized areas (Chryssolouris, 1991; Marley, 2002; Jin

and Li, 2003). This process also involves thermodynamic phenomena including: heat transfer, fluid flow, plasma effect, and lattice-phonon vibration (Bulgakova and Bulgakov, 2001).

The demand for circuit miniaturization, and small MEMS or Microfluidic components and their packaging (Cheng et al., 1998) have created the need for smaller holes and micro-vias, smaller lands, narrower lines and spaces, tighter registration, and smaller and more controllable spot-welds than before. This requires a more complete and accurate understating of the process. The variety of materials and their didactic properties induces high variability in process settings for proper sintering and it is imperative to understand these individually along with the effects and interactions with other factors. (Bruggemann, 1996).

Laser Interaction with Solid

When EM wave radiation (laser beam) strikes a surface (air/solid interface) it undergoes: reflection and transmission; the portion or percentage transmitted through the medium is adsorbed according to the Beer-Lambert law. [58]

$$I = Ie^{-\mu \cdot z}$$

Here, the absorption coefficient μ, depends on the medium and the optical properties of the material, wavelength of the radiation and the intensity I, temperature, and the plasma formation above the target, as well as changes to these as the target changes temperature. The laser energy is first adsorbed by the electrons of the solid, as the electric field is not large enough to vibrate the nucleus of the atoms. This absorption of photons is known as the "Inverse Bremsstrahlung Effect". Further loading through EM will result in more and larger vibrations of the electrons within the cloud. This vibration will re-radiate or propagate in all directions or be restrained and transmitted by the lattice phonon [98, 99, 101].

Lasers can be used to remove material (ablation) or defocused for surface functions such as: heat treatments, brazing, welding etc. To elicit this response in the material, several options are available to the user: de-focusing, raster rate, pulse rate (in the case of a non-constant wave laser). The effect of altering these factors available to the user is the same, reduction in Peak Power. This peak power is the intensity over the area over the specified time or the work function of the laser. As noted in the image below:

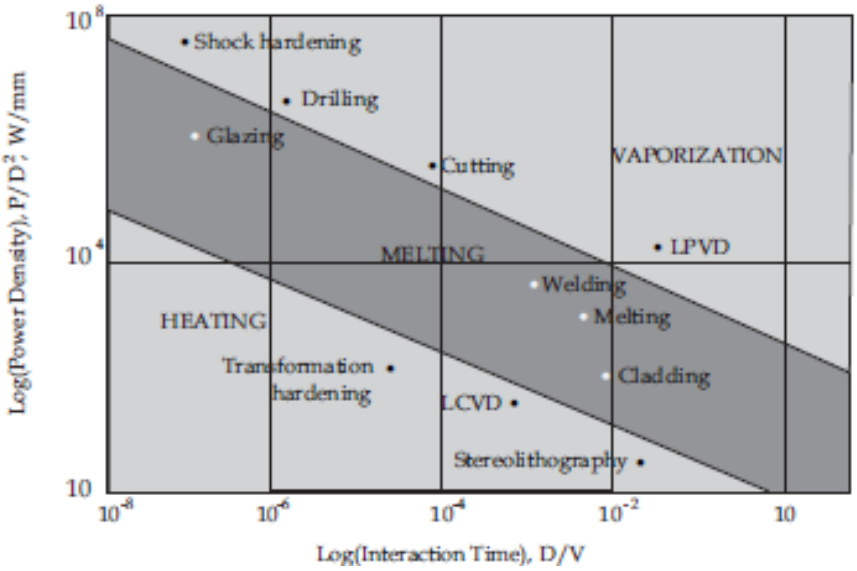

Figure 2.7: Laser Interaction with solid based on Peak Power/Area [104]

The peak power is the work function of the beam, and akin to the force impulse in physics: W=F*d. Stopping from a fast velocity (F=high) over a short distance can be the same as stopping over a longer distance (F=low). All would agree the differences to the occupants of the car would be quite different. In the case of lasers, quite complex and unexpected results can occur from high-impact or long lasing times including explosive evaporation and explosive ablation. In present case, we are interested in the change in temperature due to the impingement of the laser.

From the second law of thermodynamics: E=W+Q, The energy of a system is dependent upon the work done to or pulled from the system, and the heat added or removed. In a laser sintering process, no work is enacted upon the system and thus the only component to change the system is Q or heat added. The power added to the system happens over such a short range of time that the energy incident to the surface of the film can be reduced to the common heat transfer (heat diffusion) equation. [105]

Cojocaru, E., et al. described the fluctuations of ttemperature at the surface and regions through the following assumptions and following equations: (1) radiation from the laser is deposited to the surface (z=0). This simplification can be accepted given the proper deposition and known density of the green film layer (2-3x the diameter of the average particle). (2) The heat flows in the perpendicular direction (z) to the surface, because (3) of the difference in applied energy from the laser and heat transfer coefficient. This can easily be seen through several factors: (i)

the energy from the laser is moving horizontally limiting the constant influx of heat as it is directed only in the vertical (z) direction, (ii) the radial distribution (x-y plane) of the heat can be neglected due to the much lower transfer efficiency due to much higher porosity in this plane, (iii) the transfer of heat is also limited by local geometry and stacking density of the green film-it is the only contact area between particles which allows convective heat transfer. [98, 99, 101, 106]

The voids between particles can transfer heat at a rate much lower than that of the solid-solid or solid-liquid-solid interfaces of the particles. As such, the radial distribution of heat may be neglected. (4) The temperature dependencies of heat capacity, thermal conductivity and reflectivity are all assumed to originate at ambient temperature and end at the extrapolated level for the melt temperature of the particles. (5) Only first order terms of the equation are considered (6) Uniform density of the green layer [105].

J is the heat flow, ρ and c are the density and specific heat of the material respectively. A(r,t) is the heat source term (laser) can be understood through:

$$A(r,t) = I_m(1-R)(\pi Kc)^{-1/2}\int_0^{\tau} q(t-\tau)\tau^{-1/2}d\tau$$

Where I_m is the maximal laser intensity, R is the reflectivity, is the absorption coefficient and f(x,y) and q(t) are the normalized profiles of the laser pulse, (simplified Gaussian). From the above simplifications we assumed the f(x,y) is uniform in density. This leads to temperature increase following the equation below:

$$T(0,t) = I_m(1-R)(\pi Kc)^{-1/2}\int_0^{\tau} Q(t-\tau)\tau^{-1/2}d\tau$$

Where K is thermal conductivity of the solid. It should be noted that the laser power density is dependent upon the laser type and absorption coefficient (α) for the material. Several possibilities of temperature ramp rates may be applicable and can make calculations quite complex especially when considering feed-rate and factoring in a densification term. For example: a CW laser, the ramp may be treated as a single step-function as the laser continues to input power during the "on" phase. Other factors in the above equation are functions of

temperature, and phase change as well. It is important to take these into account, for example sample absorption will change during the heating phase.

Determination of Proper Thickness of Powder-bed

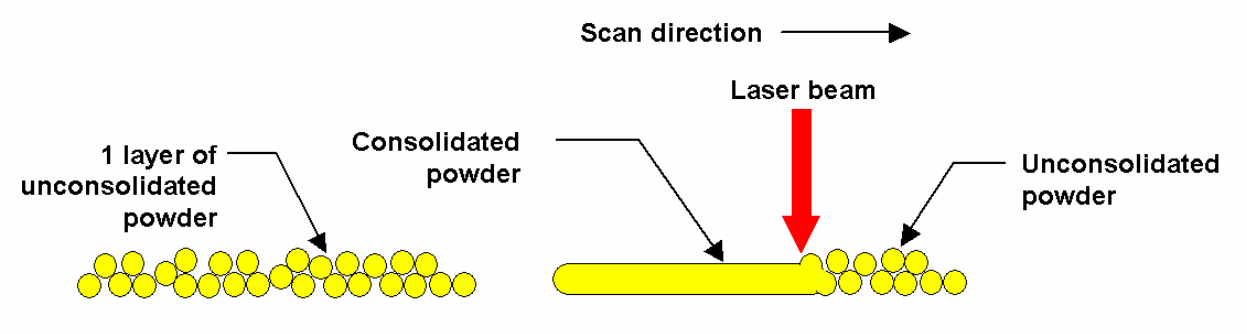

Figure 2.8: Laser Sintering of Powder Bed [104]

The optimal layer thickness has been empirically determined at 2-3 times the average particle diameter [104]. An explanation for the layer thickness can be ascertained through the realization that when the powder bed is 2-3 particles thick, most of the particles will receive direct energy from the laser. If the powder bed is thicker than this, the laser will not have the interaction volume equal to the remainder of the powder below this distance and general heat transfer through convection will become the dominant mechanism for temperature rise.

Layer Addition

After the first layer is placed and sintered together, a second layer (green-film) may be added to the original followed by laser sintering. This layer should also be of the same thickness as the previous one. In case of too thick a of an initial layer, peeling or curling can occur as the upper surface heats, densifies and then shrinks without adhering to the substrate below. An example of this can be seen in the SEM image shown below:

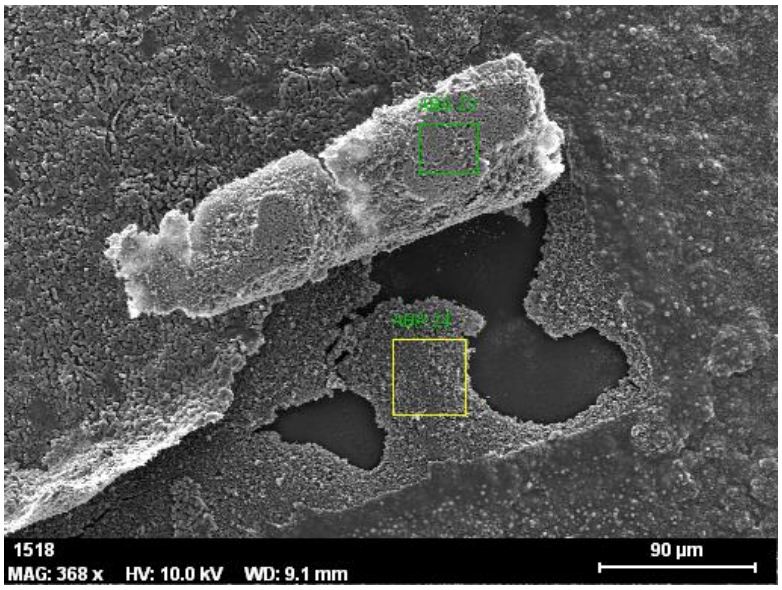

Figure 2.9: Laser Delamination Post Heat Treatment: The green film was too thick.

Sintering Models

Several models for sintering have been introduced since the 1950's taking different factors under consideration, and while the time for laser processing is so rapid that no temperature change can be accurately measured, it is important for the comprehensive understanding of laser sintering to understand the basic theory, driving forces, and processes at work. Therefore, a separate non-numerical technique will also be discussed from the point of view of process factor optimization. This method can be found in the works of Nelson, and is not a direct sintering model, but rather a design of experiments resulting in proper sintering factor settings from statistical analysis. All models presented in literature, Frenkel, Scherer and Mackenzie-Schuttleworth (MS), discuss sintering following the classic viscous sintering or amorphous liquid, or an Arrhenius shrinkage model[Ref.]. It is generally accepted that the Fenkel and MS models are a well thought out description of amorphous materials though the validity for predictions, but are limited to larger particles than those under consideration here as well as liquids which are Newtonian in nature. This leads to errors in predictions for systems based in smaller particles and through reliance of using the liquid surface tension as the sole driving force for compaction.

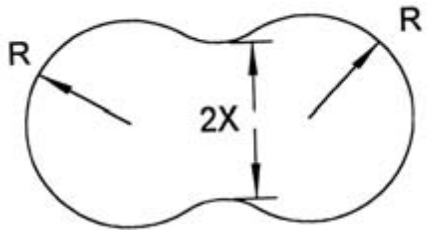

Figure 2.10: Frenkel Sintering [107]

Lee et. al. [108] provided some reduction to this error by assuming that the contact between particles significantly grows prior to viscous flow due to deformation. Lee further stressed that the contact growth is dependent on the initial radius and contact angles between adjacent artifacts. From these results on self-alignment in particulate inks, attractive surface forces such as Van Der Waals and surface tension have been shown as large driving forces for contact growth prior to flow provided they exist within a critical distance from one another.

Nelson's approach [94] to the development of a laser sintering system is based on the laser input factors and response variables. It has merit in that it developed a process for the final product of the system, not solely on the numerical solutions of the equations with given boundary conditions. Numerical models like that of Lee, Frenkel, Shuttleworth, Kendall offer no reproducibility, predictability and have shown to be inapplicable for processing in terms of settings, much less no measuring device exists which can measure temperature fluctuations over the short durations of laser heating. While numerical models can aid in the understandings via the fundamental relationships between material properties, transport phenomenon, boundary conditions, a closed form analytical solution for the prediction of temperature distribution and resulting densities of the film is absent.

References Chapter 2

1. Eric Savitz, *Manufacturing The Future: 10 Trends To Come In 3D Printing.* Forbes, 2012(http://www.forbes.com/sites/ciocentral/2012/12/07/manufacturing-the-future-10-trends-to-come-in-3d-printing/).
2. Wadhwa, V., *The End of Chinese Manufacturing and Rebirth of U.S. Industry*. Forbes, 2012(http://www.forbes.com/sites/singularity/2012/07/23/the-end-of-chinese-manufacturing-and-rebirth-of-u-s-industry/).
3. Hopkinson, N., *Additive Manufacturing: What's happening and where are we going with printing in the third dimension?* Word Document available at http://www. Becta. org. uk, 2010.
4. Campbell, I., D. Bourell, and I. Gibson, *Additive manufacturing: rapid prototyping comes of age*. Rapid Prototyping Journal, 2012. **18**(4): p. 255-258.
5. Olson, P. *Airbus Explores Building Planes With Giant 3D Printers - Updated With Video*. Forbes 2012 [cited 2012 7-11-2012].; TECH:[
6. Levy, G.N., R. Schindel, and J.-P. Kruth, *Rapid manufacturing and rapid tooling with layer manufacturing (LM) technologies, state of the art and future perspectives.* CIRP Annals-Manufacturing Technology, 2003. **52**(2): p. 589-609.
7. Cable, J., *GM, Ford and Chrysler Get Big Chunk of Advanced-Vehicle Funding.* http://www.industryweek.com/global-economy/gm-ford-and-chrysler-get-big-chunk-advanced-vehicle-funding, 2011.
8. Anonymous, *All together now; Collaborative manufacturing*, in *The Economist*2012, The Economist Intelligence Unit: London. p. 18-19.
9. Maxey, K., *IBM Sees 3D Printing Changing Manufacturing.* http://www.engineering.com/3DPrinting/3DPrintingArticles/ArticleID/5478/IBM-Sees-3D-Printing-Changing-Manufacturing.aspx, 2013.
10. Wohlers, T., *Additive Printing Technology.* MoldMaking Technology, 2012.

11. Gibson, I., D.W. Rosen, and B. Stucker, *Additive manufacturing technologies: rapid prototyping to direct digital manufacturing*. 2010: Springerverlag Us.

12. Cooper, K.G., *Rapid prototyping technology: selection and application*. 2001: Marcel Dekker, Inc.

13. Kruth, J.-P., *Material incress manufacturing by rapid prototyping techniques.* CIRP Annals-Manufacturing Technology, 1991. **40**(2): p. 603-614.

14. Noorani, R., *Rapid prototyping*. 2006: Wiley.

15. Jamieson, R. and H. Hacker, *Direct slicing of CAD models for rapid prototyping.* Rapid Prototyping Journal, 1995. **1**(2): p. 4-12.

16. Roscoe, L., *Stereolithography interface specification.* America-3 D Systems Inc, 1988.

17. Specification, S.I., *The STl Format.* Valencia, CA: 3Dsystems Inc, 2000.

18. Halloran, J.W., et al., *Photopolymerization of powder suspensions for shaping ceramics.* Journal of the European Ceramic Society, 2011. **31**(14): p. 2613-2619.

19. Sachs, E., M. Cima, and J. Cornie, *Three-dimensional printing: rapid tooling and prototypes directly from a CAD model.* CIRP Annals-Manufacturing Technology, 1990. **39**(1): p. 201-204.

20. Kruth, J.-P., M. Leu, and T. Nakagawa, *Progress in additive manufacturing and rapid prototyping.* CIRP Annals-Manufacturing Technology, 1998. **47**(2): p. 525-540.

21. Chua, C.K., K.F. Leong, and C.C.S. Lim, *Rapid prototyping: principles and applications*. 2010: World Scientific Publishing Company.

22. Burns, M., *Automated fabrication: improving productivity in manufacturing*. 1993: Prentice-Hall, Inc.

23. Pham, D. and R. Gault, *A comparison of rapid prototyping technologies.* International Journal of Machine Tools and Manufacture, 1998. **38**(10-11): p. 1257-1287.

24. Wong, K.V. and A. Hernandez, *A Review of Additive Manufacturing.* ISRN Mechanical Engineering, 2012. **2012**.

25. Shivpuri, R., et al., *Evaluation of 3D printing for dies in low volume forging of 7075 aluminum helicopter parts.* Rapid Prototyping Journal, 2005. **11**(5): p. 272-277.

26. Systems, E.d.p. *e-Manufacturing Systems*. Available from: www.EOS.com.

27. Systems, d. *Stereolithography and selective laser sintering machines*. Available from: http://www.3dsystems.

com.

28. Systems, d. *ZCorp Systems*. Available from: http://www.zcorp.com/en/home.aspx.

29. *Soligen*. Available from: http://www.soligen.com.

30. Sachs, E., *Three dimensional printing*, 2001, DTIC Document.

31. Pfister, A., et al., *Biofunctional rapid prototyping for tissue-engineering applications: 3D bioplotting versus 3D printing.* Journal of Polymer Science Part A: Polymer Chemistry, 2004. **42**(3): p. 624-638.

32. Lipke, D.W., et al., *Near net-shape/net-dimension ZrC/W-based composites with complex geometries via rapid prototyping and Displacive Compensation of Porosity.* Journal of the European Ceramic Society, 2010. **30**(11): p. 2265-2277.

33. Tang, H.-H., M.-L. Chiu, and H.-C. Yen, *Slurry-based selective laser sintering of polymer-coated ceramic powders to fabricate high strength alumina parts.* Journal of the European Ceramic Society, 2011. **31**(8): p. 1383-1388.

34. Salmoria, G.V., et al., *Microstructural and mechanical characterization of PA12/MWCNTs nanocomposite manufactured by selective laser sintering.* Polymer Testing, 2011. **30**(6): p. 611-615.

35. Kruth, J.-P., et al., *Binding mechanisms in selective laser sintering and selective laser melting.* Rapid Prototyping Journal, 2005. **11**(1): p. 26-36.

36. Taminger, K.M. and R.A. Hafley. *Electron beam freeform fabrication: a rapid metal deposition process*. in *Proceedings of the 3rd Annual Automotive Composites Conference*. 2003.

37. Liu, Z., et al. *Selective laser sintering of high-density alumina ceramic parts*. in *Proceedings of the 35th International MATADOR conference*. 2007. Springer.

38. arcam. *Electron beam welding*. 2012; Available from: www.arcam.com.

39. Exner, H., et al., *Laser micro sintering: A new method to generate metal and ceramic parts of high resolution with sub-micrometer powder.* Virtual and physical prototyping, 2008. **3**(1): p. 3-11.

40. Murr, L.E., et al., *Metal fabrication by additive manufacturing using laser and electron beam melting technologies.* Journal of Materials Science & Technology, 2012. **28**(1): p. 1-14.

41. Kummailil, J., *Process Models for Laser Engineered Net Shaping*, 2004, WORCESTER POLYTECHNIC INSTITUTE.

42. Balla, V.K., S. Bose, and A. Bandyopadhyay, *Processing of bulk alumina ceramics using laser engineered net shaping.* International Journal of Applied Ceramic Technology, 2008. **5**(3): p. 234-242.

43. Liao, Y., H. Li, and Y. Chiu, *Study of laminated object manufacturing with separately applied heating and pressing.* The International Journal of Advanced Manufacturing Technology, 2006. **27**(7-8): p. 703-707.

44. *LENS System*. 2012; Available from: www.optomec.com.

45. Atwood, C., et al., *Laser engineered net shaping (LENS (TM)): A tool for direct fabrication of metal parts*, 1998, Sandia National Laboratories, Albuquerque, NM, and Livermore, CA.

46. Corp, K.; Available from: www.kiracorp.co.jp/EG/pro/rp/top.html

47. dimensions, S. *Solido Machine*. Available from: www.solidimension.com

48. Vaupotič, B., M. Brezočnik, and J. Balič, *Use of PolyJet technology in manufacture of new product.* Journal of Achievements in Materials and Manufacturing Engineering, 2006. **18**(1-2).

49. *Fab@home*. Available from: www.fabathome.org.

50. Reprap.

51. Facchini, L., et al., *Microstructure and mechanical properties of Ti-6Al-4V produced by electron beam melting of pre-alloyed powders.* Rapid Prototyping Journal, 2009. **15**(3): p. 171-178.

52. Grimm, T., *User's guide to rapid prototyping*. 2004: Sme.

53. Kim, H., J.-W. Choi, and R. Wicker, *Scheduling and process planning for multiple material stereolithography.* Rapid Prototyping Journal, 2010. **16**(4): p. 232-240.

54. Szilvśi-Nagy, M. and G. Matyasi, *Analysis of STL files.* Mathematical and Computer Modelling, 2003. **38**(7): p. 945-960.

55. Wohlers, T., *Wohlers Report*, 2009, Fort Collins, Colorado, USA: Self. www. wohlersassociates. com.

56. *<Capillary-Assembled Microchip for Universal.pdf>*.

57. Singh, R., *Process capability study of polyjet printing for plastic components.* Journal of mechanical science and technology, 2011. **25**(4): p. 1011-1015.

58. Petrovic, V., et al., *Additive layered manufacturing: sectors of industrial application shown through case studies.* International Journal of Production Research, 2011. **49**(4): p. 1061-1079.

59. Prinz, F.B. and L.E. Weiss, *Novel applications and implementations of shape deposition manufacturing.* Naval research reviews, 1998. **50**: p. 19-26.

60. Martinez, A.W., et al., *Programmable diagnostic devices made from paper and tape.* Lab Chip, 2010. **10**(19): p. 2499-504.

61. Whitesides, G.M., *The origins and the future of microfluidics.* Nature, 2006. **442**(7101): p. 368-73.

62. Glunz, S., *High-efficiency crystalline silicon solar cells.* Advances in OptoElectronics, 2007. **2007**.

63. Jain, K., et al., *Flexible electronics and displays: High-resolution, roll-to-roll, projection lithography and photoablation processing technologies for high-throughput production.* Proceedings of the IEEE, 2005. **93**(8): p. 1500-1510.

64. Lankelma, J., et al., *Paper-based analytical device for electrochemical flow-injection analysis of glucose in urine.* Anal Chem, 2012. **84**(9): p. 4147-52.

65. Martinez, A.W., et al., *Patterned paper as a platform for inexpensive, low-volume, portable bioassays.* Angew Chem Int Ed Engl, 2007. **46**(8): p. 1318-20.

66. Martinez, A.W., S.T. Phillips, and G.M. Whitesides, *Three-dimensional microfluidic devices fabricated in layered paper and tape.* Proc Natl Acad Sci U S A, 2008. **105**(50): p. 19606-11.

67. Sachs, E., M. Cima, and J. Cornie, *Three-Dimensional Printing: Rapid Tooling and Prototypes Directly from a CAD Model.* CIRP Annals - Manufacturing Technology, 1990. **39**(1): p. 201-204.

68. Xiong, Z., et al., *Fabrication of porous scaffolds for bone tissue engineering via low-temperature deposition.* Scripta Materialia, 2002. **46**(11): p. 771-776.

69. Mironov, V., G. Prestwich, and G. Forgacs, *Bioprinting living structures.* J. Mater. Chem., 2007. **17**(20): p. 2054-2060.

70. Sukeshini, A., et al., *Aerosol Jet Printing and Microstructure of SOFC Electrolyte and Cathode Layers.* ECS Transactions, 2011. **35**(1): p. 2151-2160.

71. Sukeshini, M.A., et al. *Aerosol Jet Deposition for SOFC Fabrication*. in *Meeting Abstracts*. 2010. The Electrochemical Society.

72. Optomec, *AJ300 User Manual.* 2011.

73. Optomec, M.R. *New and Developing materials fof Ink Formulations*

2011.

74. Aliseda, A., et al., *Atomization of viscous and non-newtonian liquids by a coaxial, high-speed gas jet. Experiments and droplet size modeling.* International Journal of Multiphase Flow, 2008. **34**(2): p. 161-175.

75. Chhabra, *Bubbles, Drops, and Particles in Non-Newtonian Fluids, Second Edition.* Taylor and Francis, 2007.

76. Orzechowski, L.P.B.a.Z., *Liquid Atomization* Taylor and Francis, 1993.

77. Roman, M. and F. Navarro, *Deposition of Cellulose Nanocrystals by Inkjet Printing.* 2010. **1019**: p. 157-171.

78. Utela, B., et al., *A review of process development steps for new material systems in three dimensional printing (3DP).* Journal of Manufacturing Processes, 2008. **10**(2): p. 96-104.

79. <*Schultz_Disertation.pdf*>. 2005.

80. Hu, J.-B., Y.-C. Chen, and P.L. Urban, *Coffee-ring effects in laser desorption/ionization mass spectrometry.* Analytica Chimica Acta, 2013. **766**(0): p. 77-82.

81. Choi, S. and S. Samavedam, *Modelling and optimisation of rapid prototyping.* Computers in industry, 2002. **47**(1): p. 39-53.

82. Syms, R.R., et al., *Surface tension-powered self-assembly of microstructures-the state-of-the-art.* Microelectromechanical Systems, Journal of, 2003. **12**(4): p. 387-417.

83. Folgar, C.E., C. Suchicital, and S. Priya, *Solution-based aerosol deposition process for synthesis of multilayer structures.* Materials Letters, 2011. **65**(9): p. 1302-1307.

84. <*Optomec - AFRL - AJ Printing of SOFCs - JUN10.pdf*>.

85. Nanotech, A. *Aluminum Nano Ink*. 2012; Available from: http://www.appliednanotech.net/tech/conductive_inks.php.

86. <*laser sintered barium titaninate.pdf*>.

87. .

88. <*powder densification maps SLS.pdf*>.

89. <*Schultz_Disertation.pdf*>.

90. Kingery, W.D.B., H. K.; Uhlmann, Donald R. , *Introduction to Ceramics (2nd ed.).* John Wiley & Sons, Academic Press. I, 1976.

91. <*Sonicator_nanotechnology_applications.pdf*>.

92. Nelson, J.C., et al., *Model of the selective laser sintering of bisphenol-A polycarbonate.* Industrial & Engineering Chemistry Research, 1993. **32**(10): p. 2305-2317.

93. Rahaman, M.N., *Ceramic processing*. 2007: CRC Press.

94. *<4777014_Process_for_preparing_self_suppo.pdf>*.

95. Townes, C.H., *A Century of Nature: Twenty-One Discoveries that Changed Science and the World*, ed. L.G.a.T. Lincoln. 2003: Univeristy of Chicago Press. 380.

96. Cline, H.E. and T.R. Anthony, *Heat treating and melting material with a scanning laser or electron beam.* Journal of Applied Physics, 1977. **48**(9): p. 3895.

97. Cannon, W.R., et al., *Sinterable Ceramic Powders from Laser-Driven Reactions: I, Process Description and Modeling.* Journal of the American Ceramic Society, 1982. **65**(7): p. 324-330.

98. Cannon, W.R., et al., *Sinterable Ceramic Powders from Laser-Driven Reactions: II, Powder Characteristics and Process Variables.* Journal of the American Ceramic Society, 1982. **65**(7): p. 330-335.

99. Xiao, B. and Y. Zhang, *Laser sintering of metal powders on top of sintered layers under multiple-line laser scanning.* Journal of Physics D: Applied Physics, 2007. **40**(21): p. 6725.

100. Besling, W.F.A., *Laser-induced chemical vapor deposition of nanostructured silicon carbonitride thin films* Journal of Applied Physics, 1998. **83**(1): p. 9.

101. zheng

102. Shultz, *Modeling Heat Transfer and Densification during Laser Sintering of Viscoelastic Polymers*, 2005: Virginia Tech ETD.

103. Cojocaru, E., et al., *Free-running ruby laser annealing of boron implanted silicon.* Applied Physics A, 1981. **26**(4): p. 243-246.

104. Shuja, S.Z., B.S. Yilbas, and O. Momin, *Laser heating of moving solid: Influence of workpiece speed on melt size.* AIChE Journal, 2010. **56**(11): p. 2997-3004.

105. J., F., *Viscous Flow ofCrystalline Bodies Under the Action ofSulface Tension.* Journal of Physics (Moscow), 1945. **9 [5]. 385..91**.

106. Bourell, D., et al. *Solid Freeform Fabrication An Advanced Manufacturing Approach*. in *Proceedings of the SFF Symposium*. 1990.

Chapter 3 Case Studies: Materials and Experiments

3.1 Introduction to Materials under Investigation

Chapter 3 provides empirical information gathered in support of increasing the understanding of 3D additive printing (3D or AP) and Selective Laser Sintering (SLS). Four materials were explored in the present study, each with different characteristics. The list includes boron, Sodium-bismuth titananate (NBT-BT), polyvinyladine fluoride (PVDF), and Aluminum-Silicon (Al-Si).

Above four groups represent four classes of solids: element, ceramic, polymer, and alloy respectively. It is anticipated that these groups would each elucidate differences in handling and processing for the future directions of research in each. It is also presumed that multiple complexities and challenges would arise from the polymer and ceramic materials during sintering because of the complex reactions undertaken during energy absorption and relaxation. These include the efficacies of the varying constituents of each phase (elemental and molecular), phase transformation, molecular diffusion between grains and the substrate, melt temperatures, and others. In addition, these two materials presented a special case of phase transformation, retention or transition to a piezoelectric phase. [109-111]

3.2 Boron

Boron as an element has presented itself to be particularly difficult to characterize. Originally discovered in 1808, disagreement still existed until 2007 over the dominant phase α or β at ambient conditions [112-114]. It was not until 2011 that the complete phase diagram was mapped [1-9]. Boron and its alloys are of particular interest for several reasons: (i) compared to diamond, it is lower in atomic weight and second in hardness (27-30 GPa), (ii) high tolerance to heat, resistance to acids and corrosion and (iii) in applications within the body a low toxicity, as well as anti-fungal and anti-bacterial properties [115, 116]. In the special case of amorphous boron, there are no preferred fracture planes, making it even more desirable for impact resistant coatings [117].

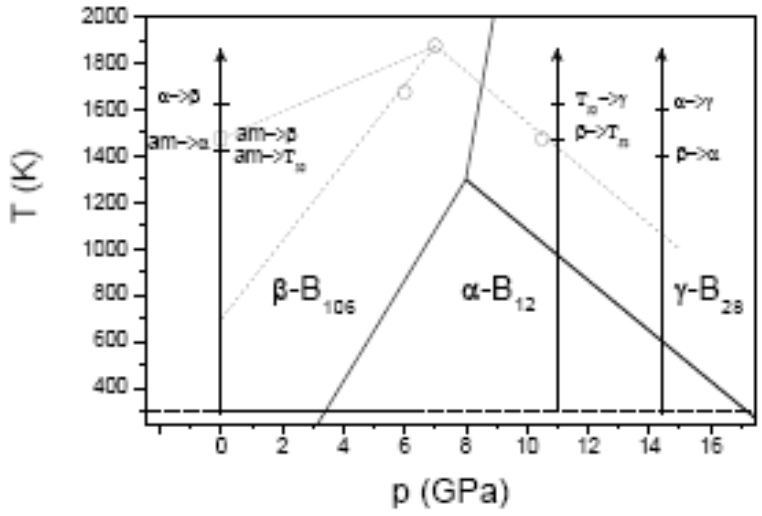

Figure 3.1: Boron Phase Diagram P-T [118]

Research into boron, boron alloys, and boron oxides have generated coatings and thin films in both crystalline and amorphous phase through chemical vapor deposition (CVD), Physical Vapor Deposition (PVD), cathodic arc deposition, magnetron sputtering, Radio Frequency (RF) sputtering, plasma arc spraying, pulsed laser deposition (PLD), and others [119-123]. The similarities and restrictions between all these systems include the limitations of enclosed geometry; elevated temperatures, high performance vacuum system, and in some cases preparation of a highly pure boron target. In all, the listed systems are restricted in application to controlled environments and the geometrical constraints of the required equipment. Additionally, previous synthesis techniques have the distinction of generating a trade-off between high growth rate and high density. Therefore, while the material characteristics of boron make it an appealing candidate for implementation in tribological coatings, bio-implants, armor plating, corrosive environment protection, and neutron absorption; as of yet it has not enjoyed industry favor owing to the extreme difficulties in processing [124, 125].

Several previous reports describing the densification and sintering of powders other than boron have had varied success in using the heat transfer equation in describing the phenomenon in the case of lasers, [119, 126-132]. The 3D printing platform of Optomec has been used recently to overcome some of long standing hurdles of top-down manufacturing, viz., geometrical restrictions and phase selection involved with standard lithography and rapid prototyping [85, 133, 134]. The major discussions for this section revolve around the ink preparation, green-film deposition, packing density enhancement and the optimization of the 1000 mW-830 nm diode

laser parameters. Several Design-of-Experiments (DOE) were conducted to systematically optimize the above processes. If proven, the M3D process would eliminate the current art requirements, allowing a highly dense film to be grown rapidly on substrates. The importance of this can be readily seen in the application of boron coatings to unrestricted part size, in-the-field application and repairs in ambient or possibly adverse environments [135].

Characterizations of the as prepared samples utilized: SEM (FEI Quanta 600 FEG environmental SEM/EDS Bruker EDX, Karlsruhe Germany with a Silicon Drifted Detector), LEO Zeiss 1550 field-emission, XRD (PANalytical X'Pert, CuKa; Philips, Almeleo, the Netherlands), Hystitron TriboIndentor, and Veeco Dimension 3100 Nanoman AFM.

3.2.1 Experimental Design

The constituents for ink composition are boron powder (97%, 2 μm powder, supplied by AeroTech industries), Acetone (99.9% Alfa-Aesar), IPA (99.7% Sigma Aldrich), Ethanol (99.9% Alfa-Aesar), Methanol (99.9% Alfa-Aesar), Ethylene-Glycol (99.9% Alfa-Aesar), and PVA (99.9% Sigma-Aldrich).

Since previous work from the lab had been directed to construct an ink for the UA system, it was decided to prepare a similar series of four solutions (TABLE 3.1) comprised of Boron (3-10% wt. to total solvent wt.), Ethylene-Glycol (15% volume of solutions), and PVA (0.5% of major solvent weight). The above components were added to the matching major-solvent (85% volume) of Di-H20, IPA, Methanol, Ethanol or Acetone and mixed to determine optimum ink composition.

Ink Generation

Boron has a higher affinity for polar solvents and therefore Di-H2O, Acetone and IPA are expected to be excellent base solvent candidates. A methanol solution, having lower polarity, was prepared to run as a control. Ethylene Glycol was used to reduce the Marangoni or "coffee-ring" effect, it also affects the surface tension and wettability [136]. PVA was included to aid in the suspension and stability of the solution as well as act as a binder once the solution had dried, though other carbomers may work equally well. [137, 138]

The determination of optimum ink composition was based on several factors including: stability, agglomeration tendencies, printing duration, low self-assembly characteristics, and consistent evaporation rates. For proper analysis, all solutions were placed in an ice-bath and treated with

two 2-minute ultra-sonication using a Ningbo HaiShu Sklon homogenizer with one minute interval in between Following this, they were closed in sealable polyethylene bottles and immersed in a Cole-Parmer Ultrasonic Bath for one hour, then split into two equal volumes of solution.

To test for stability, the first half of the solution remained undisturbed for three days, except occasional pipetting at pre-determined time intervals to remove a minor amount of fluid from the top 50% of the volume. To test for mixing affinity, the second half of each solution had three 5mm ZrO_2 balls placed inside. Prior to each measurement, the container was vigorously hand-shaken for 15-20 seconds. Each measurement from the above sample populations used a single drop of solution placed on a glass-cover slide which was dried at room temperature on a level surface. Upon complete drying, the sample was analyzed under a Zeiss Optical microscope for particulate-size population and agglomeration and self-stacking characteristics. (Data not presented)

From the above test, the best two base compositions were selected and sealed in a container placed in an ultrasonic bath for 20 minutes. Optomec recommends a solids loading content for films at up to 20%. Each solution was serially tested at 3%, 5%, 7% and 10% solids loading content within the following parameters.

1 ml was extracted using a pipette and placed in the AJP vial, the atomizer voltage turned on, adjusted, and the mixture and allowed to achieve a steady dense mist formation. The investigators chose 12 machine factors in testing for optimum deposition of the green-film and compared them with the first seven response variables from Table 2.3. If completed as a two-level full factorial, the above description would entail 212 experiments (runs) to investigate all primary effects and interactions. While this would yield excellent resolution for all factors, the time invested would be large. Instead several Orthogonal Arrays known from Taguchi's work with Design of Experiments called L-18 were used.

Green Film Production

Design of Experiments is a method to elucidate which factors from many are the driving forces for the resultant of the process. Typically, Full-Factorial experiments are used in the case of a low total number of factors and levels of each factor. However in many cases where the process is not fully understood, or if there are factors with unknown influences, Full-Factorial

experiments can become unwieldy because of the number of runs. In these cases, a better approach is to use a screening method to reduce factors and their levels. Taguchi developed several outer arrays known as "L", the digits following the L show the number of runs the experiment will take. These specialized arrays consider only main affects from the inputs with no consideration for influences between factors. It was hoped that this portion of the experiment would aid in the elimination of some factors, allowing only important ones to be further investigated.

Table 3.1: Factors Investigated for Green Film

Green Film Factors (Ultra Sonic Atomizer)	
1. Slurry Composition	2. Sheath Pressure
3. Atomizer Pressure	4. Atomizer Voltage
5. Platen Temperature	6. Deck Speed
7. Fill Pattern	8. Overlap Percentage
9. Number of Passes	10. Z-Height
11. Fill Angle	12. Trace Width

An L-18 DOE with 4-levels for each of the 12 factors was compiled, the remaining 6 columns were not used and do not affect the results or data, each experiment was blocked against two substrates Si (100) wafer and a polished Stainless Steel 304 coupon, (see Appendix for DOE designs). For the synthesis of a green film, a Computer Aided Design (CAD) file was created for the pattern outline, a (0.3 mm x 0.3 mm) square. A separate file for each run was created wherein each of the factors 7-12 were altered (Programs are listed in the Appendix), the remaining factors 1-6 were altered manually during a run at the VM interface of the machine. The general procedure for each run progressed as:

1. Selection of the pattern from the Auto Cad File, translation of the file to the VM Toolset.
2. Alterations for factors 1-6 from Table 3.2 using the VM Toolset
3. Allow the machine to arrive at steady-state from changes to flow rates (30 sec)
4. Process the file and deposit green film

The subsequent films were dried on the platen at elevated temperature (70^{o}C) and analyzed with XRD to ensure they remained at an amorphous phase.

Laser Sintering

A second series of experiments, utilizing a similar but larger Taguchi L25 design, were carried out in the laser sintering portion (programs listed in Appendix). Factors and variations thereof can be found in Table 2.1 and Table 3.2 below. Further refinements and a broadening of factor ranges were tested serially to arrive at the optimized film.

Table 3.2: Laser Sintering Parameters

Selective Laser Sintering Parameters	
Wattage	Overlap Percentage
Focal Plane	Time to return
Dwell Time (speed)	Angle of Raster
Layer Thickness	Substrate Material
Raster Pattern	O_2 Content of environment

An XPS characterization was completed on the initial samples which were developed in ambient atmospheric conditions. It was found that the films showed high variability in both oxygen and boron content, noted by the heights of their respective peaks. While these are not quantitative studies, they are indicative of general percentages of the film. Further analysis through high resolution showed varying degrees of B_2O_3 and other sub-oxides. It was theorized that because of this reactivity with oxygen, despite the short time duration, a shielding gas might be able to reduce the oxide build up.

In an attempt to reduce the oxide layer, a small detachable argon purging chamber was designed and CNC machined to enable the shielding gas to flow over the surface of the sample, Figure 3.2 (a-d). The purge box allows installation of up to a 25x25x15mm object. The purging box can be installed to the AJP within one minute and integrated to process flow, Figure 3.3. The chamber was CNC machined from a solid Teflon billet, a small diffuser at the distal end from the sintering area creates turbulent flow inside of the entry chamber. The entry chamber vents to the sample area through the ported metal divider. A gas exchange rate based on volume of the open section of the chamber of 100% per minute was calculated to be 10 cfh. The gas was allowed 5

exchanges prior to sintering with the laser. Flow rates for argon were altered from 5 cfh to 15 cfh. Images can be seen below with the cover on and off.

A	B
	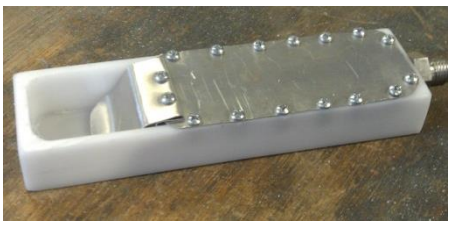
C	D
	

Figure 3.2: Purging Box

Argon purge box: (a) isometric view showing cover removed (b) isometric view cover installed (c) bird's eye view from front with cover (d) bird's eye view from front cover removed

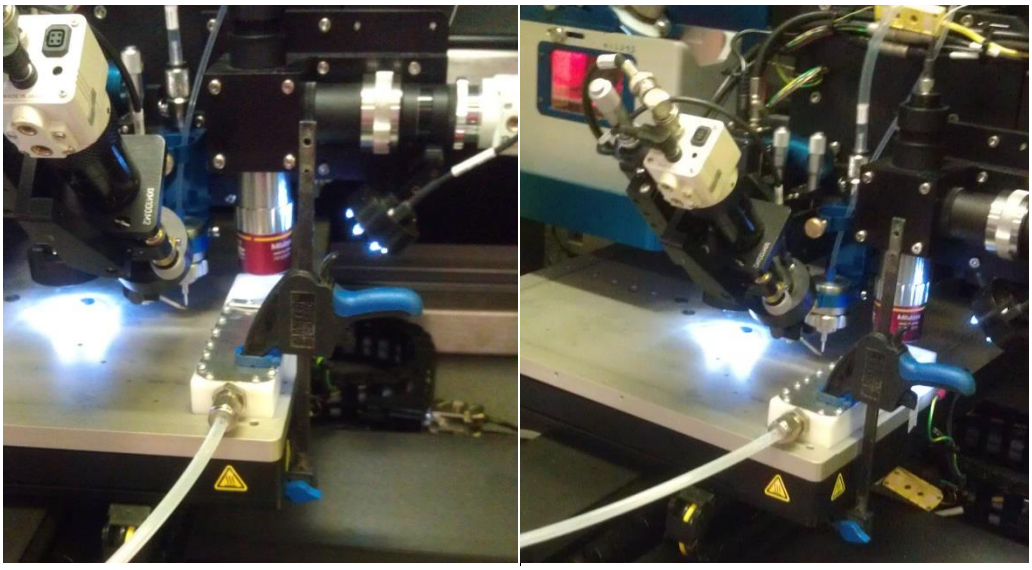

Figure 3.3: Purge Box Installed on AJP

Results

Ink

In the time lapsed test, the H_2O solution, despite having a strong polar character, performed the worst and showed highest separation rate. To test wettability, all solutions were spun coat on a Si substrate at 300rpm for 30 sec followed by a 500 for an additional 30 seconds. All solutions showed excellent wettability on the Si substrate. However, additional Ethylene Glycol was required at 10-15% of the original-volume to enhance wetting on the polished Stainless-304. Acetone was the best combined performer in dispersion and suspension analysis; IPA and methanol illustrated the best times for retained suspension.

Based on the above, the acetone and IPA based solutions were selected for further study. Testing showed excellent deposition characteristics for drying rate, low-agglomeration and fouling potential, run-length times, re-suspension, and percentage of solution available for deposition for the acetone but mixed results with IPA based solution. Issues with the IPA solution included clogged tips, inconsistent deposition rates (as calculated by mass deposited/second or average mass/sample). The calculated amount of the acetone solution which could not be aerosolized was estimated at 5-10% of initial volume. This remaining amount could be recycled with no deleterious effects by another 1 ml addition. Based on the above results, the IPA based solution was discontinued and further experiments proceeded with the acetone based solution only.

Deposition within the 3-10% solids loading showed a sweet-spot at 7%, at this solids-loading a film could be deposited quickly without clogging in the aperture in longer run times or additional sample constructions.

Green Film Deposition

To determine the quality of the film from the AJP system, four controls using the acetone solution were engaged. The control samples were produced by a spin-coat with an iterative five layer repeats at 300 rpm on Si wafer. Control-1 and 2 were pressed using a Cold-Isostatic-Press (CIP) for 1 minute at 30 MPa, Control-3 and 4, had no densification treatment.

Investigation though Design of Experiments proved to be an excellent choice. Through modification of the various factors, patterns emerged elucidating the main affects and interactions (Figures 3.4 through 3.17). The reduction of micro-pores (Figure 3.17-i), overspray (Figure 3.17-d,f) and veining (Figure 3.17-j) were accomplished as was the construction of a high density green-film(Figure 3.17-c) approaching 40-50% density. Final process ranges were atomizer voltage 45V, Sheath 52-57 ccfm, Atomizer Flow 10-15 ccfm, Platen Temperature 70 degrees, 2-4 passes, Platen Speed 3-4 mm/s, a serpentine fill pattern with 90 degree rotation between each pass, 10-15% Overlap, and a trace-width of 0.015 mm.

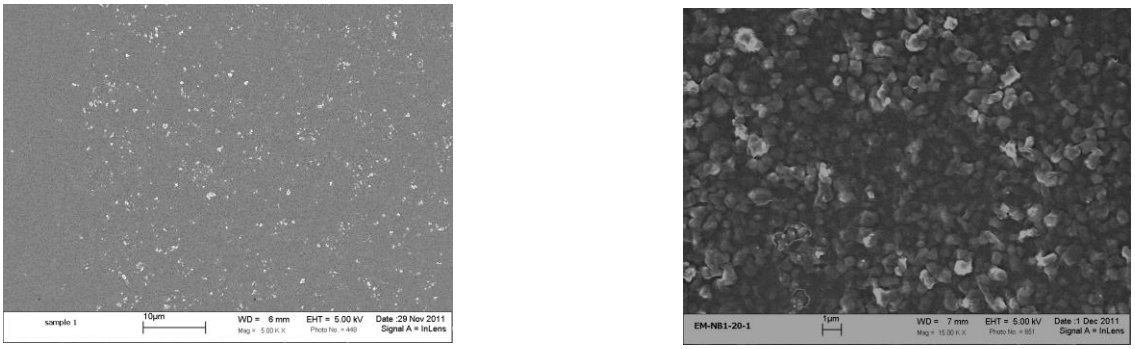

Figure 3.4: Film Densities

Sparse and inconsistent deposition, (b) excellent high density deposition

The ink used in (a) and b is the same, only process variables change.

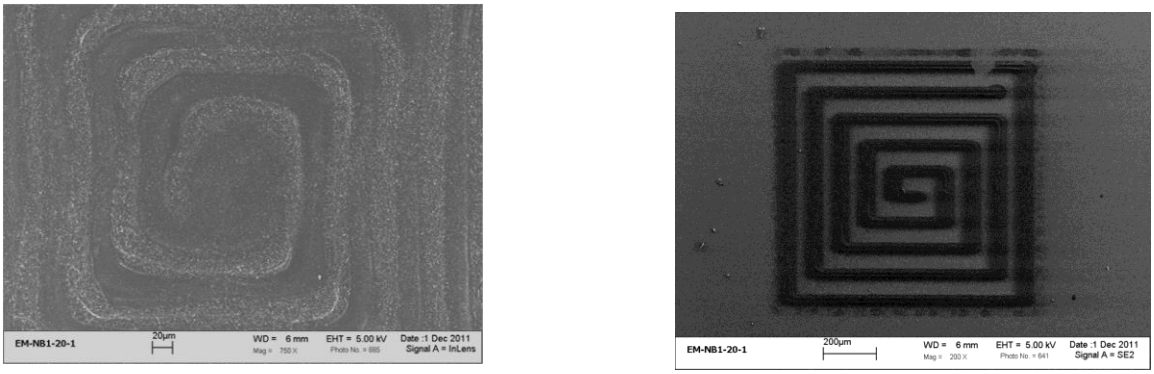

Figure 3.5: Film Spreading

(a) High wetting and spreading on substrate, (b) high aspect printing on the same substrate. Both examples use the same solids loading, varying main ink solvents

Phase analysis of the green films with XRD showed that the deposition of the green-film did not alter the boron phase for any of the samples and they remained amorphous.

Laser Sintering

Final factor ranges for control samples had a broad range in Laser Power 0.4W–1.7W, with power increasing for thinner films. In addition it was determined that a platen speed ranging from 0.5mm/s to 1.375mm/s, Trace-Width 0.001mm, Overlap 15-20%, Serpentine raster pattern with a second pass at a 90 degree rotation produced the best films. It is readily apparent from the SEM images that the AJP samples have a much higher density than the control spin-coated sample. With this knowledge, attempts were made to increase the density of the control films with additional sintering treatments (up to 8 additional passes). However matching densities could not be achieved. These less dense films did not adhere to the substrate.

AJP derived green films found optimized settings for the laser at 2.0 W and platen speeds ranging from 1.0-0.03 mm/s, all other factors from the control samples are identical (Figure 3.4). XRD analysis showed these films to remain amorphous. However, analysis with XPS showed a high concentration of oxides and sub-oxides. A further High Resolution scan showed these signatures have a high content of B_2O_3. While not a directly quantitative method, the height of the peaks at respective energy bands is indicative of the general amount of each oxide. In the High Resolution XPS graph below, the B_2O_3 peak can be seen as a completely separate peak from the main B_2 peak. In each case the films were deposited under the same conditions and

sintered under the same laser settings. Boron Peak is at 187.3 eV , B_2O_3 peak is at 192.9 eV. The intermediate peak and shoulder formations are B_4C at 186.6 eV and BN at 189.8 eV [139, 140].

In the below figures 3.6-3.12 the red line represents films sintered under argon, the blue line under ambient conditions.

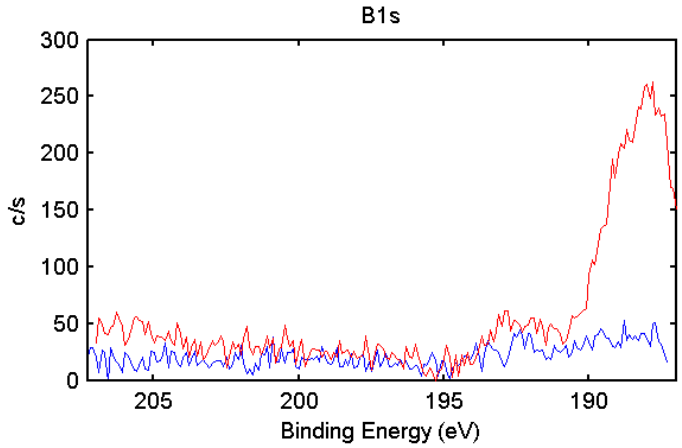

Figure 3.6: 2-Layer Green Film, Sintered at 2.0 Watts, 0.5mm/s

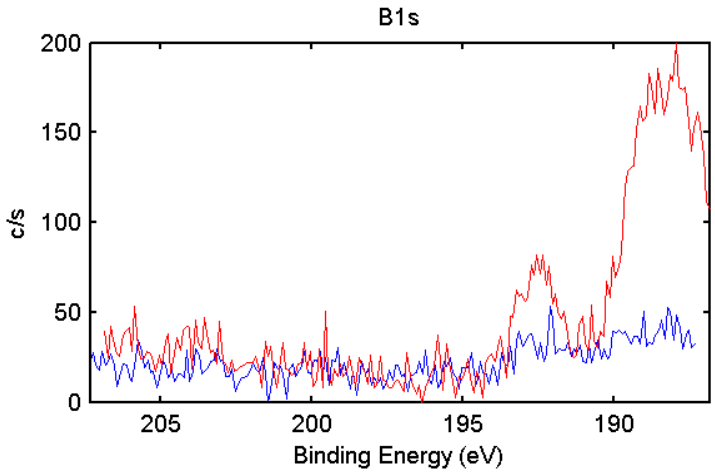

Figure 3.7: 5-Layer Green Film Sintered at 2.0 Watts 0.5 mm/s

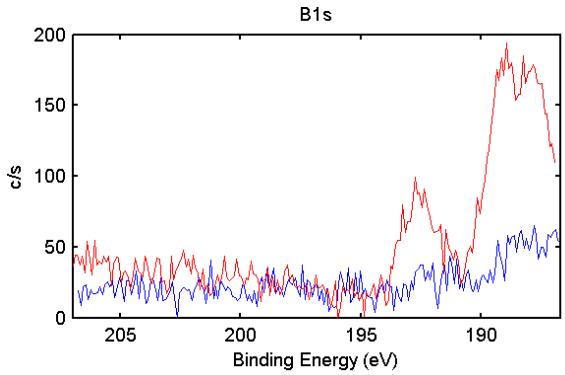

Figure 3.8: 10-Layer Green Film Sintered at 2.0 Watts 0.5 mm/s

The above graphs illustrate a marked increase in boron retention and elimination of B_2O_3 at the settings of 2 layer, 2.0 Watts and 0.5 mm/s deck speed. With this information a second set of experiments was devised to repeat proof of concept. In this experiment, the optimum settings from the above experiment are repeated for a multi-layer structure as well as including 5, 10 and 30 layer additions at 3 repeats each. Shown below are the results.

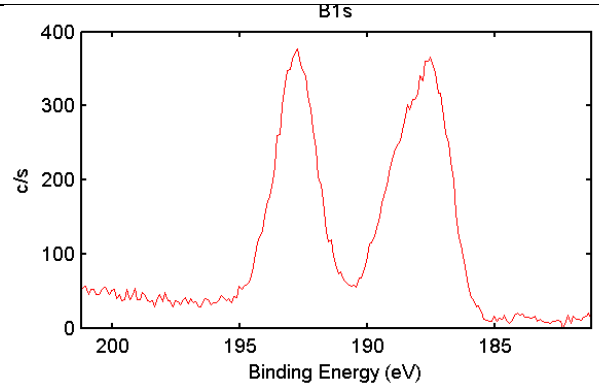

Figure 3.9: XPS Further Study

Green Film as deposited, notice the B_2 and B_2O_3 peak already in formation.

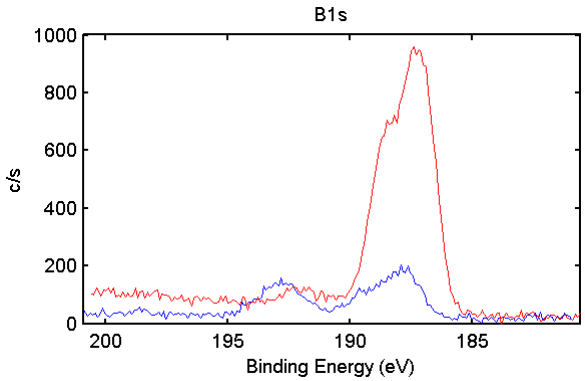

Figure 3.10: 5 Layer at 1.0 mm/s and 2.0 Watts

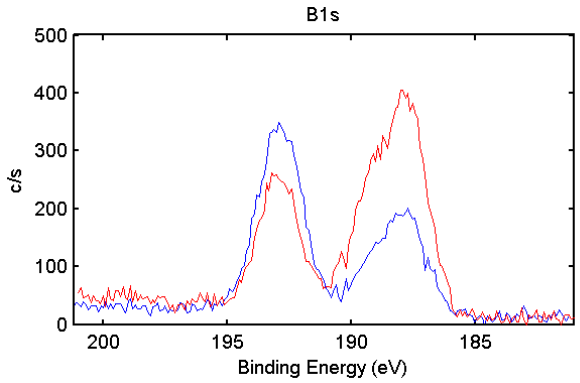

Figure 3.0.11: 10 Layer at 1.0 mm/s and 2.0 Watts

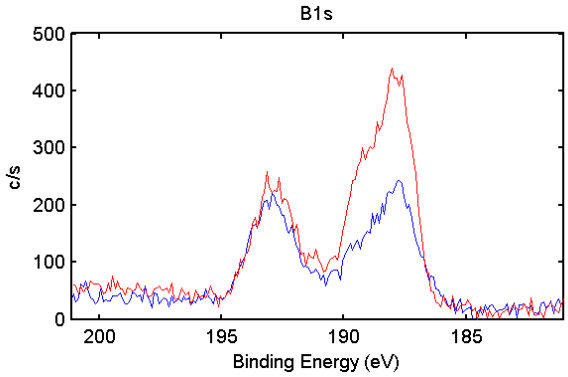

Figure 3. 12: 30 Layer at 1.0 mm/s and 2.0 Watts

As the above data illustrates, argon flow reduces the formation of B2O3 and then the evaporation of the compound.

Ultimate strength for the films arises as the density proceeds towards 100% of the bulk. To elicit this increase in density, boron deposited at 5 layers was sintered at 2.0 W with a platen speed of 0.5 mm/s and an argon flow of 10 cfh was sintered four times. A raster pattern with a second pass at a 90 degree rotation was used. In the case of adding layers. The beam has a Gaussian dispersion and power at the surface reduces exponentially with deviations from the optimum focal plane, and the z-offset must be adjusted in parallel to this increase. Density increases for these films are exhibited below. Morpologically they appear glassy and non-crystalline. Final films showed 1-2 micron grain-like formations and visible indications of flow on the surface for both SEM and AFM characterizations.

XRD tests (data not shown) confirm these still remain amorphous. Film thickness was increased via additional treatments with the above process in order to achieve a maximum thickness of a calculated 5 μm. Final tests from XRD showed these films remain amorphous.

Large scale surface topography measurements show fairly dense surfaces with surface heights reaching a maximum of approximately 400 nm. Most evident are the differences in topography from the varying treatments with the laser and associated energies with them. All samples were completed a 2.0 Watts laser power. The differences lie in the platen speed and number of passes or sintering steps used. As the energy directed to the surface grows higher, and denser, smoother surface is observed. Speeds ranged from 1.0mm/s(a), 0.5mm/s (b), to 0.05 mm/s (c).

AFM imaging from three separate areas on the sample show high density and possible flow (Figures 3.13-3.17). The first sample 12.5x12.5 micron and maximum height variation of 1.8 micron, the second shows 5x5 micron and 1.2 variations, the third and final is an 800x800x nm segment illustrating larger structures than that of the original particle size, and a maximum height difference of 400nm. All samples are quite smooth over these ranges with maximum surface roughness of 2 μm but most in the 100 nm range. This result shows the samples apparent porosity to be near full density.

3.2.3 Discussion

Ink

The high polarity, large branched structure of the molecule and high molecular weight of acetone are presumed to play important roles in the stability and excellent dispersion characteristics of the ink. In comparison to alcohol and water it is a much larger molecule. In addition, solutions employed in the AJP are heavily affected by viscosity, vapor pressure, and surface tension. The table below lists the main characteristics for each of the four major solvents.

Table 3.3: Main Solvent Characteristics

	Methanol	Acetone	Di-Water	IPA*	units
Molecular wt.	CH_4O	C_3H_6O	H_2O	C_3H_8O	
Molar mass	32.04	58.08	18.015	60.10	g mol^{-1}
Viscosity	5.9×10^{-4}	0.3.75	1.002	1.96 (25°C)	cP
Vapor Pressure	13.02 (20°C)	24.46–24.60 (20°C)	2.3 (20°C)	5.33 (24 °C)	kPa
Density	0.7918	0.791	1	0.786	g cm^{-3}

* (IPA calculated values)

Green Film

Part of this investigation was dedicated to optimization of process parameters and the development of a process for supreme film deposition. Analysis of the largest influences for response variables (Table 2.3) showed coupled interactions between the sheath and atomizer flow rates crossed with platen speed for deposition rates. Sheath and Atomizer flow rates crossed with aperture and z-height for focused lines (I). For this ink, an elevated platen temperature was necessary to achieve dense films with lower porosity (II). Beyond these, green film uniformity (III) was most heavily influenced by fill method and overlap percentage. The adherence to the substrate (IV) in the pre-annealed state was unaffected by all process parameters as expected, most likely this intermediate stage is only influenced by choice of polymer and plasticizer additives. Continuous film printing outside of solids content (V) is most heavily influenced by atomizer voltage setting and the stability of the misting rate within the vial. These settings were adequate for both printing on Si and metal substrate. It should be noted that the packing density and consistency of the applied film are also highly dependent upon the rheology of the solution and the general particle size. Due diligence should be taken in adjusting parameters.

Sintering

This strict numerical formula cannot be applied to this situation because of the highly complex surface reactions, the extremely short time frame of temperature fluctuations, changes in material coefficients, and packing density variations within the green film. All equations available to the author at the time of this publication exhibit reliance on the bulk material property (100% density); not a sphere stacked model or one more apt for complex nano-material alloys.

In practice, because amorphous materials exist at a higher energy state than their crystalline phases, the temperature transition must happen over an extremely short time period to reduce or eliminate nucleation and competitive driving forces. The crystallization function of amorphous boron is a result of complex interactions of time at temperature, heating rate and purity of the original material [113, 141].

The issue with sintering of powder via laser is that as each particle is sintered and attaches to the next, the material ceases to be a nano-particle and behaves more like the bulk material as more particles are added. After this initial sintering and compaction, the particles can no longer be treated as nano-particles because they belong to a collective matrix. An optimum film thickness for sintering exists; this thickness may be dependent upon material. Within this sweet-spot the material could be sintered in a layer by layer fashion.

Initial compaction identified the interaction between laser power and deck speed as the most critical parameters for sintering. These two parameters together yield the impact or work function which the film must absorb.

3.2.4 Discussion on Boron and Oxide Layer Formation

As boron has a high affinity for oxygen, and indeed creates boric acid in presence of water at room temperature, the sequential heating and cooling of the laser pass along with ambient humidity and available oxygen most likely created a B_2O_3 layer.

3.2.5 Conclusions

Implementation of the AJP system allowed the development of a process for fusing amorphous particles to one another under ambient conditions with high density and final phase remaining amorphous-like. We have shown the AJ printing system from Optomec is flexible enough to allow deposition of low viscosity, high vapor pressure inks with evaporation restrictors. Through a Design of Experiments optimization strategy, superfluous factors were eliminated or

set to a median level. The main affects were determined and allowed generation of a dense green film along with proper sintering via laser to create an amorphous-like boron film.

From the experiments with boron and laser sintering at ambient conditions we can expect that oxide formations can be reduced by a reducing or shielding gas at proper rates and containment. This method has been used in other processes [46, 47, 139]. These results point to the possibility overcoming similar issues with oxide formations on other alloys. The AJP has shown increased versatility in overcoming some of the current problems in materials development and Future investigations are expected to use this process to continue on this trajectory.

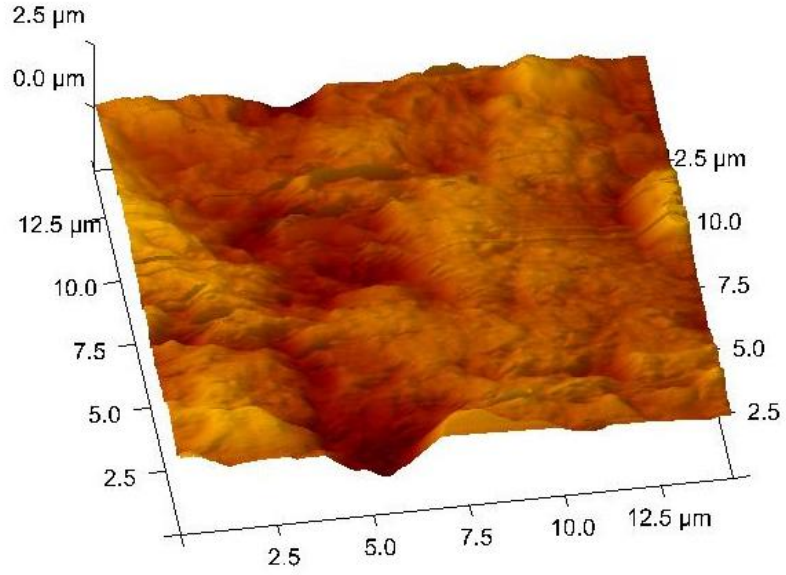

Figure 3. 13: Area #1- 12.5x12.5 micron square area sample from 4 pass laser annealed multi layer sample. Settings were 2.0W, 0.05mm/s, shielding gas at 10 cfh.

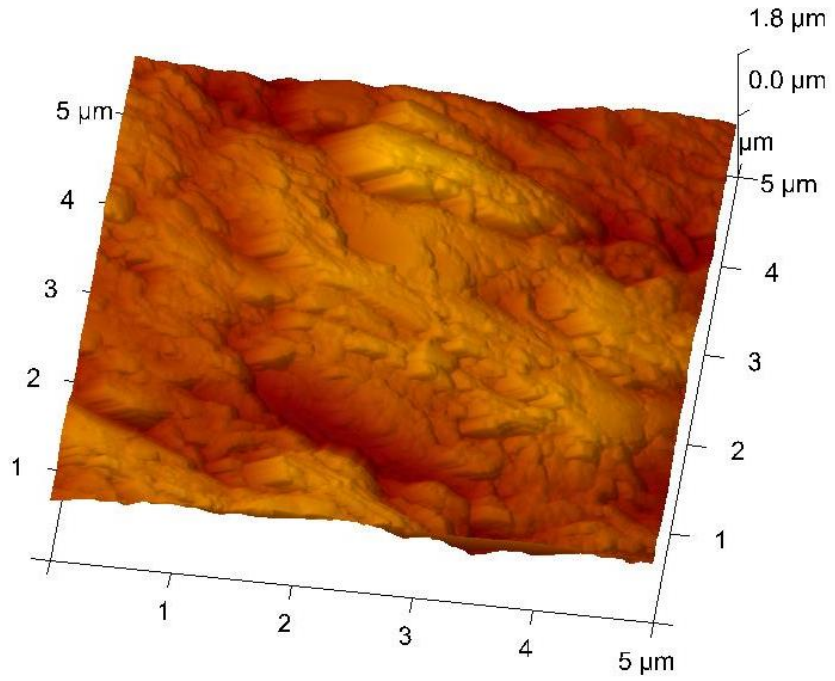

Figure 3.14: Area #2- 5.0x5.0 micron square area sample from 4 pass laser annealed multi-layer sample.

Settings were 2.0W, 0.05mm/s, shielding gas at 10 cfh.

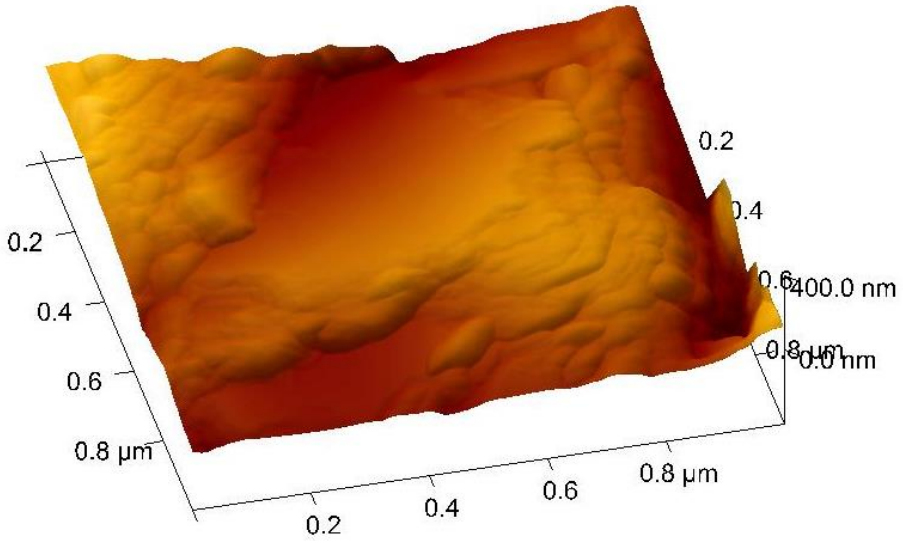

Figure 3.15: Area #3- 0.8x0.8 micron square area sample from 4 pass laser annealed multi-layer sample.

Settings were 2.0W, 0.05mm/s, shielding gas at 10 cfh.

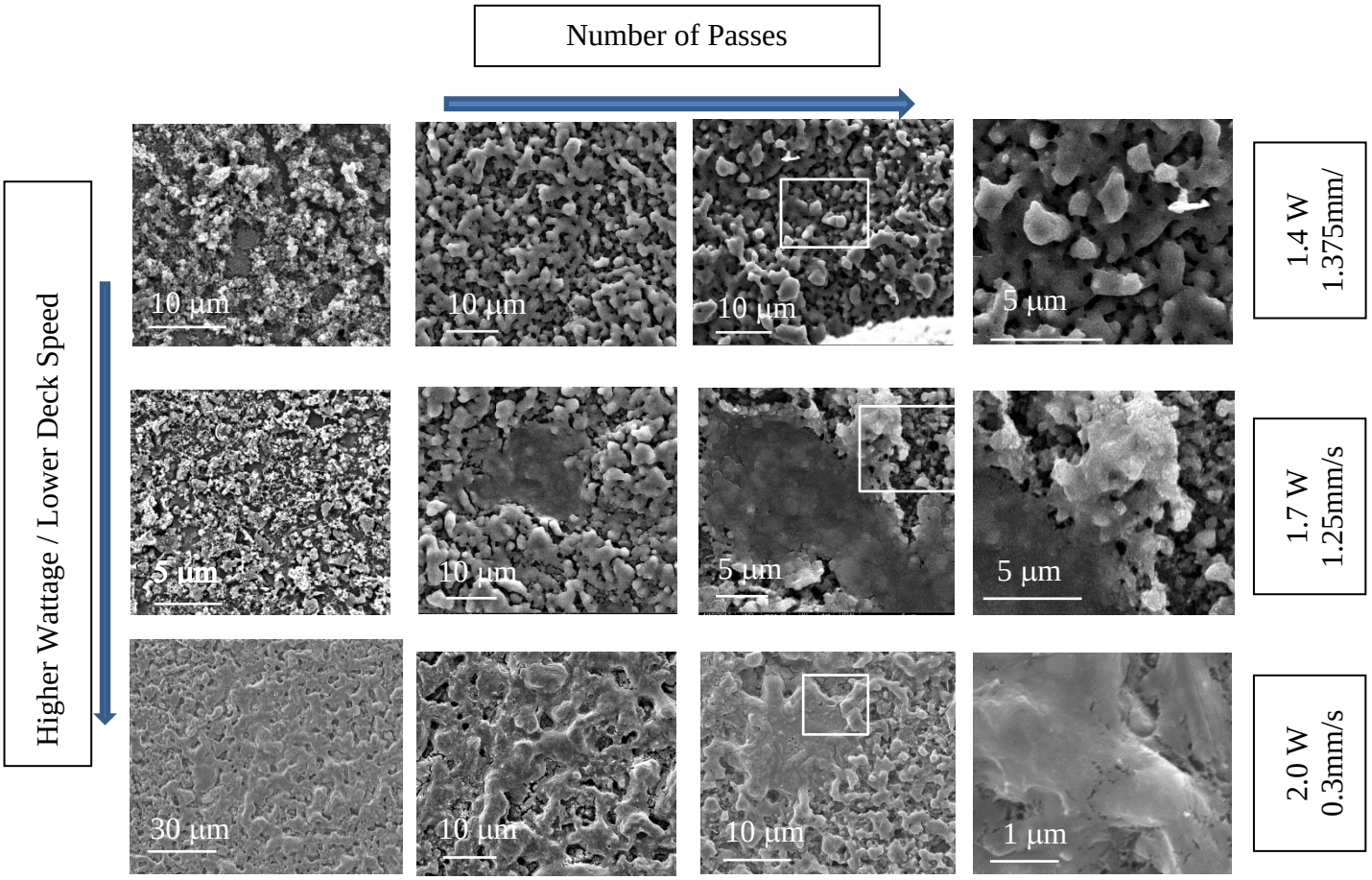

Figure 3.16: Microscopy results from Wattage vs. deck speed vs. number of passes

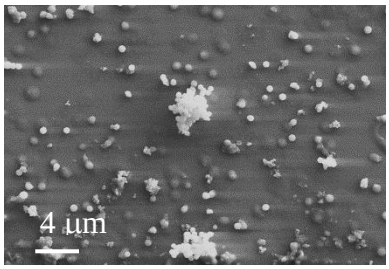

a. Poor deposition

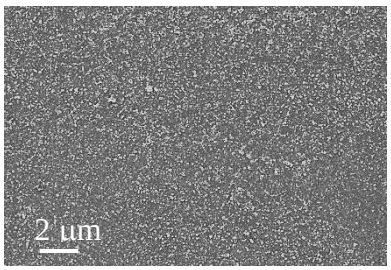

b. Mediocre deposition

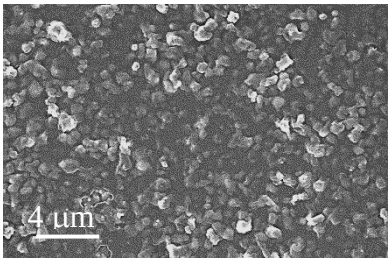

c. Excellent deposition

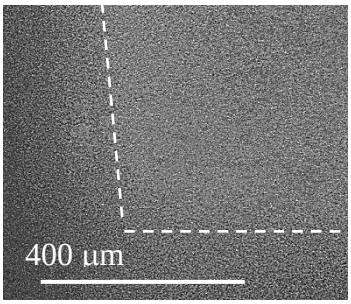

d. Over Spray: Dotted line represents area to be covered

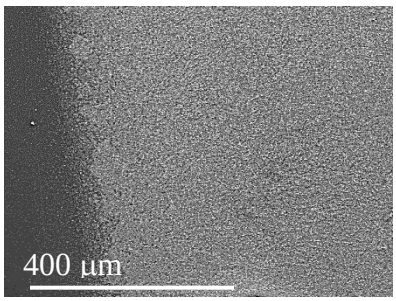

e. Marangoni

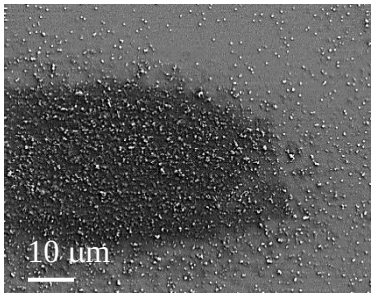

f. Over-spray: platen height issue

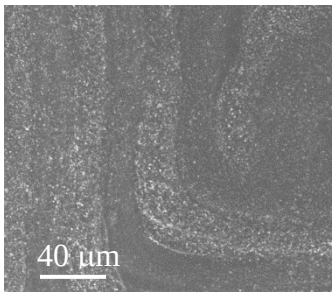

g. Over Deposition: Platen Speed Low, improper overlap %

Figure 3.17 (a-j): Defect Categorization and Main Factors

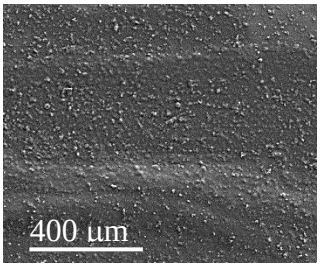

h. Over Deposition: Platen speed and sheath too low

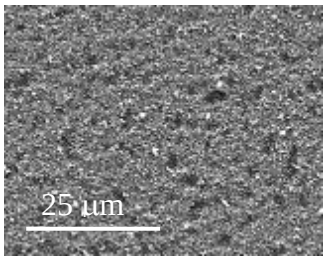

i. Porosity: Due to incomplete atomization

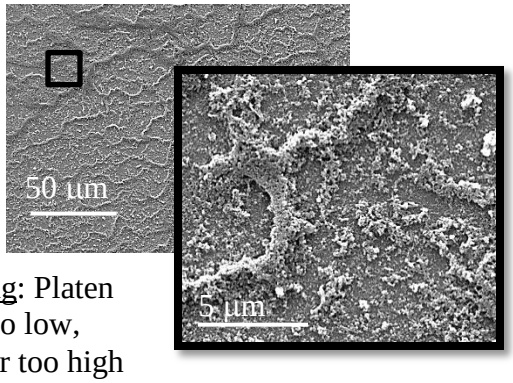

j. Veining: Platen Speed too low, Atomizer too high

3.3 Sodium Barium Titananate (NBT-BT)

Piezoelectric effect, first characterized and noted by the Curies, [109, 142] is associated with the production of electricity by squeezing or pressing. Thus, piezoelectricity can be defined as the ability of materials (crystals, ceramics and some polymers) to generate an electric field or potential as a result of an applied mechanical stress [1]. The applied stress results in a change in the materials volume, actuating a polarization density change. The converse effect in materials causes a stress and change in orientation of the crystal structure and volumetric changes when an external voltage is applied. Piezoelectric materials have been found extraordinarily useful for many of the common devices from sensor to transducer implementations. Further, production and detection of sound, generation of high voltage, ultrafine focusing of optical assemblies, microbalances and electronic frequency generation are primarily based on the principle of piezoelectric effect. It is also the basis of many scientific instrumental techniques with atomic resolution such as scanning probe microscopies such as AFM, STM, MTA, and SNOM. Piezoceramics have been used commercially since WWII, and experienced a much greater use since the last decade, most particularly due to the success of the incorporation of multilayer capacitor technology [143] Within the commercial realm, the most dominant piezoceramic has been lead zirconate titananate (PZT).

Concurrent with the development phase and exponential growth of the electronics industry, so to have the environmental concerns surrounding toxicity and lead pollution grown. With the increased use of PZT in electronic devices, added lead is released to the environment through calcination, the machining of the sintered parts, and PZT in spent devices through improper disposal. To counter environmental impact, European Union (EU), directives and legislature (in 2003 and 2006) has adopted the Waste Electrical and Electronic Equipment (WEEE) policy along with the restriction of hazardous substances (RoHS) to promote the transition and focus of finding a suitable replacement of PZT. Review articles describing these restrictions and efforts in fabrication, characterization of micro and nano-sized structures can be located here: [144-149]. Currently PZT is allowed through these restrictions imposed but in the advent of an alternative material suitable for these components, will be banned from use.

PZT belonging to a special class of perovskite structure oxides, exhibits many desired characteristics for functional applications including a desired morphotripc phase boundary

(MPB, the phase boundary which allows rearrangement of the crystal structure and change in shape) where in the figure of merit such as piezoelectric coefficients, dielectric permittivity, and coupling factors are maximized [142, 147]. PZT experiences a shape alteration or strain of 0.1 – 0.2% of original dimensions at 80 μm thicknesses [144, 147]. Further, suitable doping in PZT can enhance the piezoelectric coefficients as large as 779 pm/V [144]. PZT also has the notoriety of an elevated temperature regime (up to 175 ^{o}C and a Curie depoling temperature of 300-400 ^{o}C) where in the material can provide these properties, allowing applications to a variety of environments, along with the production of both hard and soft piezoelectrics [143, 150].

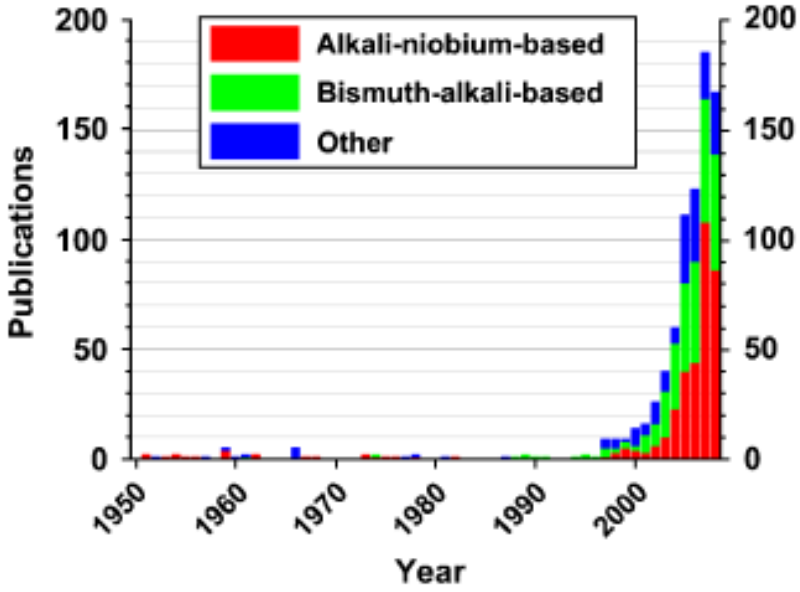

Figure 3.18: Publications on lead-free piezoceramics in refereed journals.

For the time range from 1950 to November 2008.

The search for an apt replacement has led to a variety of possible solutions. In the quest for viable alternatives, several items must be kept in mind, viz., the magnitude of the piezoelectric effect, temperature dependence, resonance frequency and available bandwidth. Beyond these major considerations, limitations are placed on materials based on intrinsic material characteristics such as crack initiation and propagation (usually related to Young's modulus). Additionally ease of production and cost per unit volume and in the case of aeronautical applications the cost of weight, as a lower piezoelectric effect will increase the weight of a component for the same force to that of a higher efficiency device. Among the possible candidates for replacements to PZT, sodium bismuth titananate (NBT) has emerged as a potential system.

Sodium Bismuth Titananate (NBT) is a well-known lead-free dielectric material with large dielectric constant. Nanostructures such as these are highly sought, however the synthesis of them is extremely challenging as the dimensional reduction most often results in cubic crystal structures and further compounds difficulties during high temperature processing by forming isotropic structures. Examples of this in literature show several variations of approach for anisotropic shape production notably these include: template-directed method [151], vapor phase synthesis[152], vapor-liquid-solid (VLS) growth[153], solution –liquid-solid (SLS) technique,[154] solvothermal synthesis,[155] solution phase growth based on capping reagents,[156] self-assembly,[157] and lithography[158].

As mentioned in the introduction of this chapter, all of the above include several steps, increased complexity and additional processes with which stringent controls need be held over for manufacturing and may not result in the net or near net shape of the final product, it is hoped that the AJP system would allow a work around to this issue. A recent study on molten salt synthesis of lead free 0.5Bi0.5TiO3-BaTiO3 (NBTBT) ferroelectric whiskers through a topochemical transformation using Na2Ti6O13 as a host structure was proven to be a highly cost effective method of producing a high purity, large volume of NBT [159, 160]. This method has been successfully used for synthesis of shape anisotropic ABO3 type perovskite using Aurivillius type PbBi4Ti4O15 and Bi4Ti3O12 oxides as host structure [19,20]. The development of a new powder (perverkosite) structure through 3D printing would be highly desirable.

Structure of Sodium Bismuth Titanate

This section briefly describes the structure of sodium bismuth titanate. Interested readers are referred to the bibliography for excellent references describing the structure, functionalities as well as mechanisms for power generation from these structures. Figure 3.19 shows the typical ABO_3 perovskite structure of cubic NBT system. The $Bi3^+$ and Na^+ of $Na_{0.5}Bi_{0.5}TiO_3$ (NBT) have standard effective charge of +3 and +1 respectively of (NBT) on A-site of the ABO_3 perovskite structure with rhombohedral symmetry [2]. The system demonstrates a large remnant polarization at room temperature and therefore considered as one of the prospective candidates for lead-free piezoelectric ceramic [3] 11].

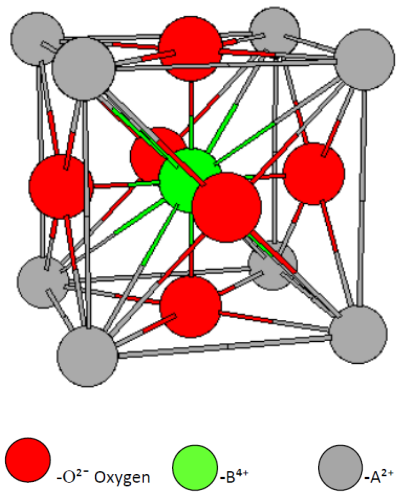

Figure 3.19: Perovskite Structure of Cubic NBT [3].

Doping in Sodium Bismuth Titanate

Because of the ABO_3 structure, NBT-BT has been subject of repeated tests for replacement atoms on one of the unit cell sites. These dopants and their concentrations within the matrix may possibly lead to the enhancement of its properties [144]. In ABO_3 perovskite structure both the A-site and B-site doping have been studied. Ba, Zr, Bi, La, Sr, K are examples of some dopants which affects different properties of NBT ceramics [13-17].

3.3.1 Experimental

The general experiment and ink preparation for NBT-BT progressed similar to the one outlined in section 3.2. In preparation of the NBT-BT inks, the seed crystals were prepared as in Mayura et. al. [159, 160] To further reduce the particulate size, they were ball milled for an additional 24 hours and allowed to remain in IPA overnight.

To select the smallest particles and grains, the top portion of the liquid was syphoned and filtered through 200# filter paper. The paper was removed from the funnel and allowed to dry. The powder was transferred to a sealable container reserving a portion of the powder to be analyzed by SEM to determine distribution of particle, (data not presented). After which, four separate ink bases were prepared from the list in Chapter 2 for use in the PA.

Previous studies on SOFC suggested that ceramics had realized a good success with a Terpineol based solution [72, 73]. From the compatible solvents listed in Chapter 2, it was known that Xylene is good candidate as a solvent. Tuning of the ink rheology would be accomplished by

varying the overall composition between Xylene and the other co-solvent, keeping in mind that Xylene has a high vapor pressure and is sometimes problematic within the transfer tube [75]. Ethylene Glycol was used as an evaporation reducer and held between 10-15%. These constructions were compromised of Xylene-Terpineol (X-T), X-T Di-H_2O, X-T-IPA and X-T – Acetone. They were mixed with varying concentrations of polyvinyl-acetate (PVA), Ethylene Glycol and 3% weight powder (Table 3.4). These solutions were placed in sealable containers with a magnetic stirring rod and allowed to mix over an 8 hour period at 300 rpm. The bottles were then removed from the stirring plates and observed for separation. Each container was tested over a 2 hour period or until sufficient separation was observed. A small amount (3 drops) was pipetted onto an inclined slide at approximately 30 degrees and allowed to dry.

Table 3.4: Final Ink Composition

Ink Constituent:	Percent Weight
NBT-BT	7%
PVA	0.5%
Ethylene Glycol	15%
Turpineol	52.5%
Xylene	25%

Once the primary solution was selected from the initial four, the main solvent constituents were varied at 10% intervals to arrive at an ink which was optimum for deposition, again relying as in previous work, on inclined drop test and spin coating observations at 300 rpm. From these results the best selection of ink based on low agglomeration, high consistency in serial testing and stability within solution was selected for use in the PA. Once the solution was finalized it was remixed for 1 hour at 300 rpm and 30 ml was directly transferred to the PAVI container. The PAVI was sealed with a magnetic stirring rod and installed onto the AJP. This container remained under constant stirring at 300 rpm to aid in suspension of particles.

Utilizing the same method outlined in previous work, a Taguchi L18 was used to determine the optimum settings for Main Affects, (Table 3.5). Once a suitable pattern for deposition and factor levels were arrived at, a separate Taguchi L-25 laser sintering experiment was devised and tested.

3.3.2 Results

Ink

From the initial analysis using SEM, it was observed that the particulate size was very close in standard deviation and largest particles observed were approximately 1 micron, smallest particles were on the order of 200 nm with most particles hovering at 500 nm. As such no further refinement on the particles was required for ink formulation.

Drop Test

The initial solutions showed the X-T solution performed the best; lowest agglomeration on inclined test, good suspension characteristics and good wetting on the slides. This solution was chosen to continue with the experiment. To test this solution, the ratio of Xylene to Terpineol was altered at 10% increments. It was observed that a continued increase of the ratio of xylene to Terpineol allowed smoother dry profiles for powder on the drop deposition as well as lower agglomeration rates. As it was known that Xylene can be a concern for evaporation within the transfer tube causing clogging a reasonable assumption that additional Xylene would produce diminishing returns and perhaps add deposition difficulties was made. The final solution was compromised of the levels set in Table 3.5.

Table 3.5: Final Deposition Settings for NBT-BT Ink

Final Deposition Settings:	
Tip Aperture-style	300 mm-long
Sheath	125-150 ccfm
Exhaust	190-217 ccfm
Deck Speed	4 mm/s
Virtual impactor	175
Platen Temperature	70
Z-Offset	4.5mm
Pattern Style	Raster
Layer Repeat	5 repeats

Initial testing in the PA showed very inconsistent deposition. Continued issues with nozzle clogging, tube condensation, over deposition and overspray were difficult to eliminate. Eventually, the largest tip aperture of 300 μm and uncharacteristically high flow rate with low

mass transfer (High Sheath and High Atomizer flow - Table 3.5) were able to produce stable depositions for 15-30 minutes after which the nozzle, tube, and jet system would have to be broken down cleaned and re-installed. Though these problems were difficult to deal with, patterns and shapes showed excellent resolution for lines with little to no overspray. Final deposition settings are listed below.

Sintering

Laser testing showed a high rate of fluctuations for proper settings. Over 100 tests were completed on varying thicknesses of films estimated at 10-300 μm in thickness of which none were completely successful. Energy densities were altered over a wide enough range producing samples appearing unaffected with no sintering taking place to consistent laser blow-outs on all portions of the trace line. In all cases where densification and sintering began, characteristic blow-outs could be viewed, and in most cases multiple sections were affected and the run was stopped prior to completion.

3.3.3 Discussion

Xylene and Terpineol solution seems to work exceedingly well for sustaining small particulates up to 1 micron in diameter of NBT-BT at solid contents up to 10%. In speaking with the manufacturer, 300 μm is the largest tip they produce and while they have had requests for larger sizes, they do not plan on production. As lower clogging was observed moving from 100 to 300 micron openings, it is rational to believe increasing this size would continue this trend. There was notable condensation within the tube and it is believed this is a function of the Xylene drying in the tube and allowing particles to disrupt the air flow both within the transfer tube and the deposition head. Increasing Turpineol may reduce this issue, additionally switching to the PFTE tube which was not an option for this experiment may provide a longer run time. Further using a bubbler where the dry N_2 gas is run through first to saturate it with Xylene may also aid. In all, the deposition rate allowed for close to 40-50 patterns to be printed at one time before deleterious effects were noted.

In addition to the above physical indications of processing issues, fluctuations in deposition gauges for flow rate were noted. No known temperature or humidity issues should affect this as it is a closed system. Tanks were checked for pressure and fill. All were found to be within

specifications and more than ½ full. Apertures for deposition were cleaned and inspected via an optical microscope. It is theorized that the main culprit was the evaporation of xylene in the tube which Optomec has also agreed with. Additional EG was added to the solution at up to 5% additional by weight, but did not eliminate this issue.

Laser Sintering

The most interesting part of these failures is the seeming cascade sintering to exponential levels within the samples at any indication of sintering initiation. After several iterative experiments, it was observed that the direction of these conditions was resulting in a better finish and color closer to that of properly sintered NBT-BT. It is believed this can be overcome with a full-factorial experiment with 4 levels per factor within the following boundary conditions.

Table 3.6: Recommended Laser Settings Design of Experiments

Laser Power	1.0W	1.3W
Speed	0.5mm/s	1.0 mm/s
Layer	4	5
Trace Width	0.001	0.002
Percent Overlap	5%	10%

However it should not necessarily be expected to result with the same grain-boundaries as in samples produced by furnace heating. Several others have noted that ceramics, and piezoelectric ceramics do not have the same grain formations after undergoing a laser sinter. These results are most likely because of the short time frame reactions take place and driving forces for diffusion, kinetics and re-solidification. Additionally, the NBT-BT system is quite complex elementally. Sodium individually has a low melting temperature, hovering just above 200^{o}C and can react with oxygen readily as well as water [161]. Bismuth is also reactive with oxygen and has four separate morphotrophs, two of which are close to the melt temperature of sodium [162].

3.4 Al-Si

Aluminum alloys with high silicon content have captivated many due to their high wear resistance, lightness, high corrosion resistance and low thermal expansion. As an example, NASA has shown the promise of an Al-Si composite alloy capable of being utilized as pistons in two-stroke engines (MSFC- 398 hypereutectic and eutectic MSFC-388) [ref]. These engines run in excess of 700 degrees and the pistons are subjected to the extreme forces of explosions. They have shown excellent resistance to thermal expansion hold superior numbers in tensile and fatigue testing. Both alloys can provide three to four times the tensile strengths of conventional alloys test at 600°F-800°F for more than 100 hrs. Below are images for both alloys.

7].

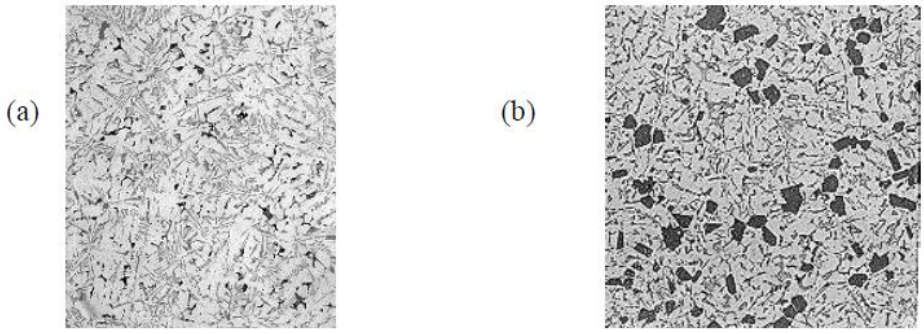

Figure 3.20: Microstructures of Eutectuc abd Hpereutectuc Al-Si

(a) Eutectic and (b) Hypereutectic Aluminum-Silicon Alloy 398

Other automotive manufacturers in pursuit of lighter engine blocks with increased durability and low weight utilizing the A390 composition [163]. Casting of high silicon Al-Si alloys (greater than 17% Si) generates large degrees of segregation and coarse microstructures due to the low rates of solidification. Hypereutectic aluminum–silicon alloys offers the possibility of an in situ natural composite (the silicon acting as the reinforcing phase) with properties that make them attractive for a number of automotive applications. However, conventional casting techniques result in excessive growth of the silicon particles in the melt, which adversely affects the mechanical properties. Thixoforming allows hypereutectic Al–Si alloys containing 40–50% fraction liquid to be shaped into complex near net shape components, whilst keeping the silicon particle size quite fine [163]. Proposed and successful solutions to casting problems with ingot

casting of hypereutectic Al-Si alloys (including those of Al, Si, Zr, Cu, Mg, Fe and Ni) have been in the direction of rapid solidification processing such as spray, weld, and chill methods.

One recent paper investigated microstructure and property modifications of Al–12.6Si alloy induced by high current pulsed electron beam (HCPEB) treatment, while operating at a higher energy density than traditional lasers, this treatment may offer some insight to the possibilities of heat-treatment of an already cast structure [164] and to the possibility of deriving a microstructure during 3D processes. Characterization results show a refined grain structure and gradient approximately 10 μm thick. Further testing illustrated a 2.5 factor of strengthening due to this finer grain. As with previous suggestions, 3D printing with SLS may offer some insights to alternative solutions. As outlined below proposals show the potential of the AJP system for the solution to this problem:

Recuperators for Aircraft:

Recuperators provide the necessary boost in thermodynamic efficiency to make gas turbine engines competitive with other propulsion systems. To match the thermal efficiency of diesel or natural gas reciprocating engines, small gas turbine engine pressure and hot section temperatures must be taken higher, requiring the recuperator to take on an even higher thermal-mechanical load. To make the lifecycle cost of recuperated gas turbines comparable, the unit cost must be reduced.

The relative gap sizes, leakage flows and aerodynamic losses of small engines cause gas turbines to be passed over for diesel or natural gas alternatives. Typical thermal efficiencies of simple cycle gas turbine engines are on the order of 20% [4]. To realize the weight and maintenance savings of a gas turbine, thermal efficiencies of 30% are required. Thermal efficiencies of this level in a simple cycle gas turbine make a recuperator a necessity. The recuperator utilizes the hot exhaust to pre-heat the compressor air, requiring less fuel consumption. To achieve a thermal efficiency in excess of 40%, Turbine inlet temperatures in excess of even exotic metal alloy operating limits are required.

Beyond a recuperator, small gas turbine engine designers are left with two primary alternatives, viz., higher pressure, or higher temperature. With small gas turbines, additional compressors to drive the pressure ratio higher can cause a disproportionate trade-off between performance and

weight. Higher temperatures necessitate exotic materials or complex film cooling geometry. Film cooling is not an option for most small engines so material has been a large focus of research. Traditional metals reach their lifetime operating limit around 750^{o}C [5]. After which super alloys and exotic materials are required which lead to increased materials cost. Ceramic materials have been investigated by previous researchers, but the main deterrents are identification of acceptable materials and ease of manufacturing. Primary surface heat exchangers provide the greatest density but can be painstaking to machine. Methods have been proposed to produce metallic recuperators quickly and continuously but not without issues. The mass production of ceramic recuperators presents even greater issues.

Recuperators of both Composite Metal Ceramic (CMC) and metal-alloy have been fabricated previously. The current designs and methods of fabrication has a long history of problems ranging from durability to leakage, undoubtedly due to the complex manufacturing methods and materials used in them.

As examples several current studies rely on a few old manufacturing methods to construct the complex parts. These include the ability to tape cast individual layers and subsequently serially stack / assemble and then sinter the combined unit, individually machine each layer and conduit matrix with final assembly taking place with welding one stack upon the next and finally constructing a ceramic matrix around a metal mesh by spray adhesion and heat treatment [6-8].

It is no wonder the parts have failed to live up to expectations; the parts are small and delicate requiring care in handling and assembly, the final product is complex and the methods of attachment do not allow nor lead to proper inspection and sound attachment as many are hidden. These issues arise in reduction of operating parameters; temperature resistance, longevity, repeatability, operating efficiency and the like.

3.4.1 Opportunity

As all of the above methods have proven to be inadequate for the employment within gas turbine engines due to leakage, structural compromises and longevity issues, our proposal entails a novel method of fabrication for a CMC recuperator. The method and results herein describe the deposition and sintering of a CMC powder contained within a liquid carrier, treated through laser sintering in ambient environment to create a complete 3d structure from the top-down with controllable depth and high aspect ratio resolution [9].

The main issue in the utilization of these materials for this purpose has been the problem of manufacturability: These materials are available in powder form and generally lend themselves to casting scenarios; it is difficult to make them into the complex shape of a recuperator efficiently and elegantly. In a literature search, it was discovered that there has already been investigation to the absorption spectrum and electron band-gap of Al-Si/Al-Cxx (Aluminum-Silicon-Carbide) alloys. It has been shown that use of a CO or YAG laser would properly heat and sinter Al-Si material. As this laser exists already and the system is well understood, it could be incorporated to a system like the AJP and be used to clear the current boundaries that exist [11]. Alternatively, Optomec revealed results of an Aluminum ink developed by Nanotech. Data from the material shows the following material characteristics for electronics use. Detailed information from SEM and other characterization shows that the main issue with high density of this material is the growth of aluminum-oxide and the resultant higher temperature needed to melt these grains. Previous work with boron has shown a marked reduction in oxidization during SLS with the implementation of a shielding gas box, and it is reasonable to speculate this would enable a more complete sinter of the material.

While an 830nm CW laser is ineffectual on Si because of the band gap in Silicon eliminates absorption at that wave length, several other papers have shown the promise of using the surrounding matrix to melt and create alloys with another material which is unaffected by the laser due to conductive heating [98, 99]. For this case, it is already known a supply of Si nanoparticles in the size order of 4-9nm exists from a laboratory in Korea. The proposed investigation would entail using the Nano-tech ink (a known and customizable Al solids loading content of 20-40%) and using an addition of Si nanoparticles to arrive at the proper percentages. Optimization of the green film and laser sintering would proceed as outlined previously. For elimination of oxides, use of the laminar gas shielding box would be necessary. The difficulty for the completion of the above rests with the nearly insurmountable hurdle of printing a “roof”. As the Optomec was designed to print on a supportive substrate, another suitable printing material for support that would be removed at a later date would be difficult to produce and several aspects of the machine would present difficulties to this challenge. The main premise for solution would be to print a water soluble or low temperature polymer ink which would be dissolved after completion of the part. These can be found in a variety of areas and are currently used in practice. Alternatively, because it is easy to calibrate and set-up times are low, the part

could be moved between each later, rotating the roof plane from a horizontal member to a vertical member, eliminating this issue. A second alternative might be to install a multi-head printing unit if there is a compatible one for this machine.

Time constraints limited further investigation to this proposal.

3.5 PVDF

With the discovery of piezoelectricity in polyvinylidene fluoride (PVDF) by Kawai in 1969, a flexible, highly processable material was introduced. Until that time, piezoelectrics were within the realm of highly brittle structures [30]. The desirable mechanical properties of PVDF are the result of its semicrystallinity (roughly 50%) and low glass transition temperature of -40 °C. The aliphatic repeat unit (CH_2-CF_2) allows for two dominant crystalline phases, referred to as α and β. As shown in Figure 3.21, the α phase has a Trans-Gauche-Trans-Gauche' (TGTG') confirmation, with the chains arranging in a centrosymmetric unit cell, resulting in an antipolar crystal. The β phase is an all trans (TTTT) planer zigzag confirmation that results in a noncentrosymmetric crystal [165]. The alternating fluorine and hydrogen groups on the PVDF backbone allow for a large dipole moment in the β phase crystalline region when electrically poled, resulting in stable polarization and piezoelectricity.

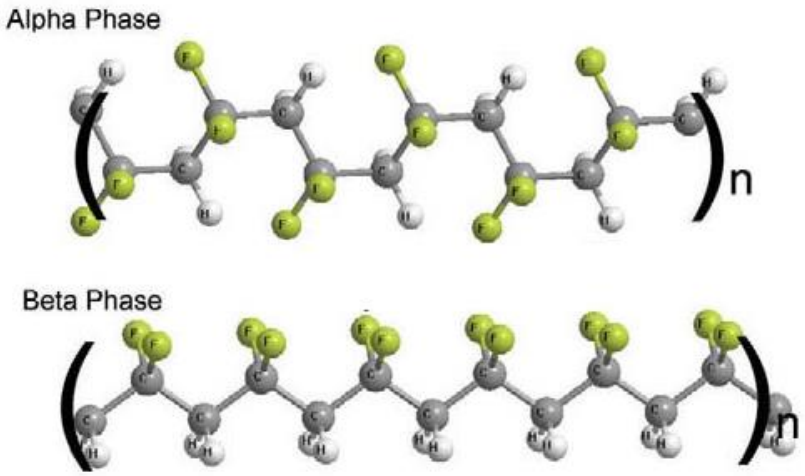

Figure 3.21: Structure of α Phase (left) and β Phase (right) PVDF

Values as high as d_{31} = 30 pC/N for uniaxially drawn samples have been attained in PVDF [166]. More recently, polymers such as odd numbered nylons and aliphatic and aromatic polyuria have

been found to possess piezoelectricity slightly lower than PVDF [167],[168]. These piezoelectric polymers, generally referred to as electroactive polymers (EAPs), offer elastic compliance and low dielectric impedance, resulting in efficient energy conversion and large mechanical actuation in response to electrical stimuli. Due to these desirable properties, EAPs to be incorporated into a broad range of applications such as actuators, integrated microelectromechanical systems, sensors, and ferroelectric memory devices [169]. EAPs also show small acoustic impedance on the scale of water and human tissue, making them useful for hydrophonics and ultrasonic imaging. However, low voltage and force generation capabilities have greatly limited their use [170].

In order to improve the properties of polymers, Newnham et. al introduced an electroactive composite material in which piezoelectric ceramic particles were dispersed into a passive polymer [171]. Composites such as these have gained popularity since they combine the processability and low mechanical impedance of polymers with the high piezoelectric performance and dielectric constant of ceramics. By adjusting the parameters of these materials, the stiffness, dielectric constant, and piezoelectric response can be optimized for specific applications [172]. These materials, however, are not without drawbacks, requiring high ceramic loading levels around 50% and the large particle size (generally micrometer) creates stress points that lead to mechanical weakness and early failure when cycled [170]. The requirement of large poling voltages for ceramics also leads to a polarization inhomogeneity of the material and inconsistent performance [173],[174].

Alternatively, nanoparticles can be added into an EAP matrix to improve material properties such as elastic moduli and dielectric behavior while retaining the properties of the host material. Carbon nanotubes (CNTs), due to their electrical conductivity, thermal stability, and high mechanical strength, have been used to improve piezoelectric performance of composites in the past [175]. Additionally, the high aspect ratio of CNTs (1000-10000) make them very effective at loading levels below 1 wt%, allowing for a large increase in force generation capabilities and charge storage while retaining the EAPs advantageous qualities [170],[176]. Past experimentation on the effect of adding CNTs into EAPs has focused on mechanical improvements such as increasing the Young's Modulus, however, no thorough mechanism of piezoelectric enhancement has been reported [177].

In a recent collaboration with UT Dallas, composites of single walled carbon nanotubes (SWNTs) and Buckminster Fullerene (C_{60}) with PVDF were fabricated via screw extrusion methods. Analysis showed piezoelectric enhancement, charge storage, morphology changes and charge release within the material. One of the least understood phenomena with the AJP machine is conformation of polymer and ability to print. The difference in size and geometry (shown in Figure 3.22) of SWNTs and C_{60}, while possessing similar structure and electrical properties, allowed for a useful comparison to be made, and mechanisms of enhancement illustrated.

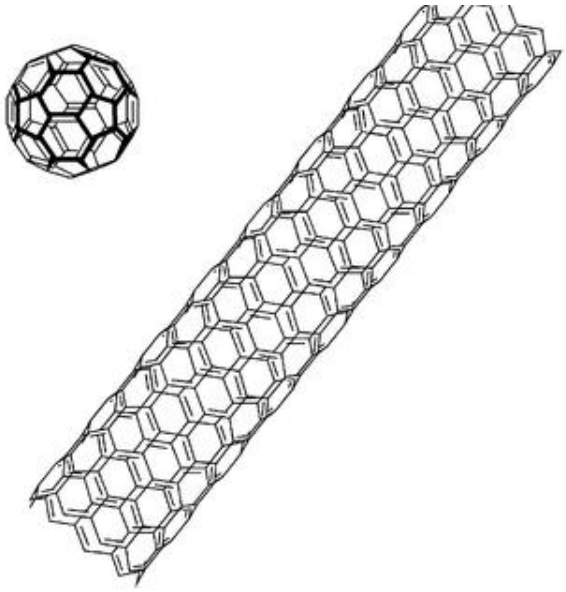

Figure 3.22: Structure of C60 (left) and SWNT (right)

Reported within was the result of twice the performance of pure PVDF, roughly 60 pC/N. While this experiment was based on the atypical screw extrusion process, an alternative method is presented here.

3.5.1 Experimental

Optomec has been demonstrated that PVDF can be dissolved in NMF (15% vol./vol.) and DMF (85% vol/vol.) and 2% wt Kynar powder. The solution can be dispenced onto the substrate using the outlined procedure in previous sections using the PAVI at a sheath 175 ccfm and atomizer flow rate of 160 ccfm. Previously, Optomec has shown the ability to print a 100mm thick PVDF sample on a glass slide along with the necessary electrodes. As proper transformation to the aligned crystalline phase is necessarily provided by uniaxial stretching under heated conditions,

the above process would not have produced a piezoelectric response. Instead, the sample must be removed either by blade, dissolution of the substrate or other means and then follow the below procedure. Attempts were made within the lab to remove samples from the glass substrates using a razor-blade but failed removal without serious damage.

In previous work in a combined effort between UT-Dallas and Virginia Tech samples were drawn using a custom designed and fabricated variable speed stretching system, Figure 3.23. The rack can be used to pull PVDF samples of variable dimensions (25-40mm wide, 25mm-100mm long, 50-150 micron thick).

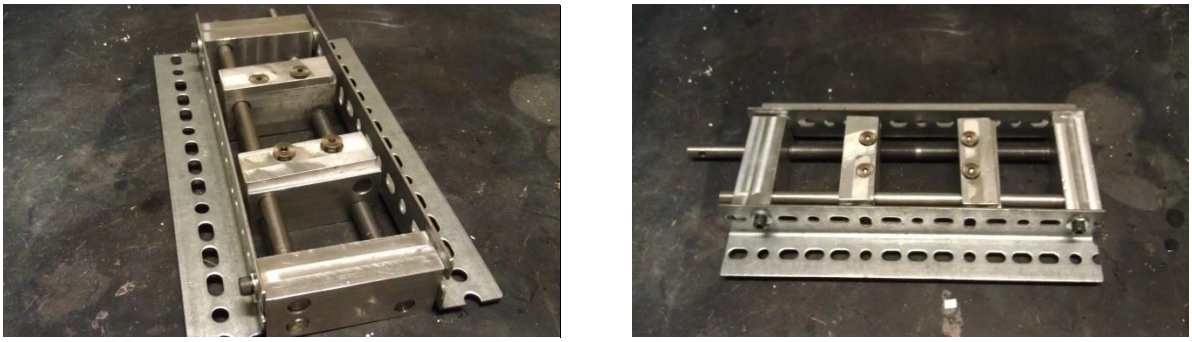

Figure 3.23: Variable Speed Stretching Rack

Blanks approximately 62.5cm x 25cm were drawn to 400%-500% their original length on a heated platform at 80 °C. Samples were roughly 50 μm in thickness after drawing and cleaned then electrode with gold with a Ladd vapor deposition system. They were then poled at 20 kV/m at 80 °C for twenty minutes in a high dielectric liquid (Silicon Oil) and rapidly quenched to room temperature while remaining under voltage.

Table 3.7: PVDF Sample Stretching and Poling Treatment

Sample	1	2	3	4	5	6
Percent Elongation	3.8	4	4	4	4	4
Stretching Rate	1.25mm/s	1mm/s	1.25mm/s	1.25	1.25	1.25
Temperature at Stretch	70	80	90	70	80	90
Poling Temperature	80	80	80	80	80	80
Poling Voltage	20MV/m	20MV/m	20MV/m	20MV/m	20MV/m	20MV/m

It has been demonstrated that through the addition of SWNTs and C_{60} to PVDF at under 0.25 wt%, the piezoelectric coefficient d_{31} can be enhanced to double that of pure PVDF. This is

achieved through a multi-mechanistic enhancement involving the seeding of crystalline sites, creation of internal charge, increased polarization, and the optimization of Young's modulus and dielectric constant. The calculated electromechanical coupling coefficients (k_{31}) at optimal loading levels are 1.84 and 2 times greater than pure PVDF for the PVDF-C_{60} and PVDF-SWNT composites.

3.5.2 Results

It is unfortunate that time did not allow completion of this portion of the experiments, as the only remaining hurdle was the step of removal from the substrate without damage. One proposed method for the success could be to use a water soluble substrate (as PVDF is quite a robust polymer). Once the film is removed, it could be drawn as in previous work. The singular unknown of the process remains as to what density and or porosity will the sample possess. In the case of obviously undesirable porosity, a possible solution of continued heating of the platen at temperatures above the glass transition for PVDF may result in a more desirable sample. Alternatively, vacuum forming the sample may show promise as well. However, the second suggestion would not be desirable as it adds an additional step to the process.

References Chapter 3

1. Mirfakhrai, T., J.D.W. Madden, and R.H. Baughman, Polymer artificial muscles. Mater. Today (Oxford, U. K.), 2007. 10(Copyright (C) 2012 American Chemical Society (ACS). All Rights Reserved.): p. 30-38.

2. Eric Savitz, Manufacturing The Future: 10 Trends To Come In 3D Printing. Forbes, 2012(http://www.forbes.com/sites/ciocentral/2012/12/07/manufacturing-the-future-10-trends-to-come-in-3d-printing/).

3. Wadhwa, V., The End of Chinese Manufacturing and Rebirth of U.S. Industry. Forbes, 2012(http://www.forbes.com/sites/singularity/2012/07/23/the-end-of-chinese-manufacturing-and-rebirth-of-u-s-industry/).

4. Hopkinson, N., Additive Manufacturing: What's happening and where are we going with printing in the third dimension? Word Document available at http://www. Becta. org. uk, 2010.

5. Campbell, I., D. Bourell, and I. Gibson, Additive manufacturing: rapid prototyping comes of age. Rapid Prototyping Journal, 2012. 18(4): p. 255-258.

6. Optomec. Revolutionary "Smart Wing" Created for UAV Model Demonstrates Groundbreaking Technology 2013; Available from: http://www.optomec.com/site/newsletter/news112.

7. Olson, P. Airbus Explores Building Planes With Giant 3D Printers - Updated With Video. Forbes 2012 [cited 2012 7-11-2012]; TECH:[

8. Levy, G.N., R. Schindel, and J.-P. Kruth, Rapid manufacturing and rapid tooling with layer manufacturing (LM) technologies, state of the art and future perspectives. CIRP Annals-Manufacturing Technology, 2003. 52(2): p. 589-609.

9. Cable, J., GM, Ford and Chrysler Get Big Chunk of Advanced-Vehicle Funding. http://www.industryweek.com/global-economy/gm-ford-and-chrysler-get-big-chunk-advanced-vehicle-funding, 2011.

10. Anonymous, All together now; Collaborative manufacturing, in The Economist2012, The Economist Intelligence Unit: London. p. 18-19.

11. Maxey, K., IBM Sees 3D Printing Changing Manufacturing. http://www.engineering.com/3DPrinting/3DPrintingArticles/ArticleID/5478/IBM-Sees-3D-Printing-Changing-Manufacturing.aspx, 2013.

12. Wohlers, T., Additive Printing Technology. MoldMaking Technology, 2012.

13. Gibson, I., D.W. Rosen, and B. Stucker, Additive manufacturing technologies: rapid prototyping to direct digital manufacturing. 2010: Springerverlag Us.

14. Cooper, K.G., Rapid prototyping technology: selection and application. 2001: Marcel Dekker, Inc.

15. Kruth, J.-P., Material incress manufacturing by rapid prototyping techniques. CIRP Annals-Manufacturing Technology, 1991. 40(2): p. 603-614.

16. Noorani, R., Rapid prototyping. 2006: Wiley.

17. Jamieson, R. and H. Hacker, Direct slicing of CAD models for rapid prototyping. Rapid Prototyping Journal, 1995. 1(2): p. 4-12.

18. Roscoe, L., Stereolithography interface specification. America-3 D Systems Inc, 1988.

19. Specification, S.I., The STl Format. Valencia, CA: 3Dsystems Inc, 2000.

20. Halloran, J.W., et al., Photopolymerization of powder suspensions for shaping ceramics. Journal of the European Ceramic Society, 2011. 31(14): p. 2613-2619.

21. Sachs, E., M. Cima, and J. Cornie, Three-dimensional printing: rapid tooling and prototypes directly from a CAD model. CIRP Annals-Manufacturing Technology, 1990. 39(1): p. 201-204.

22. Kruth, J.-P., M. Leu, and T. Nakagawa, Progress in additive manufacturing and rapid prototyping. CIRP Annals-Manufacturing Technology, 1998. 47(2): p. 525-540.

23. Chua, C.K., K.F. Leong, and C.C.S. Lim, Rapid prototyping: principles and applications. 2010: World Scientific Publishing Company.

24. Burns, M., Automated fabrication: improving productivity in manufacturing. 1993: Prentice-Hall, Inc.

25. Pham, D. and R. Gault, A comparison of rapid prototyping technologies. International Journal of Machine Tools and Manufacture, 1998. 38(10-11): p. 1257-1287.

26. Wong, K.V. and A. Hernandez, A Review of Additive Manufacturing. ISRN Mechanical Engineering, 2012. 2012.

27. Shivpuri, R., et al., Evaluation of 3D printing for dies in low volume forging of 7075 aluminum helicopter parts. Rapid Prototyping Journal, 2005. 11(5): p. 272-277.

28. Systems, E.d.p. e-Manufacturing Systems. Available from: www.EOS.com.

29. Systems, d. Stereolithography and selective laser sintering machines. Available from: http://www.3dsystems.

com.

30. Systems, d. ZCorp Systems. Available from: http://www.zcorp.com/en/home.aspx.

31. Soligen. Available from: http://www.soligen.com.

32. Sachs, E., Three dimensional printing, 2001, DTIC Document.

33. Pfister, A., et al., Biofunctional rapid prototyping for tissue-engineering applications: 3D bioplotting versus 3D printing. Journal of Polymer Science Part A: Polymer Chemistry, 2004. 42(3): p. 624-638.

34. Lipke, D.W., et al., Near net-shape/net-dimension ZrC/W-based composites with complex geometries via rapid prototyping and Displacive Compensation of Porosity. Journal of the European Ceramic Society, 2010. 30(11): p. 2265-2277.

35. Tang, H.-H., M.-L. Chiu, and H.-C. Yen, Slurry-based selective laser sintering of polymer-coated ceramic powders to fabricate high strength alumina parts. Journal of the European Ceramic Society, 2011. 31(8): p. 1383-1388.

36. Salmoria, G.V., et al., Microstructural and mechanical characterization of PA12/MWCNTs nanocomposite manufactured by selective laser sintering. Polymer Testing, 2011. 30(6): p. 611-615.

37. Kruth, J.-P., et al., Binding mechanisms in selective laser sintering and selective laser melting. Rapid Prototyping Journal, 2005. 11(1): p. 26-36.

38. Taminger, K.M. and R.A. Hafley. Electron beam freeform fabrication: a rapid metal deposition process. in Proceedings of the 3rd Annual Automotive Composites Conference. 2003.

39. Liu, Z., et al. Selective laser sintering of high-density alumina ceramic parts. in Proceedings of the 35th International MATADOR conference. 2007. Springer.

40. arcam. Electron beam welding. 2012; Available from: www.arcam.com.

41. Exner, H., et al., Laser micro sintering: A new method to generate metal and ceramic parts of high resolution with sub-micrometer powder. Virtual and physical prototyping, 2008. 3(1): p. 3-11.

42. Murr, L.E., et al., Metal fabrication by additive manufacturing using laser and electron beam melting technologies. Journal of Materials Science & Technology, 2012. 28(1): p. 1-14.

43. Kummailil, J., Process Models for Laser Engineered Net Shaping, 2004, WORCESTER POLYTECHNIC INSTITUTE.

44. Balla, V.K., S. Bose, and A. Bandyopadhyay, Processing of bulk alumina ceramics using laser engineered net shaping. International Journal of Applied Ceramic Technology, 2008. 5(3): p. 234-242.

45. Liao, Y., H. Li, and Y. Chiu, Study of laminated object manufacturing with separately applied heating and pressing. The International Journal of Advanced Manufacturing Technology, 2006. 27(7-8): p. 703-707.

46. LENS System. 2012; Available from: www.optomec.com.

47. Atwood, C., et al., Laser engineered net shaping (LENS (TM)): A tool for direct fabrication of metal parts, 1998, Sandia National Laboratories, Albuquerque, NM, and Livermore, CA.

48. Corp, K.; Available from: www.kiracorp.co.jp/EG/pro/rp/top.html

49. dimensions, S. Solido Machine. Available from: www.solidimension.com

50. Vaupotič, B., M. Brezočnik, and J. Balič, Use of PolyJet technology in manufacture of new product. Journal of Achievements in Materials and Manufacturing Engineering, 2006. 18(1-2).

51. Fab@home. Available from: www.fabathome.org.

52. Reprap.

53. Facchini, L., et al., Microstructure and mechanical properties of Ti-6Al-4V produced by electron beam melting of pre-alloyed powders. Rapid Prototyping Journal, 2009. 15(3): p. 171-178.

54. Grimm, T., User's guide to rapid prototyping. 2004: Sme.

55. Kim, H., J.-W. Choi, and R. Wicker, Scheduling and process planning for multiple material stereolithography. Rapid Prototyping Journal, 2010. 16(4): p. 232-240.

56. Szilvśi-Nagy, M. and G. Matyasi, Analysis of STL files. Mathematical and Computer Modelling, 2003. 38(7): p. 945-960.

57. Wohlers, T., Wohlers Report, 2009, Fort Collins, Colorado, USA: Self. www. wohlersassociates. com.

58. <Capillary-Assembled Microchip for Universal.pdf>.

59. Singh, R., Process capability study of polyjet printing for plastic components. Journal of mechanical science and technology, 2011. 25(4): p. 1011-1015.

60. Petrovic, V., et al., Additive layered manufacturing: sectors of industrial application shown through case studies. International Journal of Production Research, 2011. 49(4): p. 1061-1079.

61. Prinz, F.B. and L.E. Weiss, Novel applications and implementations of shape deposition manufacturing. Naval research reviews, 1998. 50: p. 19-26.

62. Martinez, A.W., et al., Programmable diagnostic devices made from paper and tape. Lab Chip, 2010. 10(19): p. 2499-504.

63. Whitesides, G.M., The origins and the future of microfluidics. Nature, 2006. 442(7101): p. 368-73.

64. Glunz, S., High-efficiency crystalline silicon solar cells. Advances in OptoElectronics, 2007. 2007.

65. Jain, K., et al., Flexible electronics and displays: High-resolution, roll-to-roll, projection lithography and photoablation processing technologies for high-throughput production. Proceedings of the IEEE, 2005. 93(8): p. 1500-1510.

66. Lankelma, J., et al., Paper-based analytical device for electrochemical flow-injection analysis of glucose in urine. Anal Chem, 2012. 84(9): p. 4147-52.

67. Martinez, A.W., et al., Patterned paper as a platform for inexpensive, low-volume, portable bioassays. Angew Chem Int Ed Engl, 2007. 46(8): p. 1318-20.

68. Martinez, A.W., S.T. Phillips, and G.M. Whitesides, Three-dimensional microfluidic devices fabricated in layered paper and tape. Proc Natl Acad Sci U S A, 2008. 105(50): p. 19606-11.

69. Sachs, E., M. Cima, and J. Cornie, Three-Dimensional Printing: Rapid Tooling and Prototypes Directly from a CAD Model. CIRP Annals - Manufacturing Technology, 1990. 39(1): p. 201-204.

70. Xiong, Z., et al., Fabrication of porous scaffolds for bone tissue engineering via low-temperature deposition. Scripta Materialia, 2002. 46(11): p. 771-776.

71. Mironov, V., G. Prestwich, and G. Forgacs, Bioprinting living structures. J. Mater. Chem., 2007. 17(20): p. 2054-2060.

72. Sukeshini, A., et al., Aerosol Jet Printing and Microstructure of SOFC Electrolyte and Cathode Layers. ECS Transactions, 2011. 35(1): p. 2151-2160.

73. Sukeshini, M.A., et al. Aerosol Jet Deposition for SOFC Fabrication. in Meeting Abstracts. 2010. The Electrochemical Society.

74. Optomec, AJ300 User Manual. 2011.

75. Optomec, M.R. New and Developing materials fof Ink Formulations

2011.

76. Aliseda, A., et al., Atomization of viscous and non-newtonian liquids by a coaxial, high-speed gas jet. Experiments and droplet size modeling. International Journal of Multiphase Flow, 2008. 34(2): p. 161-175.

77. Chhabra, Bubbles, Drops, and Particles in Non-Newtonian Fluids, Second Edition. Taylor and Francis, 2007.

78. Orzechowski, L.P.B.a.Z., Liquid Atomization Taylor and Francis, 1993.

79. Roman, M. and F. Navarro, Deposition of Cellulose Nanocrystals by Inkjet Printing. 2010. 1019: p. 157-171.

80. Utela, B., et al., A review of process development steps for new material systems in three dimensional printing (3DP). Journal of Manufacturing Processes, 2008. 10(2): p. 96-104.

81. <Schultz_Disertation.pdf>. 2005.

82. Hu, J.-B., Y.-C. Chen, and P.L. Urban, Coffee-ring effects in laser desorption/ionization mass spectrometry. Analytica Chimica Acta, 2013. 766(0): p. 77-82.

83. Choi, S. and S. Samavedam, Modelling and optimisation of rapid prototyping. Computers in industry, 2002. 47(1): p. 39-53.

84. Syms, R.R., et al., Surface tension-powered self-assembly of microstructures-the state-of-the-art. Microelectromechanical Systems, Journal of, 2003. 12(4): p. 387-417.

85. Folgar, C.E., C. Suchicital, and S. Priya, Solution-based aerosol deposition process for synthesis of multilayer structures. Materials Letters, 2011. 65(9): p. 1302-1307.

86. <Optomec - AFRL - AJ Printing of SOFCs - JUN10.pdf>.

87. Nanotech, A. Aluminum Nano Ink. 2012; Available from: http://www.appliednanotech.net/tech/conductive_inks.php.

88. <laser sintered barium titaninate.pdf>.

89. .

90. <powder densification maps SLS.pdf>.

91. <Schultz_Disertation.pdf>.

92. Kingery, W.D.B., H. K.; Uhlmann, Donald R. , Introduction to Ceramics (2nd ed.). John Wiley & Sons, Academic Press. I, 1976.

93. <Sonicator_nanotechnology_applications.pdf>.

94. Nelson, J.C., et al., Model of the selective laser sintering of bisphenol-A polycarbonate. Industrial & Engineering Chemistry Research, 1993. 32(10): p. 2305-2317.

95. Rahaman, M.N., Ceramic processing. 2007: CRC Press.

96. <4777014_Process_for_preparing_self_suppo.pdf>.

97. Townes, C.H., A Century of Nature: Twenty-One Discoveries that Changed Science and the World, ed. L.G.a.T. Lincoln. 2003: Univeristy of Chicago Press. 380.

98. Cline, H.E. and T.R. Anthony, Heat treating and melting material with a scanning laser or electron beam. Journal of Applied Physics, 1977. 48(9): p. 3895.

99. Cannon, W.R., et al., Sinterable Ceramic Powders from Laser-Driven Reactions: I, Process Description and Modeling. Journal of the American Ceramic Society, 1982. 65(7): p. 324-330.

100. Cannon, W.R., et al., Sinterable Ceramic Powders from Laser-Driven Reactions: II, Powder Characteristics and Process Variables. Journal of the American Ceramic Society, 1982. 65(7): p. 330-335.

101. Xiao, B. and Y. Zhang, Laser sintering of metal powders on top of sintered layers under multiple-line laser scanning. Journal of Physics D: Applied Physics, 2007. 40(21): p. 6725.

102. Besling, W.F.A., Laser-induced chemical vapor deposition of nanostructured silicon carbonitride thin films Journal of Applied Physics, 1998. 83(1): p. 9.

103. zheng

104. Shultz, Modeling Heat Transfer and Densification during Laser Sintering of Viscoelastic Polymers, 2005: Virginia Tech ETD.

105. Cojocaru, E., et al., Free-running ruby laser annealing of boron implanted silicon. Applied Physics A, 1981. 26(4): p. 243-246.

106. Shuja, S.Z., B.S. Yilbas, and O. Momin, Laser heating of moving solid: Influence of workpiece speed on melt size. AIChE Journal, 2010. 56(11): p. 2997-3004.

107. J., F., Viscous Flow ofCrystalline Bodies Under the Action ofSulface Tension. Journal of Physics (Moscow), 1945. 9 [5] 385..91.

108. Bourell, D., et al. Solid Freeform Fabrication An Advanced Manufacturing Approach. in Proceedings of the SFF Symposium. 1990.

109. Kasai, K., Piezoelectricity in helical polymer chains. J. Phys. Soc. Japan, 1969. 27: p. 1268.

110. Jaffe, B.b., W.R. Cook, and H. Jaffe, Piezoelectric ceramics. 1971, London: Academic Press.

111. Kasai, T., et al., Laser-Sintered Barium Titanate. Journal of the American Ceramic Society, 1989. 72(9): p. 1716-1718.

112. Baudis, U. and R. Fichte, Boron and Boron Alloys. 2000.

113. Runow, P., Study of the α to β Transformation in Boron. Journal of Materials Science, 1972. 7(5): p. 499-511.

114. Solov'ev, N., V. Makarov, and Y.A. Ugai, The crystallization kinetics of amorphous boron. Journal of the Less Common Metals, 1986. 117(1): p. 21-27.

115. Klepper, C.C., et al., Tribo-mechanical properties of thin boron coatings deposited on polished cobalt alloy surfaces for orthopedic applications. Thin Solid Films, 2008. 516(10): p. 3070-3080.

116. Matuda, N., S. Baba, and A. Kinbara, Mechanical-Properties of Boron Films. Thin Solid Films, 1982. 89(2): p. 139-142.

117. Balakrishnarajan, M.M., P.D. Pancharatna, and R. Hoffmann, Structure and bonding in boron carbide: The invincibility of imperfections. New Journal of Chemistry, 2007. 31(4): p. 473.

118. Oganov, A. and V. Solozhenko, Boron: a hunt for superhard polymorphs. Journal of Superhard Materials, 2009. 31(5): p. 285-291.

119. Makino, T. and H. Nakamura, Electrical and Optical-Properties of Boron Doped Amorphous Si Prepared by Cvd Method. Japanese Journal of Applied Physics, 1978. 17(10): p. 1897-1898.

120. Klepper, C.C., et al., Amorphous boron coatings produced with vacuum arc deposition technology. Journal of Vacuum Science & Technology a-Vacuum Surfaces and Films, 2002. 20(3): p. 725-732.

121. Klepper, C.C., et al., Vacuum arc deposited boron carbide films for fusion plasma facing components. Fusion Technology, 2001. 39(2): p. 910-915.

122. Monteiro, O.R., M.P. Delplancke-Ogletree, and C.C. Klepper, Boron carbide coatings prepared by cathodic arc deposition. Journal of Materials Science, 2003. 38(14): p. 3117-3120.

123. Bin Zeng a, Z.F.a., *, Siwei Li a, Yongsheng Liu b, Laifei Cheng b, Litong Zhang b, Microstructure and deposition mechanism of CVD amorphous boron

carbide coatings deposited on SiC substrates at low temperature. Ceramics International, 2009. 35.

124. Klepper, C.C., The challenge and opportunity to move amorphous boron suboxides toward commercial surface engineering applications. Surface Engineering, 2007. 23(1): p. 1-4.

125. Song, Z.F., et al., Study on boron-film thermal neutron converter prepared by pulsed laser deposition. Applied Radiation and Isotopes, 2011. 69(2): p. 443-447.

126. Bjerring, P., et al., Evaluation of the free-running ruby laser for hair removal - A retrospective study. Acta Dermato-Venereologica, 1998. 78(1): p. 48-51.

127. Cojocaru, E., et al., Free-Running Ruby-Laser Annealing of Boron Implanted Silicon. Applied Physics a-Materials Science & Processing, 1981. 26(4): p. 243-246.

128. Earles, S., et al., Nonmelt laser annealing of 5-KeV and 1-KeV boron-implanted silicon. Ieee Transactions on Electron Devices, 2002. 49(7): p. 1118-1123.

129. Hicks, J.M., et al., Can Pulsed Laser Excitation of Surfaces Be Described by a Thermal-Model. Physical Review Letters, 1988. 61(22): p. 2588-2591.

130. Kuhlmann, U., et al., Optical-Properties of Amorphous Boron. Journal of Physics and Chemistry of Solids, 1994. 55(7): p. 579-587.

131. Morita, N. and A. Yamamoto, Optical and Electrical Properties of Boron. Japanese Journal of Applied Physics, 1975. 14(6): p. 825-831.

132. Sota, H., et al., Optical and electrical properties of boron nitride oxide films. Diamond and Related Materials, 2008. 17(4-5): p. 826-829.

133. K.P. Karunakaran, D.o.M.E., Indian Institute of technology, Bombay, India), Alain Bernard, (IRCCyN, Ecole Centrale de Nantes, Nantes, France), S. Suryakumar, (Department of Mechanical Engineering, Indian Institute of technology, Bombay, India), Lucas Dembinski, (LERMPS-UTBM, Belfort, France), Georges Taillandier, (French Rapid Prototyping Association, Clermont-Ferrand, France), Rapid manufacturing of metallic objects. Rapid Prototyping Journal, 2012. 10(4).

134. Sukeshini, M.A., et al., Ink-Jet Printing: A Versatile Method for Multilayer Solid Oxide Fuel Cells Fabrication. Journal of the American Ceramic Society, 2009. 92(12): p. 2913-2919.

135. Zhu, J.Q., et al., Boron doped amorphous diamond window layer deposited by filtered arc for amorphous silicon alloy p-i-n solar cells. Solar Energy Materials and Solar Cells, 2009. 93(9): p. 1652-1656.

136. Kim, D., et al., Direct writing of silver conductive patterns: Improvement of film morphology and conductance by controlling solvent compositions. Applied Physics Letters, 2006. 89(26).

137. Gratson, G.M. and J.A. Lewis, Phase behavior and rheological properties of polyelectrolyte inks for direct-write assembly. Langmuir, 2005. 21(1): p. 457-464.

138. Tai, Y.L. and Z.G. Yang, Preparation of stable aqueous conductive ink with silver nanoflakes and its application on paper-based flexible electronics. Surface and Interface Analysis, 2012. 44(5): p. 529-534.

139. Zehringer, R., et al., Oxidation behaviour of boron carbide. Journal of Nuclear Materials, 1990. 176: p. 370-374.

140. Vincent, C., et al., Characterization by XPS and SEM of reactive chemical vapour deposited boron carbide on carbon fibre. Journal of Materials Science, 1992. 27(7): p. 1892-1900.

141. Solovev, N.E., V.S. Makarov, and Y.A. Ugai, The Crystallization Kinetics of Amorphous Boron. Journal of the Less-Common Metals, 1986. 117(1-2): p. 21-27.

142. Jaffe, B., Piezoelectric ceramics. 1971, London: Academic Press.

143. Rödel, J., et al., Perspective on the Development of Lead-free Piezoceramics. Journal of the American Ceramic Society, 2009. 92(6): p. 1153-1177.

144. Donnelly, N.J., T.R. Shrout, and C.A. Randall, Addition of a Sr, K, Nb (SKN) combination to PZT (53/47) for high strain applications. Journal of the American Ceramic Society, 2007. 90(2): p. 490-495.

145. Kounga, A.B., et al., High-temperature poling of ferroelectrics. Journal of Applied Physics, 2008. 104(2): p. 024116-024116-6.

146. Lubitz, K., et al. Material aspects for reliability and life time of PZT multilayer actuators. in Piezoelectric Materials for the end user, Conference notes, Polecer Meeting, Interlaken. 2002.

147. Moulson, A.J. and J.M. Herbert, Electroceramics: materials, properties, applications. 2003: Wiley.

148. Muralt, P., et al., Piezoelectric micromachined ultrasonic transducers based on PZT thin films. Ultrasonics, Ferroelectrics and Frequency Control, IEEE Transactions on, 2005. 52(12): p. 2276-2288.

149. Zupan, M., M.F. Ashby, and N.A. Fleck, Actuator classification and selection—the development of a database. Advanced Engineering Materials, 2002. 4(12): p. 933-940.

150. Padhi, A.S., Synthesis & Characterization of Lead Free Piezoelectric NBT-BT Ceramics by Solid State Processing Route Method. Department of Physics National Institute of Technology Rourkela India, 2012.

151. Ranjan, R. and A. Dviwedi, Structure and dielectric properties of (Na< sub> 0.50</sub> Bi< sub> 0.50</sub>)< sub> 1− x</sub> Ba< sub> x</sub> TiO< sub> 3</sub>: 0≤< i> x</i>≤ 0.10. Solid state communications, 2005. 135(6): p. 394-399.

152. Zhou, T.-S., et al., Lead-free In2O3-doped (Bi0. 5Na0. 5) 0.93 Ba0. 07TiO3 ceramics synthesized by direct reaction sintering. Applied physics letters, 2007. 90(18): p. 182903-182903-3.

153. Jones, G. and P. Thomas, Investigation of the structure and phase transitions in the novel A-site substituted distorted perovskite compound Na0. 5Bi0. 5TiO3. Acta Crystallographica Section B: Structural Science, 2002. 58(2): p. 168-178.

154. Woodward, P.M., Octahedral tilting in perovskites. I. Geometrical considerations. Acta Crystallographica Section B: Structural Science, 1997. 53(1): p. 32-43.

155. Joshi, S., Synthesis of $ Bi0. 5Na0. 5TiO_3–BiFeO_3 $ Solid Solution Via Combustion Synthesis Route, 2009.

156. Soukhojak, A., et al., Superlattice in single crystal barium-doped sodium bismuth titanate. Journal of Physics and Chemistry of Solids, 2000. 61(2): p. 301-304.

157. Park, S.-E. and K.S. Hong, Variations of structure and dielectric properties on substituting A-site cations for Sr2+ in (Na1/2Bi1/2) TiO3. Journal of materials research, 1997. 12(8): p. 2152-2157.

158. Sakata, K. and Y. Masuda, Ferroelectric and antiferroelectric properties of (Na 0.5 Bi 0.5) TiO3-SrTiO3 solid solution ceramics. Ferroelectrics, 1974. 7(1): p. 347-349.

159. Maurya, D., M. Murayama, and S. Priya, Synthesis and Characterization of Na2Ti6O13 Whiskers and their Transformation to (1−x) Na0.5Bi0.5TiO3-xBaTiO3 Ceramics. Journal of the American Ceramic Society, 2011. 94(9): p. 2857-2871.

160. Maurya, D., et al., Nanostructured lead-free ferroelectric Na0.5Bi0.5TiO3-BaTiO3 whiskers: synthesis mechanism and structure. Dalton Trans, 2012. 41(18): p. 5643-52.

161. elements, c. Sodium. 2012; Available from: http://www.chemicalelements.com/elements/na.html#citing.

162. elements, c., Bismuth. 2012.

163. Nikanorov, S.P., et al., Structural and mechanical properties of Al–Si alloys obtained by fast cooling of a levitated melt. Materials Science and Engineering: A, 2005. 390(1-2): p. 63-69.

164. Grabowski, A., M. Nowak, and J. Śleziona, Laser beam interactions with metal matrix AlSi alloy/SiCp composites. Journal of Achievements in Materials and Manufacturing Engineering, 2008. 31(2).

165. Hasegawa, R., et al., Crystal structures of three crystalline forms of poly(vinylidene fluoride). Polym. J., 1972. 3(Copyright (C) 2012 American Chemical Society (ACS). All Rights Reserved.): p. 600-10.

166. Kunstler, W., et al., Preparation and assessment of piezo- and pyroelectric poly(vinylidene fluoride-hexafluoropropylene) copolymer films. Appl. Phys. A: Mater. Sci. Process., 2001. 73(Copyright (C) 2012 American Chemical Society (ACS). All Rights Reserved.): p. 641-645.

167. Newman, B.A., et al., Piezoelectricity in nylon 11. J. Appl. Phys., 1980. 51(Copyright (C) 2012 American Chemical Society (ACS). All Rights Reserved.): p. 5161-4.

168. Fukada, E., Pyroelectricity and piezoelectricity of polyurea. Key Eng. Mater., 1994. 92-93(Copyright (C) 2012 American Chemical Society (ACS). All Rights Reserved.): p. 143-59.

169. Zhang, S., et al., Microstructure and electromechanical properties of carbon nanotube/poly(vinylidene fluoride-trifluoroethylene-chlorofluoroethylene) composites. Adv. Mater. (Weinheim, Ger.), 2005. 17(Copyright (C) 2012 American Chemical Society (ACS). All Rights Reserved.): p. 1897-1901.

170. Levi, N., et al., Properties of Polyvinylidene Difluoride-Carbon Nanotube Blends. Nano Lett., 2004. 4(Copyright (C) 2012 American Chemical Society (ACS). All Rights Reserved.): p. 1267-1271.

171. Newnham, R.E., D.P. Skinner, and L.E. Cross, Connectivity and piezoelectric-pyroelectric composites. Mater. Res. Bull., 1978. 13(Copyright (C) 2012 American Chemical Society (ACS). All Rights Reserved.): p. 525-36.

172. Ploss, B., et al., Pyroelectric activity of ferroelectric PT/PVDF-TRFE. IEEE Trans. Dielectr. Electr. Insul., 2000. 7(Copyright (C) 2012 American Chemical Society (ACS). All Rights Reserved.): p. 517-522.

173. Cui, C., et al., Improved piezoelectric ceramic/polymer composites for hydrophone applications. Synth. Met., 1997. 85(Copyright (C) 2012 American Chemical Society (ACS). All Rights Reserved.): p. 1391-1392.

174. Venkatragavaraj, E., et al., Piezoelectric properties of ferroelectric PZT-polymer composites. J. Phys. D: Appl. Phys., 2001. 34(Copyright (C) 2012 American Chemical Society (ACS). All Rights Reserved.): p. 487-492.

175. Sreekumar, T.V., et al., Polyacrylonitrile single-walled carbon nanotube composite fibers. Adv. Mater. (Weinheim, Ger.), 2004. 16(Copyright (C) 2012 American Chemical Society (ACS). All Rights Reserved.): p. 58-61.

176. Wang, L. and Z.-M. Dang, Carbon nanotube composites with high dielectric constant at low percolation threshold. Appl. Phys. Lett., 2005. 87(Copyright (C) 2012 American Chemical Society (ACS). All Rights Reserved.): p. 042903/1-042903/3.

177. Salehi-Khojin, A., M.R. Hosseini, and N. Jalili, Underlying mechanics of active nanocomposites with tunable properties. Compos. Sci. Technol., 2009. 69(Copyright (C) 2012 American Chemical Society (ACS). All Rights Reserved.): p. 545-552.

178. Guldi, D.M., et al., Multifunctional molecular carbon materials - from fullerenes to carbon nanotubes. Chem. Soc. Rev., 2006. 35(Copyright (C) 2012 American Chemical Society (ACS). All Rights Reserved.): p. 471-487.

Chapter 4 Conclusion and Future of 3D Additive Printing

4.1 Introduction

This manuscript discussed the Optomec AJP system and investigated four inorganic types of solid. The study has demonstrated a method for the development of ink, generation of a high density green film and sintering ability of the laser. The construction of high density green-film was shown to be a consequence of proper adjustment of several important parameters. In addition, sintering methods and corresponding Selective Laser Sintering (SLS) mechanism have been presented for both initial and subsequent layers along with hurdles for some more complex materials. Although some strides and successes have been achieved, other portions of the projects remain unfinished. Below lists the major achievements followed by the goals and gaps for future research, and the appendix provides the additional information on Taguchi Experimental Designs for Orthogonal Arrays along information on the ink construction calculator.

4.2 Development Thrusts

Listed here are the major knowledge gaps and suggested further research within regarding this body of work:

1. There is a complex interaction between surface tension and viscosity that is not well understood. This interaction plays an important role in many processes during 3D additive printing, such as the ability to aerosolize the ink within the initial vessel, droplet formation size and inclusion of particles by volume and or mole concentration, compaction of droplet upon impact, surface wetting and impact at the substrate.
    a. In order to understand the ability to produce an aerosol mist along with the particle size and distribution of that mist, a study on viscosity and surface tension for inks should be conducted to distinguish different contributions from polarity of the molecules, solid shape and loading concentration. This would provide an operating guideline for different inks due to better understanding of deposition capabilities, stability of misting rate, overspray minimization.
2. Laser sintering new materials has shown to be an extremely difficult problem to solve, specifically multi-material systems. As noted previously many of the laser treatments for

new materials are proprietary. However, there are some formulas and papers providing insight to the power/area and initial power per area these formulas exist for complete and dense solids.

   a. Nanoparticles with diameter less than 500 nm behave very differently than bulk materials. Complicated thermal variations exist when dealing with multi-materials, most of which arises from different melting points, varied composition percentages, different crystal structure, and random matrix distribution and orientations. Other enigmas include variable densities within the green film matrix, it is this point that was one of the main focuses of the investigation of the AJP.

   b. It is recommended that for future development of materials a design of experiments methodology be employed, because the measurement time is too short for any method of recording and all current methods of numerical solutions have failed. This is not to say numerical solutions should be abandoned, rather they should continue to be sought, but tempered with the knowledge that DOE and Nelson's work has enabled repeatable results based on the interactions between controllable factors for the experiments.

3. Additional issues with high temperatures and oxidation at ambient environments cause incredible problems with final material property and formations of oxides. In fact this issue is the major limitation to all systems listed above for sintering with any type of metal. This issue is different for a 3D system with other material synthesis method. Since the 3D system is building the object, the entire volume can be compromised by oxidation. This limits corrosion resistance at best and ultimate part strength at worst.

   a. It is recommended to utilize laminar flow gas chamber to reduce oxidation for other materials, as it has shown excellent possibilities in the boron segment of this research. However, due to time constraints was not able to be applied to other areas. There are several changes and small alterations to this chamber which can be made easily to those current in the art allowing further flexibility in use. The current system can be installed onto and disassembled from the machine in less than one minute. Re-orientation of the Optomec AJP to this new position is less

than one minute as well. Because oxidation is one of the major hurdles to additive printing, this solution of a protective gas presents an excellent, low cost, low-tech method of solution to these problems.

4. The largest hurdle for the AJP in constructing 3D parts is that this system was designed as a 2D system, and in the cases for 3D printing the design of the machine was intended for 3D printing from conception. This is not to say this system cannot be retrofit or cannot install additional accessories (such as multi-head print system), rather that these accessories might not have the same return on investment as a newer machine. In order to print in 3D, some material systems may be easily integrated such as water based solids, which can be removed through heat or other solvents.

5. Another limitation to the current system is the power and wavelength of the laser. The current system uses a 2Watt max laser, which is dedicated to the near-infrared band of the spectrum. There are several elements are unaffected by this wavelength, which are of interest both to 3D structures and electronic printing. Utilization of higher power laser, such as Nd:YAG, CO2, or other laser would be readily welcomed. The current system has a beam cross-section of approximately 20 μm under focused condition; increase the power of laser can reduce the time for annealing and heat treatments. This in turn would also decrease the oxidation possibility at the surface.

6. Finally, it is apparent that size plays a distinct role in the availability to test new materials. One of the hardest to overcome has been the limitations placed on the operator regarding powder size. At one micron of the particle size is the upper limitation of the machine, because of the energy needed to create a dense and continuous aerosol, and also the diffusion of these particle down to the deposition head. Additionally, it is a necessity that the aerosol cannot contain any particulate at a diameter larger than a percentage of the droplet size. To further complicated issues, smaller particles are less accurately dispensed onto the substrate creating overspray issues.

   One possible solution in future developments may be to use flow instability via the Raleigh equation. This equation states that the flow of water while undergoing shear stress or through turbulence will separate into droplets with an average size equal to 2.5x the diameter of the flow. It may be possible to use a jetting system to create droplets of

programmable size in 5-20 μm range, just below ink jet printing, that are deposited from a print head with sufficient stand-off distance.

7. The lone polymer used in this experiment did not use the laser for sintering as the Tg was low enough to allow sintering and flash-off via the heated platen. Not all polymers will have this characteristic, and not all polymers can absorb light. In these cases, outside of a separate laser which has an absorption coefficient with the material, it may be possible to heat the polymer first with the platen and using an absorbent material either within the polymer matrix or below it, heat the polymer.
8. One characteristic not taken into account in the polymer deposition is the confirmation of the polymer as it is being aerosolized, transmitted and deposited. To this author's best knowledge at the time this paper was submitted, there is no research on this subject using this machine.

4.3 Final Thoughts

3D printing technique develops very fast recently. Part of this progressing technology is due to the computer industry and parallel track of development for many of the sub-systems of the 3D machines, code and architecture. As decreasing in both price and volume, these printers will become more ubiquitous at home and industry. These new printers can produce everything from batteries to replacement parts for the car.

The current limitations for progress in the realm of mat

erials are really a new paradigm shift in thinking. In nano-scale devices or micro-fluidics, the typical pedestrian forces we experience and take for granted are no longer the driving forces. This realization points to two main issues: The first is that by necessity under rapid-time sintering conditions the typical phase diagrams metallurgists and materials science has relied on for decades will be incomplete or incorrect; the second is that phase transformations, diffusion, kinetics, and mixing are all time dependent. The reduction of this time-scale from hours to milliseconds is on the order of $3.6x10^6$ to $3.6x10^9$, and has a monumental effect on formations found, phase retention, and new alloys. This provides a new field of investigations to proceed with the same materials we currently have extracting new properties from them.

Appendix

Taguchi L18 **Orthogonal** Array

			P1	p2	p3	p4	p5	p6	p7	p8
Original Run#		Run #		Deck Temp	Atm cfm	Sheath Cfm	Passes	TWV	% Overlap	Deck Speed
1		1	perimeter	30	23	35	1	0.01	5:10	1.2
2		2	perimeter	30	25	40	2	0.02	10:15	1.4
3		3	perimeter	30	27	45	4	0.05	25:30	1.6
10		4	serpentine	30	23	45	4	0.02	10:15	1.2
11		5	serpentine	30	25	35	1	0.05	25:30	1.4
12		6	serpentine	30	27	40	2	0.01	5:10	1.6
4		7	perimeter	50	23	35	2	0.02	25:30	1.6
5		8	perimeter	50	25	40	4	0.05	5:10	1.2
6		9	perimeter	50	27	45	1	0.01	10:15	1.4
13		10	serpentine	50	23	40	4	0.01	25:30	1.4
14		11	serpentine	50	25	45	1	0.02	5:10	1.6
15		12	serpentine	50	27	35	2	0.05	10:15	1.2
7		13	perimeter	70	23	40	1	0.05	10:15	1.6
8		14	perimeter	70	25	45	2	0.01	25:30	1.2
9		15	perimeter	70	27	35	4	0.02	5:10	1.4
16		16	serpentine	70	23	45	2	0.05	5:10	1.4
17		17	serpentine	70	25	35	4	0.01	10:15	1.6
18		18	serpentine	70	27	40	1	0.02	25:30	1.2

Taguchi L25 DOE Template

Laser DOE						
	P1	p2	p3	p4	p5	p6
Run #	Wattage	Focal Plane	% Overlap	Deck Speed	# Repeats	--
1	1.2	-0.004	0 to 5	1.1	1	0
2	1.2	-0.002	5 to 10	1.2375	2	0
3	1.2	mid	10 to 15	1.375	4	0
4	1.2	0.002	20 to 25	1.5125	6	0
5	1.2	0.004	20 to 25	1.65	8	0
6	1.4	-0.004	5 to 10	1.375	6	0
7	1.4	-0.002	10 to 15	1.5125	8	0
8	1.4	mid	20 to 25	1.65	1	0
9	1.4	0.002	20 to 25	1.1	2	0
10	1.4	0.004	0 to 5	1.2375	4	0
11	1.6	-0.004	10 to 15	1.65	2	0
12	1.6	-0.002	20 to 25	1.1	4	0
13	1.6	mid	20 to 25	1.2375	6	0
14	1.6	0.002	0 to 5	1.375	8	0
15	1.6	0.004	5 to 10	1.5125	1	0
16	1.8	-0.004	20 to 25	1.2375	8	0
17	1.8	-0.002	20 to 25	1.375	1	0
18	1.8	mid	0 to 5	1.5125	2	0
19	1.8	0.002	5 to 10	1.65	4	0
20	1.8	0.004	10 to 15	1.1	6	0
21	2	-0.004	20 to 25	1.5125	4	0
22	2	-0.002	0 to 5	1.65	6	0
23	2	mid	5 to 10	1.1	8	0
24	2	0.002	10 to 15	1.2375	1	0
25	2	0.004	20 to 25	1.375	2	0

Boron Solutions Calculator

Solutions Calculator								
Instructions: Enter the total volume of solution to be made in the yellow highlighted boxes:								
			3.00%			5.00%		
	volume		wt		volume	wt		
Boron			1.50993	g		2.51655	g	
Methanol	51	ml	40.341	g	5.95		ml	
Ethylene Glycol	9	ml	9.99	g	1.05		ml	
PVA			0.251655	g		0.251655	g	
Totals	60			ml	7		ml	
			3% by wt of solvent			5% by wt of solvent		
Boron			1.501821	g		2.503035		
Acetone	51	ml	40.0707	g	5.95	40.0707	g	
Ethylene Glycol	9	ml	9.99	g	1.05	9.99	g	
PVA			0.250304	g		0.250304		
Totals			50.0607	g		50.0607		
Total Solvent Volume	60			ml	7		ml	
			3% by wt of solvent			5% by wt of solvent		
Boron			1.50687	g		2.51145	g	
Ethanol	51	ml	40.239	ml	5.95	40.239	ml	
Ethylene Glycol	9	ml	9.99	ml	1.05	9.99	ml	
PVA			0.251145	g		0.251145	g	
			8	ml		8	ml	
Total Solvent Volume	60	ml			7			
Total Solvent Weight			50.229					
			3% by wt of solvent			5% by wt of solvent		
Boron			1.8297	g		3.0495	g	
H2O	51		51	ml	5.95	51	ml	
Ethylene Glycol	9		9.99	ml	1.05	9.99	ml	
PVA			0.30495	g		0.30495	g	
Total Solvent Volume	60			ml	7	0	ml	
Total Solvent Weight			60.99					
Total Boron Used	16.92886	g						